Die approbierte gedruckte Originalversion dieser Dissertation ist an der TU Wien Bibliothek verfügbar.
The approved original version of this doctoral thesis is available in print at TU Wien Bibliothek.

Dissertation

Surface chemistry and pretreatment effects on Zn-Al-Mg coatings: insights into oxide and zirconium conversion layer formation

Executed for the purpose of obtaining the academic degree of Doctor of Technical Sciences under the supervision of

Univ.Prof. Dipl.-Ing. Dr.techn. Markus Valtiner
E134
Institute of Applied Physics,

submitted to the Vienna University of Technology
Faculty of Physics
by
Maria Ponomareva
Student ID number 12045340

Place, date | (Signature of author) | (Signature of supervisor)

Die approbierte gedruckte Originalversion dieser Dissertation ist an der TU Wien Bibliothek verfügbar.
The approved original version of this doctoral thesis is available in print at TU Wien Bibliothek.

Declaration

I hereby affirm that this thesis was prepared by me in accordance with the established standards for scientific papers. All resources utilized, particularly the foundational literature, are identified and enumerated in this thesis. Any passages taken verbatim from the sources are clearly marked as such. I confirm that I have not submitted the topic of this thesis as an examination paper to an assessor in this country or abroad. This thesis is in alignment with the assessment provided by the assessors. I acknowledge that the submitted work will be checked electronically and technically using suitable and state-of-the-art means (plagiarism detection software). This process ensures that the high quality standards within the framework of the applicable rules for safeguarding good scientific practice, as outlined in the TU Wien Code of Conduct, were observed in the preparation of the submitted work. Additionally, a comparison with other student theses avoids any potential violations of my personal copyright.

Linz, 18.11.2024

Signature

Die approbierte gedruckte Originalversion dieser Dissertation ist an der TU Wien Bibliothek verfügbar.
The approved original version of this doctoral thesis is available in print at TU Wien Bibliothek.
TU WIEN Bibliothek Your knowledge hub

Die approbierte gedruckte Originalversion dieser Dissertation ist an der TU Wien Bibliothek verfügbar.
The approved original version of this doctoral thesis is available in print at TU Wien Bibliothek.

Die approbierte gedruckte Originalversion dieser Dissertation ist an der TU Wien Bibliothek verfügbar.
The approved original version of this doctoral thesis is available in print at TU Wien Bibliothek.

Contents

Die approbierte gedruckte Originalversion dieser Dissertation ist an der TU Wien Bibliothek verfügbar.
The approved original version of this doctoral thesis is available in print at TU Wien Bibliothek.
TU WIEN Bibliothek Your knowledge hub

Die approbierte gedruckte Originalversion dieser Dissertation ist an der TU Wien Bibliothek verfügbar.
The approved original version of this doctoral thesis is available in print at TU Wien Bibliothek.

Die approbierte gedruckte Originalversion dieser Dissertation ist an der TU Wien Bibliothek verfügbar.
The approved original version of this doctoral thesis is available in print at TU Wien Bibliothek.

Die approbierte gedruckte Originalversion dieser Dissertation ist an der TU Wien Bibliothek verfügbar.
The approved original version of this doctoral thesis is available in print at TU Wien Bibliothek.
TU WIEN Bibliothek Your knowledge hub

Acknowledgements

This work originates from research in the iMESA (FFG 865864 CEST-K1, 2019-2022) project and the GreenMetalCoat (FFG 899594, Comet-Center (K1), 2023) project.

First, I would like to express my gratitude to my supervisor, Univ. Prof. Dipl.-Ing. Dr. techn. Markus Valtiner, for his expert guidance through this PhD thesis. Thank you for inviting me into the world of real research and being a good example of confidence, optimism, and a can-do attitude. I believe that working with you taught me valuable life lessons that I will carry forward.

I would like to thank colleagues from the Institute of Applied Physics, particularly Matthias Kogler, Elahe Akbari and Daniela Miano, for their collaboration and constant readiness to assist with the research. I also would like to thank Florian Farnberger from the Institute of Chemical Technology and Analytics for his insightful contributions to this work.

Among the people who gave me the opportunity to pursue this PhD from the CEST side is Bernhard Lutzer, whose mind-blowing networking initiated my journey to Austria and CEST, and Alexander Balatka, who gave me the time I needed to complete this thesis. Markus Nadlinger, my first project manager, and his successor, Gabi, both taught me a lot and provided valuable support. Tanja and Laura, who later managed the GreenMetalCoat project, offered constant encouragement. Special thanks go to CEST Linz technicians Phillipp and Perizat for their assistance in my projects.

This research would not have been possible without our industry partner, voestalpine Stahl GmbH, who provided both financial support and critical materials. I am deeply thankful for the expertise of Gerald Luckeneder and Roland Steger, whose contributions were instrumental to the success of this work.

I would also like to thank my research partners, Dr. Jiri Duchoslav and Assoc. Univ.-Prof. DI Dr. David Stifter from JKU Linz for their support and always

fruitful collaborations.

Lastly, I want to express my deepest gratitude to people, who have had the most positive impact on my life and this thesis. To my husband - for his dedication, patience, and a shoulder to cry on. To my psychologist - for helping me navigate anxiety and personal growth. To my friends in Austria and beyond - for being together during the pandemic and other turbulent times. As we all know, "What doesn't kill you makes you stronger", and with the support of my family and friends, this journey has truly made me stronger in unpredictable ways. My heartfelt thanks also go to my family—my parents, who made all of this possible, and my grandmother, aunt, and sister, whose constant support and understanding were invaluable.

Thank you all for being part of this journey.

Die approbierte gedruckte Originalversion dieser Dissertation ist an der TU Wien Bibliothek verfügbar.
The approved original version of this doctoral thesis is available in print at TU Wien Bibliothek.
TU WIEN Bibliothek Your knowledge hub

Die approbierte gedruckte Originalversion dieser Dissertation ist an der TU Wien Bibliothek verfügbar.
The approved original version of this doctoral thesis is available in print at TU Wien Bibliothek.

Abstract

Zn-Al-Mg hot-dip galvanized steel is one of the frequently used modern materials for an automotive industry. With high corrosion resistance and good mechanical properties, it serves as a base for consequent processes, such as painting or applying organic coatings. The influence of intermitting processes, such as chemical cleaning of the surface, surface activation and application of a conversion layer, on the Zn-Al-Mg coating surface chemistry plays an important role in later adhesion and susceptibility to corrosion. This thesis investigates the surface chemistry of Zn-Al-Mg coatings under varying chemical treatments, utilizing a combination of advanced surface-sensitive analytical techniques and others.

A comparative analysis of Angle-resolved X-ray photoelectron spectroscopy (AR-XPS), Low-energy ion scattering spectroscopy (LEIS), and Secondary ion mass spectrometry (SIMS) depth profiles is conducted to interpret compositional changes in Zn-Al-Mg coatings subjected to alkaline and acidic pretreatments. The findings reveal distinct chemical modifications depending on the treatment conditions, with alkaline treatments promoting the formation of mixed Mg/Al- and Zn-hydroxide layers, while acidic conditions result in the fast activation of Zn and dissolution of Mg-oxyhydroxides. Moreover, the results showed in practice high applicability of XPS and LEIS methods to study the surface chemistry of the industrially produced material, and the ability of SIMS to complement these results on such complex matrix material.

Further, combination of analytical (ICP-OES) and surface-sensitive approach was used to characterize the surface chemistry modifications and dissolution mechanism of Zn-Al-Mg coatings induced by industrially applicable cleaners with different pH, in mild and strong alkaline areas. While mild alkaline cleaner showed active Zn dissolution and Zn diffusion to the surface, strong alkaline cleaner advanced in Al dissolution, forming Mg/Zn-hydroxide on the surface. The results highlight the critical role of choosing the right cleaning conditions, depending on the preferrable

effects, which could be essential for the next step in the coating process.

As the next logical step in metallic coating processing the research examines the effects of alkaline and acidic pretreatments on the characteristics of Zr-conversion layers. The findings indicate that alkaline pretreatments result in double-layered coatings, consisting of an oxidic and fluoridic layer. Acidic conditions although form much thicker oxidic layer, deflect an insoluble fluoride layer formation. Therefore, strong alkaline pretreatment showed to be preferrable for building an uniform complex Zr-conversion coating.

Die approbierte gedruckte Originalversion dieser Dissertation ist an der TU Wien Bibliothek verfügbar.
The approved original version of this doctoral thesis is available in print at TU Wien Bibliothek.
TU WIEN Bibliothek Your knowledge hub

Glossary

Abbreviations

AES Auger electron spectroscopy
AR-XPS Angle-resolved X-ray photoelectron spectroscopy
AFM Atomic force microscopy
CPD Contact potential difference
FT-IR Fourier-transform infrared spectroscopy
HDG Hot-dip galvanized steel
HR-SKP Height-regulated scanning Kelvin probe
ICP-OES Inductively coupled plasma optical emission spectroscopy
IRRAS Infrared reflection-absorption spectroscopy
ISO International Organization for Standardization
LEIS Low-energy ion scattering
NSS Neutral salt spray test
SIMS Secondary ion mass spectrometry
SKP Scanning Kelvin probe
SST Salt spray test
ToF-SIMS Time-of-flight secondary ion mass spectrometry
XPS X-ray photoelectron spectroscopy

Die approbierte gedruckte Originalversion dieser Dissertation ist an der TU Wien Bibliothek verfügbar.
The approved original version of this doctoral thesis is available in print at TU Wien Bibliothek.

Die approbierte gedruckte Originalversion dieser Dissertation ist an der TU Wien Bibliothek verfügbar.
The approved original version of this doctoral thesis is available in print at TU Wien Bibliothek.

Die approbierte gedruckte Originalversion dieser Dissertation ist an der TU Wien Bibliothek verfügbar.
The approved original version of this doctoral thesis is available in print at TU Wien Bibliothek.

Part I

Introduction

TU WIEN Bibliothek Your knowledge hub
Die approbierte gedruckte Originalversion dieser Dissertation ist an der TU Wien Bibliothek verfügbar.
The approved original version of this doctoral thesis is available in print at TU Wien Bibliothek.

Die approbierte gedruckte Originalversion dieser Dissertation ist an der TU Wien Bibliothek verfügbar.
The approved original version of this doctoral thesis is available in print at TU Wien Bibliothek.
TU WIEN Bibliothek Your knowledge hub

Chapter 1

Motivation and Literature Reviews

1.1 Literature background

1.1.1 Surface chemistry of Zn-Al-Mg coatings

Mild steel is often used in the automotive industry because it is a low-cost material with good mechanical properties. However, it is prone to corrosion: the steel corrosion rate, predicted for the very low corrosivity environment C1, according to ISO 9223, is about 10 g/m^2 year [1]. The application of metallic coatings, such as Zinc coatings, should isolate the substrate from the environment, therefore protecting it (also electrochemically). This way the mechanical properties of the substrate and the anticorrosion properties of metallic coatings would prolong the life of the steel [2]. According to ISO 9223, the Zn corrosion rate in the same environment is 0.7 g/m^2 year, what would be already an effective mean for steel corrosion protection, even only by providing an isolation from the low corrosivity environment [1]. In other conditions, e.g., in Linz, at a site with urban industrial atmosphere the corrosion rate for steel is 106 g/m^2 year, while for Zn it is 11.4 g/m^2 year [3].

Thus, the application of metallic coatings, e.g., Zn coatings, became a popular way of corrosion protection, constantly improving and evolving over the years [4].

Zn-Al-Mg coatings have been known for the last few decades, since in the 2000s researchers from different steel-producing manufacturers came to the conclusion about the most effective Mg and Al percentage in such coatings. It was found that the optimal content of Mg is from 1.0 to 3.0 wt%, where Al is from 1.0 to 3.7

wt%.

The Zn-Al-Mg alloy consist of dendrite regions and granular/lamellar regions, as it is shown in **Figure 1.1**. The dendrite structure consist of Zn-rich dendrite branches, and the areas among the branches, containing Mg, where Zn to Mg ratio is 2:1. The bordering granular/lamellar region composes of Zn, Al and Mg, and often called a ternary eutectic phase. It has a complex morphology and consist of Zn lamellas, Al-wrapping Zn-granules and Zn-Mg lamellas [5–7].

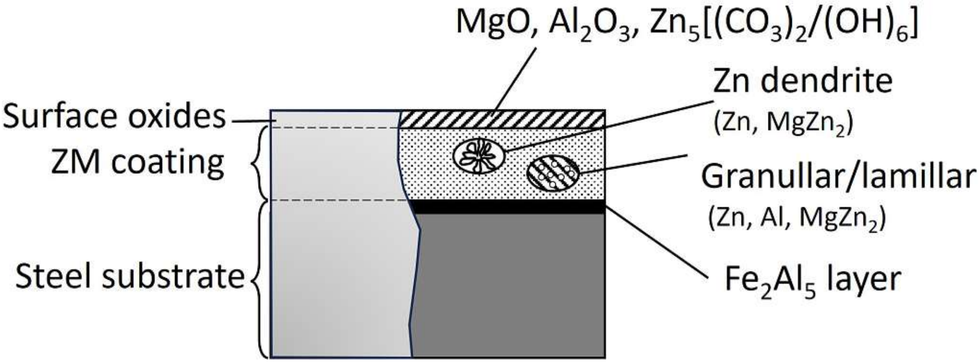

Figure 1.1. Schematic representation of Zn-Al-Mg-coating-layer cross-cut structure and surface oxide chemistry, produced by hot-dip galvanizing.

The surface of industrially produced Zn-Al-Mg coated steel surface is usually covered with initial Mg/Al-oxide, as well as basic Zn carbonate (hydrozincite) [8–10].

Demonstrating excellent corrosion resistance properties, Zn-Al-Mg coatings can hold about 2500 hours of neutral salt spray test – a standardized test used to evaluate the corrosion resistance of a material [11]. Compared to simple Zn-coated steel, that would hold for about to 100 hours of the neutral salt spray test exposure before showing first signs of red rust formation [12]. Overall, regardless of pH of the SST, Zn-Al-Mg showed better results than Zn coating any time [13]. Moreover, Zn-Al-Mg is 8-10 times better than Zn coating in automotive tests with salt load in delaying red rust appearance, and 2 times better in tests with lower salt load and in field exposure [14].

Die approbierte gedruckte Originalversion dieser Dissertation ist an der TU Wien Bibliothek verfügbar.
The approved original version of this doctoral thesis is available in print at TU Wien Bibliothek.

Die approbierte gedruckte Originalversion dieser Dissertation ist an der TU Wien Bibliothek verfügbar.
The approved original version of this doctoral thesis is available in print at TU Wien Bibliothek.

1.1.2 Alkaline and acidic treatment effects on metal coatings

The goal of cleaning as part of the hot-dip galvanization process is the removal of various substances and contaminants from the surfaces. This includes residues from soldering and welding, as well as dust, sand, salts, bacteria, and other. Depending on the type of contamination, hydrocarbons, alkaline solutions, surfactants, or sodium salts of polycarboxylic acids are used as cleaners [15].

Despite the ability of acids to dissolve relatively insoluble in other solutions oxides, the acid cleaning is more often used as an application to the other methods. Thus, such method, which includes alkaline decreasing and later acid pickling, is often used in hot-dip galvanizing plants. Alkaline cleaners, on the other hand, are efficient and economical in degreasing without other additional steps [16].

As far as an alkaline media effects the surface chemistry, degreasing with strong alkaline solution results in Al reduction on the surface of HDG Zn surface. If thorough, preceding pretreatments before the phosphating or paint application, it removes aluminium oxide layer, which brings good adhesion of exerted later organic coatings or paints [17, 18]. The composition of the oxide films changes from ZnAl hydroxide/oxide to Zn hydroxide/oxide after the cleaning [19]. Moreover, alkaline cleaning induces an increase in the real surface area, which might affect later formation of the conversion film [20]. It is reported that on Zn surfaces, the activation is achieved because of the Aluminium oxide dissolutions [21].

Similarly, on Zn-Al-Mg coated steel the sodium hydroxide solutions with pH value above 13 reduce aluminium concentration in the topmost surface layer, when highly acidic treatment dissolves Mg-compounds, including MgZn2 phases [22]. Further, it was found that strong alkaline commercially available cleaner removes Zn corrosion products, and aluminium, enriching the Zn-Al-Mg surface in Zn and Mg [23].

1.1.3 Zirconium conversion coatings

Conversion coatings are essential in metal pretreatment and commonly used in automated systems like powder and coil coating. These coatings help protect the metal surface by passivating it and creating a stable base that improves the adhesion of organic layers or paints applied afterwards.

In the past, phosphating and chromating were widely used, separately or in combination, but the environmental and health risks associated with chromates have prompted a move toward safer, eco-friendly solutions [24]. Zirconium- and titanium-based coatings have become an attractive alternative, providing effective surface protection while meeting modern health, safety, and environmental requirements, making them a strong candidate to replace chromate-based systems [25].

The conversion coatings, based on zirconium fluorides, are often referred to as the nanoceramic conversion layer and comprise a dense zirconium dioxide layer of about 20 to 50 nm. The potential for savings is significant, with the possibility of reducing water consumption and heating energy costs by up to 60 %, and waste generation by up to 80 % [26].

There are currently more than twenty commercial coating baths from manufacturers such as Henkel, Chemetall, Navair, and others reported [27]. They are mainly composed of hexafluorzirconic acid and other additives, including chrome, copper, and organic compounds. Another alternative is a combination of hexafluortitanic acid with hexafluorzirconic.

The corrosion resistance properties of Zr conversion coatings on steels are being investigated. It is important to note that Zr conversion coatings do not provide corrosion protection on their own, but they improve corrosion protection by enhancing coating adhesion [25]. E.g., chemical pretreatment by Ti/Zr enhances the adhesive strength of epoxy coatings after exposure to condensation chamber test and salt fog test, in comparison to classical chromating and phosphating [28]. Similarly, the zirconium-based conversion coating on cold rolled steel showed well-pleasing corrosion and adhesion properties as a result of corrosion performance evaluation, including adhesion test, T-bone test, NSS and warm salt water dipping test [29].

The conditions of the conversion process are also of importance when talking about the Zr layers application. The influence of convection on Zr conversion film formation was studied, the stirring at 400 rpm by 90 s immersion in conversion bath increased film thickness by a factor of 3 on HDG steel [30].

The mechanism of the process is an object for investigation. Thus, a key step in Zr conversion process on Zn surface is initial surface activation, which is prompted by the removal of hydroxyls by free fluorides. This increases the Zr deposition rate and growth of a conversion layer [31].

On Zn-Al-Mg alloy surfaces, the deposition of the Zr-conversion layer starts from Zn-rich phases, while Mg- and Al-rich phases undergo anodic dissolution. With

Die approbierte gedruckte Originalversion dieser Dissertation ist an der TU Wien Bibliothek verfügbar.
The approved original version of this doctoral thesis is available in print at TU Wien Bibliothek.

increasing immersion time, the deposition of the layer happens over all surface [32].

1.2 Motivation and outline of this thesis

1.2.1 Research aim

In the context of the "in Situ Metal Surface Analysis" and "GreenMetalCoat" projects and in light of the literature background presented above, the following research questions were formulated for this doctoral dissertation on agreement with all company and research partners:

- How do alkaline and acidic treatments impact the formation, dissolution, and composition of oxide and hydroxide layers on Zn-Al-Mg alloy coatings, and how do surface analytical techniques like AR-XPS, LEIS, and SIMS reveal these effects?
- How do mild and strong alkaline cleaning treatments affect the dissolution mechanisms and surface chemistry of Zn-Al-Mg coated hot-dip galvanized steel, and how do these processes influence the formation and stability of passive films on the coating?
- How do mild alkaline, strong alkaline, and acidic pretreatments affect the formation, thickness, and uniformity of Zr-conversion layers on Zn-Mg-Al alloy coatings, and which conditions optimize the growth and quality of Zr-based layer?
- How can one further optimize the process of Zn-Al-Mg coating pretreatment consistency before Zr-conversion or other industrially applicable processes to ensure good final product properties?

1.2.2 Thesis outline

This thesis consists of six chapters. The first chapter contains the motivation for this work and a literature review, while Chapter 2 gives an overview of the main methods used in the work. Among them are optical spectroscopy methods, electron spectroscopy, and ion emission and scattering techniques, which were used to determine the chemical composition and chemical states of the surface

Die approbierte gedruckte Originalversion dieser Dissertation ist an der TU Wien Bibliothek verfügbar.
The approved original version of this doctoral thesis is available in print at TU Wien Bibliothek.
TU WIEN Bibliothek Your knowledge hub

oxides and the elemental composition of the solution.

Chapter 3 ”Comparison of LEIS, SIMS and AR-XPS as methods for surface characterization of passivated Zn-Al-Mg steel” reports about the effects of alkaline and acidic pretreatments on ZM surface and compares the depth profile measurements of said methods between each other. The study reveals the next effects of pretreatments. Mild alkaline treatment leads to an Mg/Al-hydroxide/oxide structure with slight Zn-hydroxide inclusion. Strong alkaline treatment leads to an enrichment of Zn—and Mg-hydroxides in the upper layer. In the acidic medium Zn-hydroxide quickly becomes the dominant oxidation product, with a highly concentrated Al-oxyhydroxide forming, while Mg-oxyhydroxides dissolve completely after extended exposure.

Chapter 4 ”Alkaline cleaning of Zn–Al–Mg hot-dip galvanized steels: Mechanisms and surface oxide chemistry” focuses on the commercial mild and strong alkaline cleaners, and their influence on the surface oxide chemistry. It was found that mild alkaline cleaning increases significantly the surface concentration of Zn-oxide, while strong alkaline cleaning dissolves the native oxide and generates a transient Zn/Mg-hydroxide on the surface.

Chapter 5 ”Effect of surface pretreatments on the formation of Zr-based con- version layers on Zn-Al-Mg alloy coated steel” investigates the influence of the mild alkaline, strong alkaline and acidic pretreatments on the Zr-conversion coating formation. Strong alkaline pretreatment is found to be an optimal among others, as it leads to double-layered structure, consisting of the ZrO_2-ZrOF-oxidic layer, followed by insoluble interfacial Mg-Al-F structure.

Chapter 6 ”Conclusion and outlook” gives an overview of the most important results of this thesis as well as a brief outlook.

Die approbierte gedruckte Originalversion dieser Dissertation ist an der TU Wien Bibliothek verfügbar.
The approved original version of this doctoral thesis is available in print at TU Wien Bibliothek.

Die approbierte gedruckte Originalversion dieser Dissertation ist an der TU Wien Bibliothek verfügbar.
The approved original version of this doctoral thesis is available in print at TU Wien Bibliothek.

Chapter 2

Methodology

This section provides an overview of the main relevant methods employed in the present study. This overview is focused on the physical principles of these methods. The specific procedures for conducting the measurements can be found in the individual chapters. The methods are grouped according to the primary interactions, used in the analysis - photon emission or absorption for ICP-OES and IRRAS, electron emission for AES and XPS, emission or scattering of ions for SIMS and LEIS. FT-IRRAS spectroscopy was applied to evaluate the cleanliness of the sample surface after mild and strong alkaline cleaning, and ICP-OES was used to determine coating element concentrations in the spent cleaning solutions (**see Chapter 4**). In the same chapter AES, XPS and LEIS were applied to establish the chemical composition and vertical layering of surface oxides. Similarly together XPS, LEIS and SIMS depth profiles measurements were conducted and compared to study the influence of different preatretments on Zn-Al-Mg oxide chemistry (**see Chapter 3**). Combination of XPS and LEIS for surface oxide composition analysis and AES sepctra were studied to charachterize Zr-conversion layers, formed after different pretreatments (**see Chapter 5**).

2.1 Optical spectrosopy

2.1.1 IRRAS

The color of materials corresponds to the absorption of visible light in the range of wavelengths from 380 to 740 nm, from blue to red. Infrared radiation has even longer wavelengths than visible red light, in the range from 740 nm to 2 mm, invisible to the human eye, see **Figure 2.1**. Similarly to a visible absorption spectrum, an infrared spectrum quantitatively represents the absorption of infrared radiation over specific wavelength regions [33].

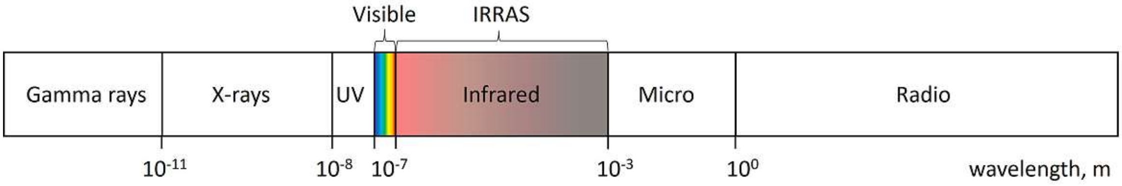

Figure 2.1. Electromagnetic spectrum.

The infrared radiation causes molecules to vibrate, stretching or bending molecular bonds. **Infrared (IR) spectroscopy** is an analytical technique used to investigate the interaction between infrared light and the vibrational motions of covalent bonds in molecules [34]. The energy involved in this interaction corresponds to infrared light, which ranges wavelengths from approximately 10 to around 14.000 cm^{-1}, and usually separated in three regions: near-infrared (14.000–4.000 cm^{-1}), mid-infrared (4.000–400 cm^{-1}) and far-infrared (400–10 cm^{-1}) [33]. This technique provides qualitative and quantitative information about the nature of chemical bonding and crystal structures by analyzing transmitted, reflected, or scattered infrared radiation.

The measuring principle based on the fact, that the energy absorbed by molecules of the sample is missing from the initial light beam. A detector transmits and collects the remaining light.

The "FT" abbreviation in **FT-IR** stands for Fourier transformation. It is a mathematical process for converting spectral information into frequency and intensity. On the practic the Fourier transformation significantly enhances the resolution and speed of IR measurements [34].

In **Fourier transform infrared (FT-IR) spectroscopy**, the IR radiation is directed through a scanning interferometer. The radiation beam is splitted by a beam splitter and directed to a fixed and a moving mirror. Then, beams return to the beam splitter, where they are recombined, causing interference, and directed to the sample, and then detector. It allows the spectral information of all wavelengths to be received simultaneously. At the end the received signal is light intensity versus mirror position. This signal is then processed with the help of Fourier transformation.

The method of measuring the infrared absorption spectra of thin layers on metal

Die approbierte gedruckte Originalversion dieser Dissertation ist an der TU Wien Bibliothek verfügbar.
The approved original version of this doctoral thesis is available in print at TU Wien Bibliothek.
TU WIEN Bibliothek Your knowledge hub

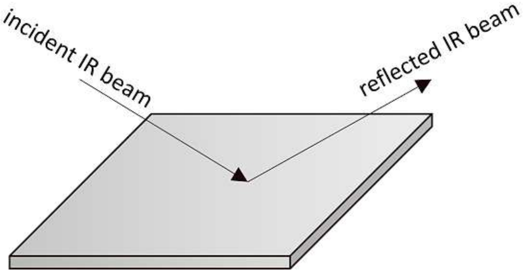

Figure 2.2. IRRAS principle

surfaces, using grazing-angle incidence of the infrared beam, is known as reflection–absorption spectroscopy (RAS), see **Figure 2.2**. This technique is more commonly referred to as **infrared reflection–absorption spectroscopy (IRRAS)**. IRRAS is particularly useful for studying thin films on reflective substrates [33].

In our case, the IRRAS technique is perfect as a fast and simple method of detecting organic matter, specifically organic contaminations on the surface of solvent- and alkaline-cleaned metal surfaces, see Chapter 4.

2.1.2 ICP-OES

Inductively coupled plasma optical emission spectroscopy (ICP-OES), often called ICP-AES or ICP-**atomic emission spectroscopy** operates on the principle that atoms and ions, when excited, emit radiation at characteristic wavelengths as their electrons transition back to lower energy states, see **Figure 2.3**.

The excitation source (transmitting thermal or electrical energy) causes an excited state of an atom, when electrons elevated to higher energy levels. As soon as the excitation source is removed, the atom rapidly returns to its ground state. The energy absorbed during excitation is released as the electrons return to their original energy levels. The resulting emission spectrum, which consists of these quanta of energy, is unique to each atom and provides information about its composition [35].

In the **ICP-OES** process, the sample is introduced into the high-temperature **plasma** - an ionized gas created at extremely high temperatures. The plasma is maintained by the energy from an electromagnetic induction coil. The strong heat inside of the plasma dissociates all chemical bonds, and as a result, analysis is not affected by the sample's chemical composition. When exposed to plasma, atoms and ions are excited and emit electromagnetic radiation. The emitted radiation lies primarily in the approximate 170-800 nm range, what corresponds to ultraviolet and

TU Bibliothek Your knowledge hub WIEN
Die approbierte gedruckte Originalversion dieser Dissertation ist an der TU Wien Bibliothek verfügbar.
The approved original version of this doctoral thesis is available in print at TU Wien Bibliothek.

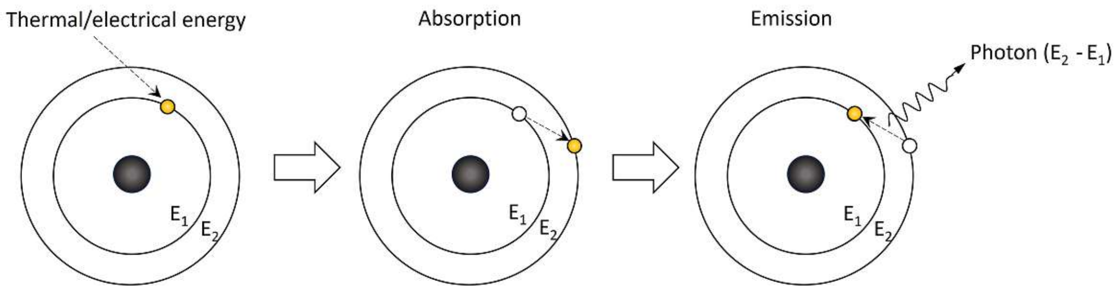

Figure 2.3. Optical emission principle

visible regions of the spectrum.

The measurement result is presented in the form of individual spectral lines, each corresponding to specific wavelengths. The lines are separated by diffraction optics, what enables the detection and quantification of elemental constituents of the sample [36].

In this thesis the ICP-OES techniques will be used to determine concentrations of dissolved Zn-Al-Mg coating elements in used cleaning solutions after mild and strong alkaline cleaners application.

2.2 Electron Spectroscopy

2.2.1 AES

Auger Electron Spectroscopy (AES) is a long-established technique for studying the chemical composition of solid surfaces.

An AES system consists of an **electron beam**, typically operating at energies between 3 and 30 keV, and an **electron energy analyzer**. The sample is bomarded by electrons from the electron beam and the analyzer measures the kinetic energy of emitted from the surface electrons.

These incident electrons from the electron beam penetrate the sample to a depth ranging from 0.1 to 1 micrometer, depending on their energy.

The physics base for AES, the **Auger process**, occurs when an inner-shell electron near the nucleus is ejected by high-energy radiation, creating an excited ion, see **Figure 2.4**. The ion could return to a lower energy state through several possible processes, one of which is the Auger process. It involves the emission of an electron from an atom or ion with a vacancy in an inner shell. This process is called ”radiationless” because no photons are released. The energy of the emitted

Die approbierte gedruckte Originalversion dieser Dissertation ist an der TU Wien Bibliothek verfügbar.
The approved original version of this doctoral thesis is available in print at TU Wien Bibliothek.
TU Bibliothek, WIEN Your knowledge hub

Auger electron is characteristical value for the origin atom and is not dependent on the energy of the incident radiation. This fact distinguishes AES from techniques like XPS, where the kinetic energy of emitted electrons depends on the incoming photon energy. As a result, AES allows for precise identification of the elemental composition by measuring the kinetic energy of the Auger electrons.

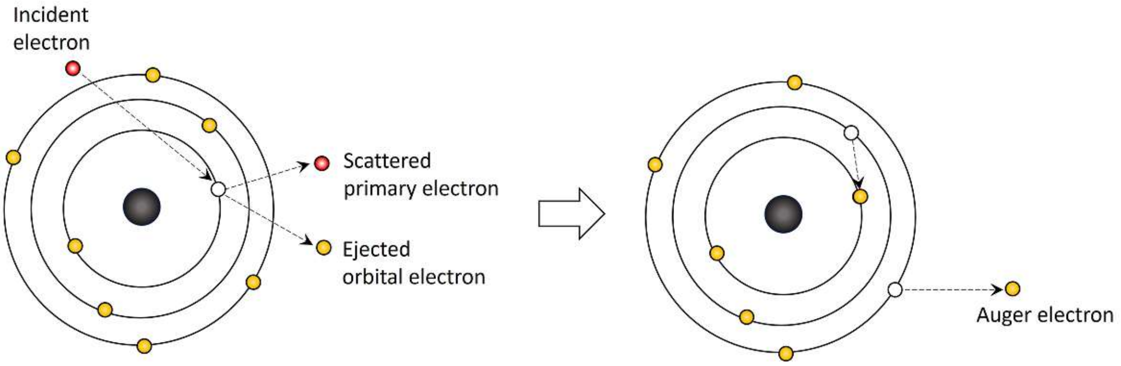

Figure 2.4. Auger effect

As this kinetic energy is characteristic, for accurate detection the emitted electrons must escape the surface without undergoing **inelastic scattering**. The **attenuation length** is the average distance that an electron or photon can travel through a material before losing energy due to inelastic scattering. For AES and XPS, the attenuation length is very short, 1-10 nm on the top of the surface. This short value is a reason for the high surface specificity and limited depth information in both techniques [37].

The electron beam can be focused to analyze nm-sized areas, what offers excellent lateral resolution. Moreover, the AES can be used to create high-resolution elemental maps, similar to ones produced by Scanning electron microscopy, by scanning the beam across the surface.

Though AES primarily uses electron beams, it can also be performed with X-rays or high-energy ions, although these are less common due to their lower lateral resolution. In terms of limitations, AES requires atoms to have at least three electrons, therefore, making hydrogen and helium impossible to analyze [38].

In this thesis, the AES elemental mapping will be used in Chapter 4 to evaluate the surface elemental composition after alkaline cleaning and the AES spectra of Zr-based coating on top of Zn-Al-Mg coated steel in Chapter 5 to evaluate .

Die approbierte gedruckte Originalversion dieser Dissertation ist an der TU Wien Bibliothek verfügbar.
The approved original version of this doctoral thesis is available in print at TU Wien Bibliothek.

2.2.2 XPS

X-ray photoelectron spectroscopy is based on photoelectron production.

It occurs through a single-step process, where a photon causes the ejection of an electron bound to an atom or ion. Photons, having no mass and no charge, are entirely absorbed during this interaction, transferring their energy to the electron. If this energy is sufficient, the electron is released from both the atom or ion and the material itself. The **kinetic energy (K.E.)** of the emitted electron is then measured, which is particularly useful as it has a distinct value determined by the electron's **binding energy (B.E.)**, which varies depending on the element and its surrounding environment [39], see **Figure 2.5**.

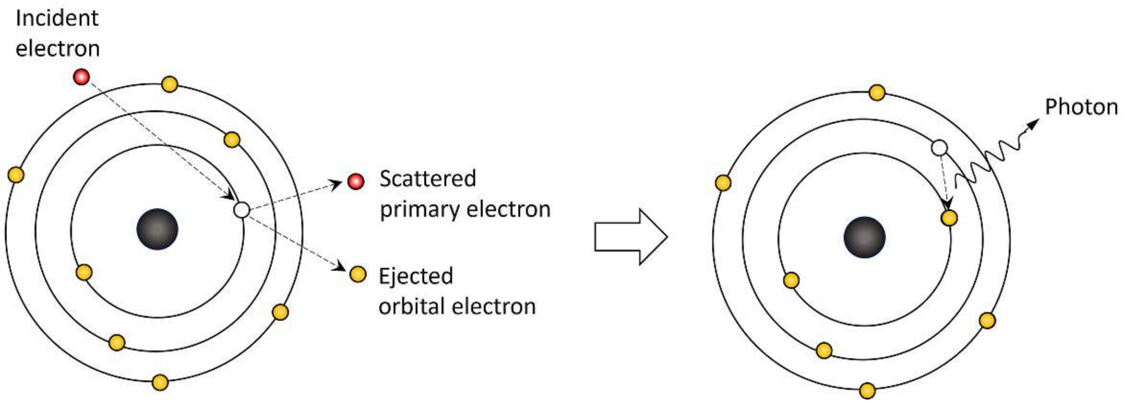

Figure 2.5. Photon emission

The relationship between kinetic energy and binding energy is inverse, meaning that lower kinetic energy corresponds to higher binding energy. Typically, kinetic energy is plotted on the x-axis, increasing from left to right, so binding energy increases from right to left. The inelastic mean free path of photoelectrons is influenced by the likelihood of energy loss, while the attenuation length, accounting for both inelastic and elastic scattering, reflects the probability that an electron will be detected by the energy analyzer. Both kinetic energy and the matrix material set limits on the depth of information, typically within the nanometer scale. Similar to AES, this makes XPS highly surface-sensitive [37].

The unique electron level structure of each element allows for its identification. The composition of a sample's surface can be determined by analyzing the intensity, or area, of the photoemission peaks. The chemical states of examined elements could be determined thanks to shifts in electron energy levels due to chemical bonds with

Die approbierte gedruckte Originalversion dieser Dissertation ist an der TU Wien Bibliothek verfügbar.
The approved original version of this doctoral thesis is available in print at TU Wien Bibliothek.

heteroatoms [40].

In this thesis the XPS technique used in Chapter 4 and 5 for a chemical analysis of species on the modified surfaces, and AR-depth profile is measured in Chapter 3.

2.3 Ion Analysis Techniques

2.3.1 SIMS

Secondary Ion Mass Spectrometry (SIMS) determines the composition of a surface by analyzing ions, ejected from the surface, as a result of ion bombardment.

Specifically, a focused beam of energetic ions, known as **primary ions**, directed towards the sample surface, causes the ejection of atoms and molecules, with a small fraction of these being ionized, see **Figure 2.6**. The resulting ionized particles, called **secondary ions**, are subsequently collected and analyzed using a mass spectrometer.

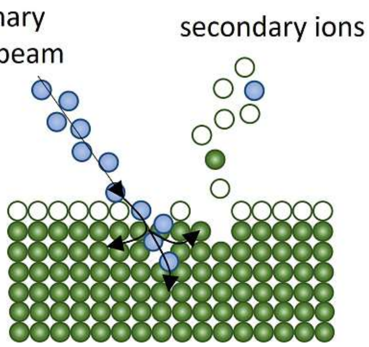

Figure 2.6. SIMS principle

The ejection of atomes and molecules from the target area is also called **sputtering**. The small percentage of the sputtered population existing in an ionized state is at first collected and focused, and then passed through a mass spectrometer.

The identification of isotopes, elements, or molecules is based on analyzing the mass to charge ratio (m/z) of the emitted secondary ions. As the mass remains constant, SIMS is defined as a spectrometry as opposed to a spectroscopy [41]. Modern mass analyzers are based on electromagnetism so ions are required to undergo separation. The analyzer will then separate ions coming from the source according to their m/z. A **time-of-flight (TOF) mass analyzer** separates ions based on the time-of-flight of an ion from the sample surface to the detector [42].

Die approbierte gedruckte Originalversion dieser Dissertation ist an der TU Wien Bibliothek verfügbar.
The approved original version of this doctoral thesis is available in print at TU Wien Bibliothek.
TU Bibliothek WIEN Your knowledge hub

Is it noteworthy that SIMS is able to detect all of the elements of the periodic table as well as their combinations. In many cases, this information can be collected almost simultaneously from the same surface.

The known SIMS disadvantage is difficulty of quantification of recorded signal. This is due to the fact that the intensity of the recorded signal often varies unpredictably depending on the type of substrate and analysis conditions. As an outcome, quantification requires the analysis of reference materials with matching matrix in conjunction with the sample of interest.

SIMS analysis can be performed in two modes, such as Static SIMS and Dynamic SIMS. Static Static SIMS illustrates the elemental or molecular distributions from the outer monolayer, whereas Dynamic SIMS provides the elemental or molecular distributions in depth [41].

SIMS depth profile technique and SIMS total intensity count measurement are applied in the Chapter 3 for alkaline and acidicly pretreated surface evaluation.

2.3.2 LEIS

Low-energy ion scattering (LEIS) is the sensitive technique that provides the quantitative elemental composition of the outermost surface layer. When combined with sputtering, LEIS can also reveal elemental composition as a function of depth within the surface region [43].

An incident beam of noble gas ions, such as He^+ or Ne^+, with energies in the range of 0.1–10.0 keV, is directed at the surface and arrives at an angle α ($\prec 60^\circ$) to the surface normal, causing the scattering of ions, see **Figure 2.7**. The energy of the scattered ions is then measured at a specific emission angle (θ) [43, 44].

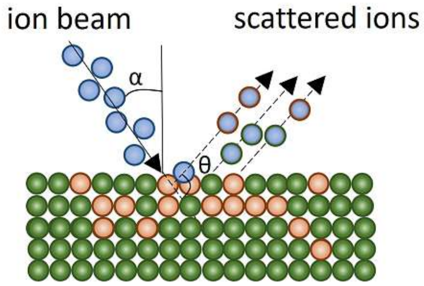

Figure 2.7. LEIS principle

Scattering occurs primarily from **binary collisions**, when the total momentum of the ion and the surface atom is conserved.

Die approbierte gedruckte Originalversion dieser Dissertation ist an der TU Wien Bibliothek verfügbar.
The approved original version of this doctoral thesis is available in print at TU Wien Bibliothek.
TU WIEN Bibliothek Your knowledge hub

The recoil of a stationary surface atom causes energy loss. The magnitute of the energy loss depends on the relative masses of the incident ion and the surface atom, resulting in a backscattered ion having a certain energy. These masses and scattering angle define the kinematics of the binary collision. According to the classical mechanics principles, each element at the solid surface produces a unique scattered peak at a kinetic energy related to the momentum transfer between these elements. This allows LEIS to determine the masses of surface elements by measuring the **kinetic energy** of the scattered ions, making it one of the most surface-sensitive characterization techniques [43].

The neutralization of the incident ions in the solid - is one of the reasons of LEIS high sensitivity in outer layer measurements. For example, 1 keV He ions have a 99% probability of neutralization after passing through a single atomic layer. Thus, most ions detected are those that scattered from the outermost layer or were reionized upon exiting the solid. The detection of these low-energy particles requires an electrostatic analyzer, meaning only ions are detected [45].

The LEIS depth technique is used in Chapters 3, 4, and 5 for an analysis of the Zn-Al-Mg surface after alkaline and acidic pretreatment, alkaline cleaning, and application of Zr-based conversion coating.

TU WIEN Bibliothek Your knowledge hub
Die approbierte gedruckte Originalversion dieser Dissertation ist an der TU Wien Bibliothek verfügbar.
The approved original version of this doctoral thesis is available in print at TU Wien Bibliothek.

Die approbierte gedruckte Originalversion dieser Dissertation ist an der TU Wien Bibliothek verfügbar.
The approved original version of this doctoral thesis is available in print at TU Wien Bibliothek.

Part II

Results and Discussion

Die approbierte gedruckte Originalversion dieser Dissertation ist an der TU Wien Bibliothek verfügbar.
The approved original version of this doctoral thesis is available in print at TU Wien Bibliothek.

TU Bibliothek WIEN Your knowledge hub

Die approbierte gedruckte Originalversion dieser Dissertation ist an der TU Wien Bibliothek verfügbar.
The approved original version of this doctoral thesis is available in print at TU Wien Bibliothek.

Die approbierte gedruckte Originalversion dieser Dissertation ist an der TU Wien Bibliothek verfügbar.
The approved original version of this doctoral thesis is available in print at TU Wien Bibliothek.
TU WIEN Bibliothek Your knowledge hub

Chapter 3

Comparison of LEIS, SIMS and AR-XPS as methods for surface characterization of passivated Zn-Al-Mg steel

The following chapter is based on the article accepted under the same title in Materials and Corrosion [46] and reproduced under the corresponding copyright agreement.

This study was performed to evaluate the ability of the mentioned above methods in depth profile mode, to characterize the industrially produced surface of Zn-Al-Mg coating after alkaline and acidic pretreatments.

The experiments were performed by a group of researchers, including Jiri Duchoslav, who performed XPS measurements, Matthias Kogler, who performed LEIS depth measurements, and Florian Fahrnberger, who performed SIMS measurements. The author herself prepared the samples for the surface analyses, evaluated and described results.

The combination of different surface-sensitive techniques is frequently employed in material sciences to analyze complex systems. How these methods compare in terms of quantitative, and qualitative information is often unclear. In this study, we directly compare angle-resolved X-ray photoelectron spectroscopy (AR-XPS), Low-energy ion scattering spectroscopy (LEIS), and Secondary ion mass spectrometry (SIMS) depth profiling analyses. Therefore, we use Zn-Al-

Mg model coatings after alkaline and acidic treatments in model solutions.

The combined use of AR-XPS and LEIS depth profiling proved effective in studying compositional and elemental changes in the surface oxides of Zn-Al-Mg coatings after alkaline and acidic treatments. Additionally, by combining these methods, SIMS depth profiling can be effectively calibrated for matrix effects. Here, we find that e.g. Mg is considerably more sensitive to SIMS detection, based on effective secondary ionisation. Such effects must be considered for data interpretation.

3.1 Introduction

Based on different physical principles, such as photoemission, ion scattering, and sputtering of secondary ions, X-ray Photoelectron Spectroscopy (XPS), Low-Energy Ion Scattering spectroscopy (LEIS), and Time-of-Flight-Secondary Ion Mass Spectrometry (ToF-SIMS) are often compared [47–49] and applied together for analysis. However, how they compare quantitatively and qualitatively is often not considered.

Both XPS and LEIS are quantitative, with the advantage of chemical information in XPS. In contrast LEIS offers only elemental sensitivity, yet it is sensitive to the very top atomic layer of a surface. Hence, XPS is commonly used to determine chemical structure [50–54] and depth profiling [55–57], while LEIS is frequently applied to catalysts, semiconductors and solid oxide fuel cells [58] where the atomic composition of the outer surface is essential for function [59–61]. ToF-SIMS is ordinarily implemented for mapping [62–64], structural analysis by fragment ions detection [65], and depth profiling [66], as well as biologic sample analysis [67]. Here, quantification is complex and often requires careful selection of reference materials due to strong matrix effects on secondary ion yield, but mass fragmentation makes it very interesting also for soft matter and coated samples [68].

For the last few years, different groups of authors used these techniques while analyzing various coatings and steels - stainless, advanced high strength or hot-dip galvanized [69–76]. There ToF-SIMS depth profiles showed the influence of the oxidizing atmosphere on the formed oxide layer, while XPS defined its chemical composition on stainless steel after cesium iodide deposition and thermal treatment [77]. Another group of authors employed ToF-SIMS to investigate liquid metal embrittlement susceptibility. Three-dimensional reconstruction of ion distribution indicated more pronounced Si enrichment of dual-phase “high ductility” steel compared to a

Die approbierte gedruckte Originalversion dieser Dissertation ist an der TU Wien Bibliothek verfügbar.
The approved original version of this doctoral thesis is available in print at TU Wien Bibliothek.

conventional dual-phase steel after thermal cycling at 700° C [78].

In a study on a 304L stainless steel surface oxide chemistry after exposure to air and steam at different temperatures, XPS and LEIS spectra provided qualitative information of surface oxides, while the SIMS depth profile denoted oxides thickness growth along the profile [79]. In surface science, combined SIMS depth profiling, LEIS and XPS methods are frequently used. For instance, Sutara et al. [80] used XPS to probe suboxidial changes for Zr3d, V2p3, O1s and C1s after thermal activation and then Ar^+ sputtering. At the same time, LEIS characterized the dynamic of Zr, V, and O peaks after treatments, deducting the location of the residual oxide and activated surface zirconium enrichment. Tof-SIMS contributed to the time evolution of ion intensity ratios by dynamic depth profiling.

The more common combination of XPS and SIMS for analyzing Zn-Al-Mg alloy coatings has been applied in the following cases. E.g., plasma induced surface effects on Zn-Al-Mg alloy were studied by SIMS depth profiling of Zn, Al and Mg ions and XPS for chemical characterization - removal of surface carbon, conversion from carboxylates to carbonates and the oxidation and hydroxylation of Al after plasma treatment [81]. Cetinskaya et al. implemented XPS and ToF-SIMS together with Glow-discharge optical emission spectroscopy (GD-OES) to study the impact of alkaline and acidic solutions on Zn-Al-Mg coated surface chemistry. In this case SIMS provided information about changing element concentrations based on the total count ratio of signals in the first nanometer [22]. The authors concluded that acidic solutions are more consistent than alkaline for Zn activation, although highly concentrated alkaline solutions are also effective. Another approach of ToF-SIMS for Zn-Al-Mg coating analysis was carried out for high-temperature phase evolution investigation. The positive ion analysis of Zn^+, Al^+, Mg^+, and Fe^+ showed a three-dimensional distribution of elements throughout the coating before and after a high-temperature tensile test at 700, 800, and 900° C [82].

Saarimaa et al. presented an interesting inquiry into cleaning and titanium hexafluoride pretreatment on the hot-dip galvanized steel (HDG) surface. XPS sputtering provided information about element depth profiles and aluminium removal in two differently concentrated cleaning solutions. In addition, ToF-SIMS element maps showed deformation twinning for the HDG sample cleaned with a 4g/L concentrated solution [83].

In our previous work, we studied the modifications of the surface oxides chemistry on Zn-Al-Mg coatings after treating them with mild and strong alkaline industrial

Die approbierte gedruckte Originalversion dieser Dissertation ist an der TU Wien Bibliothek verfügbar.
The approved original version of this doctoral thesis is available in print at TU Wien Bibliothek.
TU WIEN Bibliothek Your knowledge hub

cleaners using Inductively Coupled Plasma Optical Emission Spectroscopy (ICP-OES), Auger Electron Spectroscopy (AES), XPS, and depth LEIS measurements [84]. We found that mild alkaline cleaning leads to Mg and Zn dissolution, with Zn oxyhydroxides forming on the surface while the Al-oxide layer is stable. Strong alkaline cleaning leads to the formation of an Mg/Zn mixed oxyhydroxide upper layer on the surface.

In this investigation, we focus on comparing methods for surface analysis, namely AR-XPS, LEIS, and SIMS methods. We show how results compare quantitatively and qualitatively, providing a basis for analysis of complex thin films.

3.2 Methods and materials

3.2.1 Chemicals and Materials

Non-skin-passed Zn–Al–Mg coatings (96 wt% Zn, 2.5 wt% Al and 1.5 wt% Mg) were produced by hot-dip galvanizing on a large-scale plant of voestalpine Stahl GmbH in Linz, Austria. The average coating weight per side was about 60 g m $^{-2}$, corresponding to a thickness of 8 µm. The substrate was a DX56 low carbon steel.

The following chemicals were used to create model solutions with different pH for the treatment process simulation: sodium tetraborate decahydrate for a solution with a pH of 9.1-9.2, sodium dihydrogen phosphate for a solution with a pH of 9.1-9.2, sodium hydroxide for a solution with a pH of 12.7, and concentrated sulphuric acid for a model acidic treatment solution with a pH of 2.

3.2.2 Surface preparations

Samples were at first immersed for 1 or 10 minutes in the treatment solutions, described above, and preheated to 55°C. Then, the samples were rinsed in distilled water, at the room temperature, and dried with a stream of air. Then they were packaged in aluminium foil individually to prevent further carbon contamination.

3.2.3 LEIS

LEIS measurements were performed using a high sensitivity spectrometer ION-TOF Qtac^{100} (IONTOF, Germany) with a primary beam of He^{+} 3 keV at 1.8-1.9 nA, at an incident angle of 0° and scattering angle of 145° . The measurement area was 2 ×

Die approbierte gedruckte Originalversion dieser Dissertation ist an der TU Wien Bibliothek verfügbar.
The approved original version of this doctoral thesis is available in print at TU Wien Bibliothek.
TU Bibliothek Your knowledge hub WIEN

$2\ \text{mm}^2$. The sputter beam consisted of 500 eV Ar^+ ions at a current of 95 nA and an incident angle of 59° with a sputter area of $2.5 \times 2.5\ \text{mm}^2$. ION-TOF Surface Lab 7 was used to process the data. To quantify the measured data, reference spectra of pure Zn, Al, and Mg were measured and equated to 100% concentration. Using the measured reference spectra, the atomic fractions of Zn, Al, and Mg in the coating samples were then calculated with respect to the densities in the metallic state.

3.2.4 SIMS

Elemental depth distributions were studied using Time-of-flight secondary ion mass spectrometry (ToF-SIMS) with a ToF-SIMS 5 instrument (IONTOF GmbH, Münster, Germany). A focused 25 keV Bi^+ beam in high current bunched (HCBU) mode was employed as the primary ion source to generate secondary ions within an analysis area of $100\times100\ \mu\text{m}^2$, providing high mass resolution. Depth profiling was performed in positive ion mode using a 500 eV $O2^+$ ion beam (≈100 nA) over a sputter area of $300\times300\ \mu\text{m}^2$. Data processing and calibration were carried out using SurfaceLab 7 (version 7.1.130060), the ToF-SIMS instrument software from IONTOF. Since Mg^+ and Al^+ were outside the linear range of the detector during depth profiling, the magnesium isotope $25Mg^+$ and the ion species $Al_2{}^+$ were analyzed instead. Further, the samples have a certain degree of surface roughness (measured with a DekTakXT® profilometer (Bruker); see **Table 3.1**), making it challenging to assign a depth scale to the profiles. To enable more quantitative differentiation of the surface treatments, the surfaces (sampling depth ≈ 1-2 nm [85, 86]) were also analyzed over a larger analysis area of $300\times300\ \mu\text{m}^2$ without sputtering. For evaluation, at least eight positions per sample surface were measured, with 250 scans taken at each position.

Table 3.1. Arithmetical mean height roughness Ra, measured by a profilometer.

	Ra, μm	
sample	1 min	10 min
A	0.93	1.04
B	1.23	1.09
C	1.11	1.02
D	1.08	1

Die approbierte gedruckte Originalversion dieser Dissertation ist an der TU Wien Bibliothek verfügbar.
The approved original version of this doctoral thesis is available in print at TU Wien Bibliothek.
TU WIEN Bibliothek Your knowledge hub

Die approbierte gedruckte Originalversion dieser Dissertation ist an der TU Wien Bibliothek verfügbar.
The approved original version of this doctoral thesis is available in print at TU Wien Bibliothek.
TU WIEN Bibliothek Your knowledge hub

3.2.5 XPS

The angle-resolved measurements (AR-XPS) were performed with a Thetaprobe XPS system (Thermo Scientific, UK), using a monochromated Al Kα X-ray source and equipped with a 2-D detector, which allowed the AR-spectra to be recorded parallel without tilting the sample. The wide acceptance angle of the analyzed being 20 - 80° was split into 8 ranges (each being 7.5° broad). The AR spectra were acquired with a pass energy of 50 eV and an energy step of 0.05 eV. The virtual depth profiles were calculated using the Avantage software package (Thermo Scientific, UK). The fit model contained oxides, hydroxides and metallic forms of the detected elements. An advanced linear combination fitting method using the full-shaped spectra of reference materials was used to confirm the evaluation results obtained from AR-XPS data [87, 88].

3.3 Results and discussion

We examined the effect of mild alkaline borate and phosphate based, (samples A and B), strong alkaline (samples C), as well as strong acid treatments (samples D), on the surface chemistry of the Zn-Al-Mg alloy coating after 1 and 10 minutes. The main aim is to understand how depth profiling using LEIS, SIMS and AR-XPS, which complement each other, provides qualitative and quantitative insight into the surface chemistry.

3.3.1 LEIS

LEIS spectra are often used for quantitative surface analysis of the top layer of a surface. Furthermore, LEIS depth profiling offers elemental quantification, which is very useful for complex elemental mixtures such as high entropy materials [89].

Figure 3.1 shows LEIS sputter depth profiles for all four surface treatments. The results are quantified with elemental reference materials and presented in atomic fractions. The oxygen signal can not be directly quantified and is presented as a qualitative profile. First of all, for sample A data indicates a predominance of a Mg/Al mixture on the surface, with a small Zn inclusion. In the first 2 nm Mg:Al ratio is 2:1, then the Mg atomic fraction decreases followed by 1:1 ratio of these elements.

After 10 minutes there is a small increase in the Zn peak at the very surface. In

Die approbierte gedruckte Originalversion dieser Dissertation ist an der TU Wien Bibliothek verfügbar.
The approved original version of this doctoral thesis is available in print at TU Wien Bibliothek.
TU WIEN Bibliothek Your knowledge hub

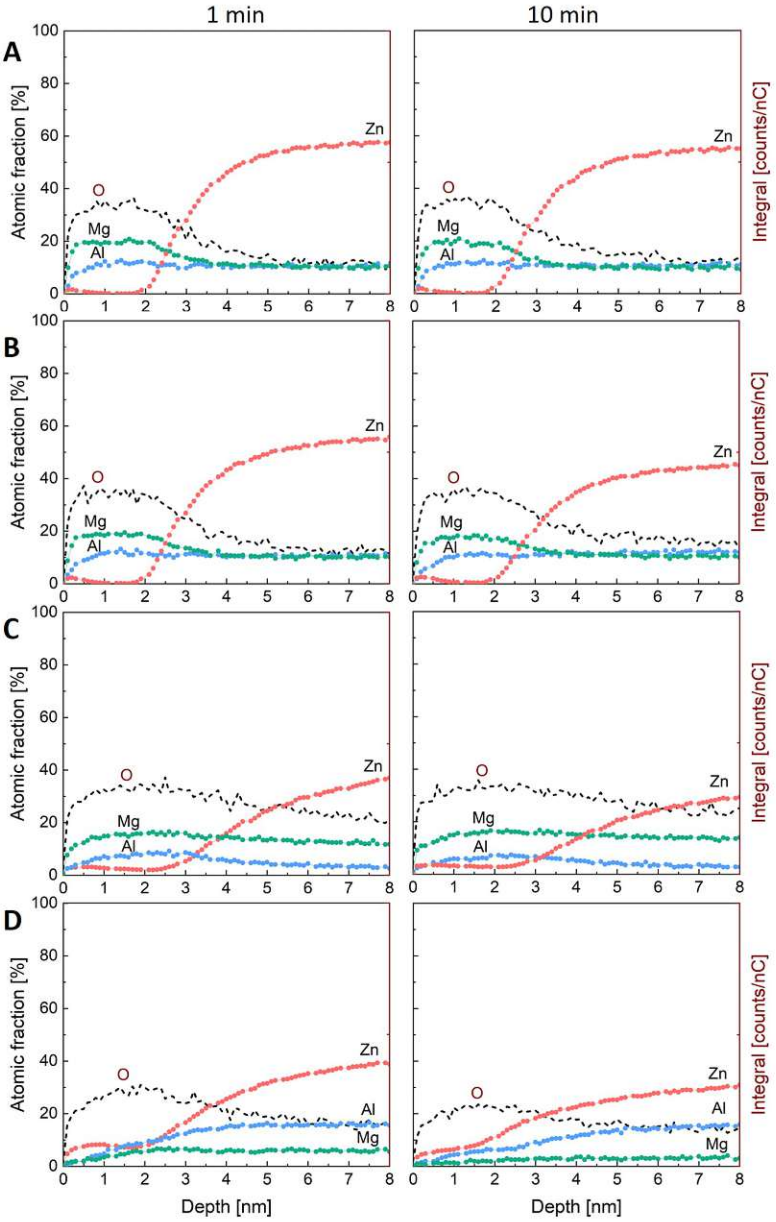

Figure 3.1. Depth profiles of alkaline and acidic treated samples by LEIS after 1- and 10-minutes treatment. A and B - pH 9.1- 9.2 by $Na_2B_4O_7$ and NaH_2PO_4 respectively; C - pH 12.7 by NaOH; D - pH 2.1 by H_2SO_4. O signal is not quantifiable and is presented as integral signal. The depth scale was established with the assistance of the IONTOF Surface Lab 7 software tool, which estimated the value of one sputter step to be between 0.1 and 0.2 nm.

one or another form Al and Mg exist in the even ratio after approximated by 4 nm in the depth. A slight increase in the oxygen depth profile intensities hints at an enrichment of oxidic species.

A similar behaviour is observed for samples B. The Zn peak on the outer surface layer is more prominent compared to A, especially after prolonged treatment times. More notable is also a decrease in the Zn percentage in approximately 3-8 nm depth after 10 minutes.

For sample C a separation of Mg from the Al profile is observed. According to Pourbaix diagrams, Al is dissolved actively in strong alkaline solutions, even more after 10 minutes. It looks like the surface is covered with Mg-oxihydroxides, as Mg and O profiles acquire similar shape. Zn is also being dissolved along the depth. Zn on the surface is thicker and higher concentrated than for A and B. Still Mg and Al are dominating elements in the first 4 nm, while Zn, dominant after that point, is being dissolved along the profile with time.

Acidicly treated sample D displays Zn enrichment on the outermost surface in the 0-2 nm range. Almost in the whole range Zn is the dominant element already after 1 minute of etching. After 10 minutes there is Zn and Mg dissolution. As a results Mg is almost removed completely, and Zn is still dominant.

The LEIS results demonstrate that for all samples Zn is the dominating element starting from 3-4 nm depth. In the upper layers Mg and Al are dominant in the alkaline treated samples A, B and C. In mild alkaline media A and B the behaviour of the elements is similar. In the strong alkaline medium C there is a faster Al and Zn dissolution and oxidation in the depth. Compared to the sample treated with A and B, Zn treated with C is already more activated on the surface after one minute and is partially dissolved in depth. In the acidic medium D Zn dominates over all depth, and on the surface in both cases. It appears that prolonged treatments only dissolve already activated Zn and Mg.

3.3.2 SIMS

Although SIMS depth profiles do not provide precise quantitative information due to the typically strong matrix effects, surface roughness and SIMS lateral resolution, provide complementary insight into surface chemistries.

Figure 3.2 presents the ToF-SIMS depth profiles for various treatment solutions and durations. It is immediately visible that Mg is measured with considerably higher intensity in SIMS. When comparing the ratios of LEIS and SIMS data (shown in **Figure A.1**) Mg is about 10 times as sensitive compared to Al and Zn.

Further, the depth profiles of samples A and B appear similar, despite differences

TU Bibliothek Die approbierte gedruckte Originalversion dieser Dissertation ist an der TU Wien Bibliothek verfügbar. The approved original version of this doctoral thesis is available in print at TU Wien Bibliothek.

Die approbierte gedruckte Originalversion dieser Dissertation ist an der TU Wien Bibliothek verfügbar.
The approved original version of this doctoral thesis is available in print at TU Wien Bibliothek.

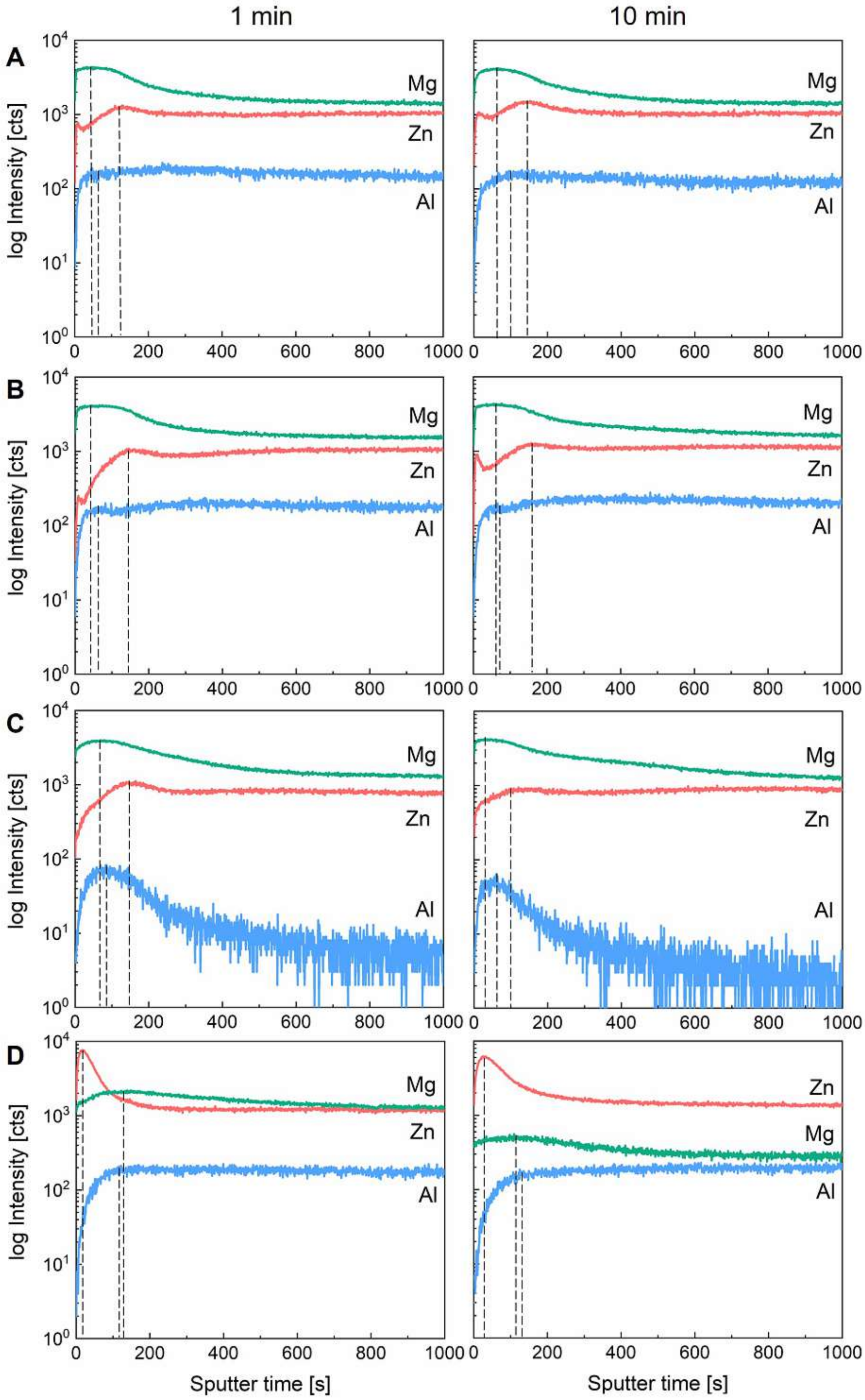

Figure 3.2. Not quantified depth profiles of alkaline and acidic treated samples after 1- and 10- minutes treatment by SIMS of the surfaces in an area of 100×100 µm^2 . The estimated sputter rate is ≈ 0.3 nm/s. A and B - pH 9.1- 9.2 by $Na_2B_4O_7$ and NaH_2PO_4 respectively; C - pH 12.7 by NaOH; D - pH 2.1 by H_2SO_4.

TU WIEN Bibliothek Your knowledge hub

in their treatment times and when compared to each other, with only slight shifts in the signal maxima. Both samples A and B exhibit an increase in the signal maxima of Zn, Mg, and Al as treatment time increases. This suggests that the treatment influences the coating composition beyond the surface layers. The observed shift of all profile maxima toward longer sputtering times may indicate the formation of a deeper oxide layer. As this oxide layer develops, the oxidized material may extend deeper into the sample. The maxima of oxidic AlO^-, MgO^-, and ZnO^- also shift slightly to the longer sputter times, see **Figure A.2**.

In sample C, treated for 1 and 10 minutes, the elements Mg and Zn exhibit signal propagation similar to that observed in samples A and B, see **Figure 3.2**. However, Al shows a markedly different profile when treated with a more basic solution, such as NaOH. While the secondary ion signal of Al increases from the surface and remains constant in the bulk for the other two treatments, in this case, we observe a further, progressive decrease in the bulk following a clear signal maximum. Additionally, by tracking the shifts in signal maxima between 1 and 10 minutes of treatment, the data suggests that this is may be due to contamination or the removal of the initial oxide layer. The oxidic signals, shown in **Figure A.2**, also demonstrate a slight shift to the left. AR-XPS data indicate that this is more likely to be the latter, namely the removal of Al-hydroxide.

For sample D, we observe different signal propagation in depth compared to the samples treated with basic solutions, see **Figure 3.2**. The signal maximum of the Zn profile occurs earlier than the maxima for Mg and Al. While the Al signal intensity remains steady, the SIMS depth profile for sample D indicates a decline in Mg intensity. This is evident both when comparing with samples A, B, and C, and across varying treatment times with H_2SO_4 for sample D. This behavior is consistent with the rapid dissolution of Mg in sulfuric acid, as observed in XPS and LEIS analyses. The slight shift in the Zn maximum toward longer sputtering times may suggest an increase in oxide layer thickness. AlO^- and ZnO^- signals also shift to the longer sputter times, while MgO^- demonstrates depletion, see **Figure A.2**.

While SIMS depth profiling is not quantified, it can be employed as a supplementary analysis for LEIS depth profile. SIMS observes the growth of oxides following an extended treatment period for samples A and B, the initial removal of oxides for C, the dissolution of Mg, and the significant activation of Zn by an acidic solution for sample D.

In examining the application of SIMS depth measurements to the industrially

Die approbierte gedruckte Originalversion dieser Dissertation ist an der TU Wien Bibliothek verfügbar.
The approved original version of this doctoral thesis is available in print at TU Wien Bibliothek.
TU Bibliothek, WIEN Your knowledge hub

produced rough surface, it was interesting to consider signals on a typical estimated sampling depth, approximately 1-2 nm of the surface, using the total signal intensities of the elements.

As illustrated in **Figure 3.3**, the trends extracted from the total count ratios are consistent across all alkaline cleaned samples with an increase in the Zn signal compared to relatively equal Mg and Al ratios after a longer treatment time. On average, all three elements decrease in secondary ion signal on the surface due to the longer treatment. For the acidicly treated sample D, on the other hand, an increase in Zn and Al and a decrease in the Mg signal are observed. The stated trends of elemental behavior in the first nanometer align with the LEIS results, discussed above.

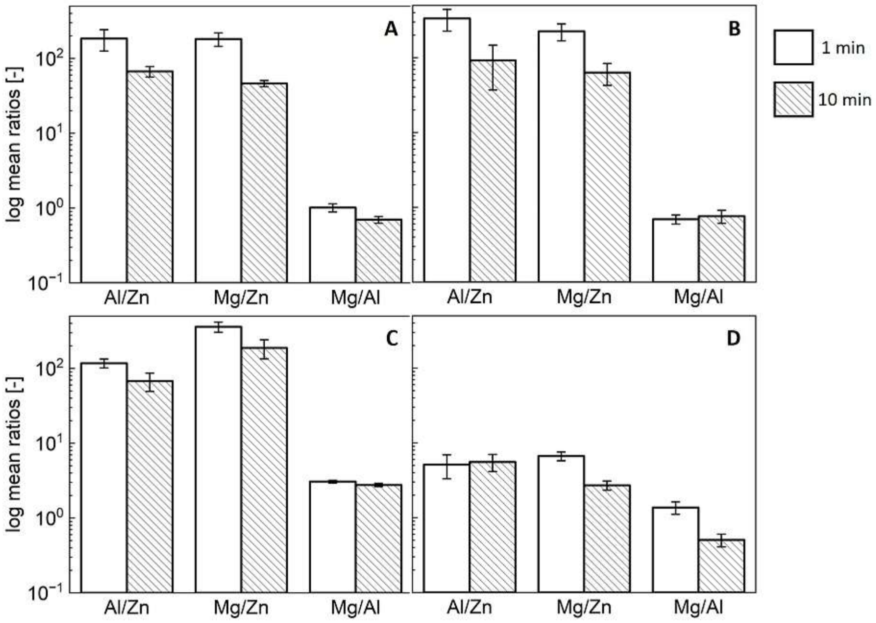

Figure 3.3. Relative ratios of Al to Zn, Mg to Zn and Al to Mg in the 1st 1-2 nm of the surface after 1 and 10 minutes, calculated based on measured total counts by SIMS in an area of 300×300 µm^2. Eight positions per sample surface were measured. A and B - pH 9.1- 9.2 by $Na_2B_4O_7$ and NaH_2PO_4 respectively; C - pH 12.7 by NaOH; D - pH 2.1 by H_2SO_4.

Die approbierte gedruckte Originalversion dieser Dissertation ist an der TU Wien Bibliothek verfügbar.
The approved original version of this doctoral thesis is available in print at TU Wien Bibliothek.

Die approbierte gedruckte Originalversion dieser Dissertation ist an der TU Wien Bibliothek verfügbar.
The approved original version of this doctoral thesis is available in print at TU Wien Bibliothek.

3.3.3 AR-XPS

Given our existing knowledge of elemental depth profiles, which has been gained with the help of LEIS and SIMS techniques, we have found the AR-XPS to be an effective tool. The principal advantage of XPS is its capacity to distinguish between the diverse species of a chemical element. This approach, in particular, allows for the separation of an initial Al/Mg-oxide from its hydroxide in the top layer. As shown in **Figure 3.4** the principal constituents in the AR-XPS depth profiles are organic contaminations, a layer, combining hydroxides, oxides and substrate. In addition, the AR-XPS depth measurements are expected to yield highly quantitative results with excellent depth resolution [90].

Figure 3.4 demonstrates that the treatment with the mild alkaline $Na_2B_4O_7$ solution of sample A results in the formation of an about 2-times thicker oxyhydroxide layer after 10 minutes, including Zn-hydroxide layer, which concentration and thickness increases on the outer surface layer. Further, in comparison to LEIS technique, see **Figure 3.1**, AR-XPS was able to detect carbon contamination here, and in all other samples.

Interestingly, on the surface of sample B, treated in a similar mild alkaline solution, the layer of $Zn(OH)_2$ becomes more prominent and concentrated in the same 2 nm depth after 10 minutes. Additionally, the extended treatment differs in the Al and Mg concentrations, with Al as a prevailing element, probably due to notable Mg dissolution in the mild alkaline solution [84].

Moreover, after one minute of strong alkaline treatment, see sample C in **Figure 3.4**, the peak of $Zn(OH)_2$ on the outer surface layer becomes comparable in concentration to the ones of Mg and Al-hydroxides, staying in 1:1 ratio to each other. Further, the concentration and thickness of $Zn(OH)_2$ and $Mg(OH)_2$ increases evenly, resulting in the formation of a Zn/Mg hydroxide layer, as described for an industrial strong alkaline Cleaner 2 in our first publication [84]. Mg tends to form a mixture with Zn, while Al is found in deeper regions.

The acidic treatment D rapidly activates Zn after just one minute, making Zn the dominant element in the 0-2 nm range. Additionally, Mg-oxyhydroxides fully dissolve and transition to (Mg/Zn)carbonate is observed, while Al-oxides and hydroxides significantly thicken. After 10 minutes, the concentration of the $Zn(OH)_2$ layer is grown to the 2-4 nm range, and there is an overall decrease in Al concentration, with its thickness remaining the same. After acid treatment, the presence of

Die approbierte gedruckte Originalversion dieser Dissertation ist an der TU Wien Bibliothek verfügbar.
The approved original version of this doctoral thesis is available in print at TU Wien Bibliothek.

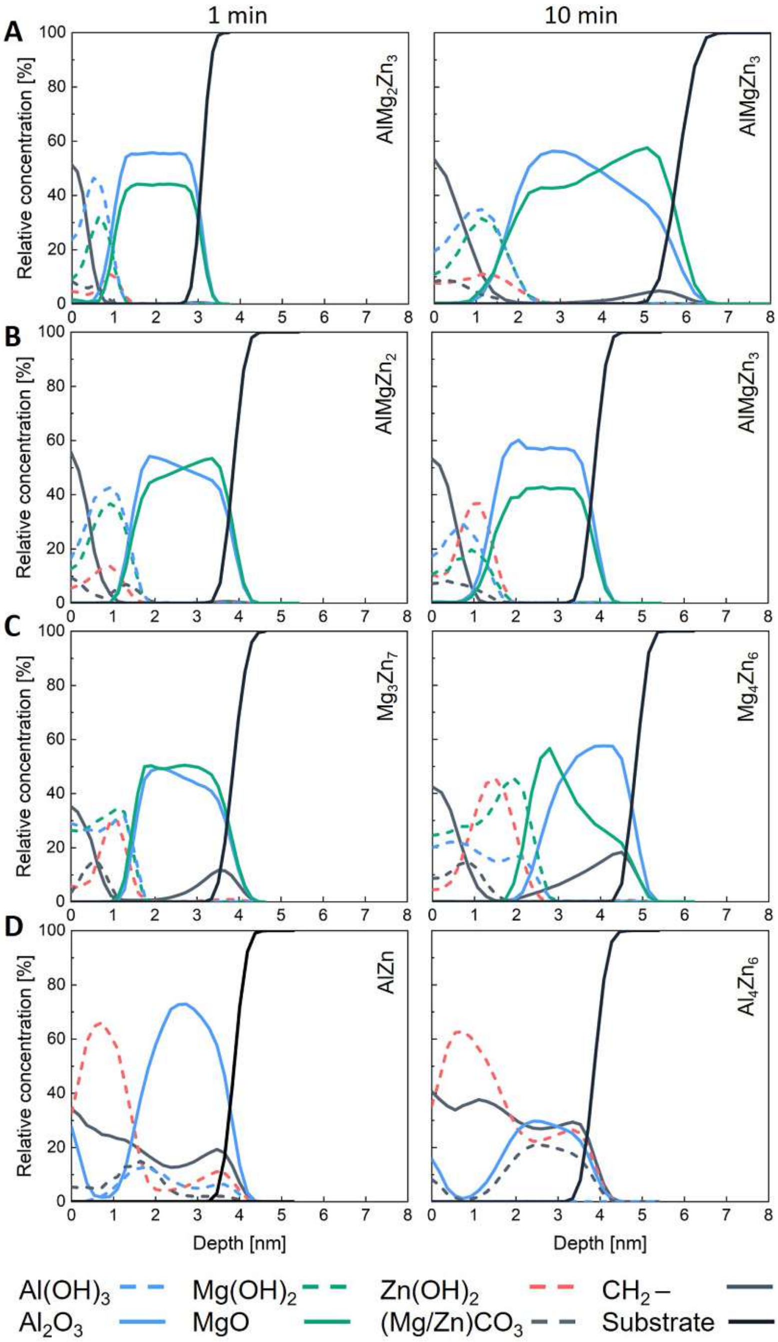

Figure 3.4. Virtual depth profiles of alkaline and acidic treated samples by angle resolved XPS after 1- and 10-minutes treatment. Here A and B - pH 9.1-9.2 by $Na_2B_4O_7$ and NaH_2PO_4 respectively; C - pH 12.7 by NaOH; D - pH 2.1 by H_2SO_4.

CH_2-containing compounds has become more significant. The surface is relatively smooth in comparison to the other samples, see **Table 3.1**.

The chemical composition of the surface without the angle-resolving and depth profiling shows an averaged result over the measured area. High-resolution spectra exhibit hydrozincite $Zn_5(CO_3)_2(OH)_6$ (HZ) on alkaline cleaned samples A,B and C, see **Figure A.3** and **Figure A.4**. In AR-XPS data, shown in **Figure 3.4**, it is reflected as Zn carbonate and Zn hydroxide. The averaging method underlines the shift of the balance from MgO towards $Mg(OH)_2$ in samples B and C as s well as Al hydroxide dehydration to AlOOH in strong acid environment D. This is indicated in the virtual depth profile by a declining and depleted Al hydroxide concentration.

3.3.4 Comparison of the methods

The combination of AR-XPS and LEIS provides a comprehensive understanding of surface modifications resulting from alkaline and acidic treatments.

Following these treatments and subsequent air exposure, $Zn(OH)_2$ forms in the uppermost surface layers. In alkaline media, this $Zn(OH)_2$ shares the outermost layer with Mg- and Al-hydroxides, which remain prevalent even after 10 minutes of treatment. Strong alkaline conditions lead to Al dissolution and the destruction of initial Mg/Al oxides. In the acidic medium, the $Zn(OH)_2$ quickly dominates after the first minute, while Mg dissolves across various depths. Al is resistant to further acidic dissolution, forming oxyhydroxides and later only hydroxide. Acidic treatment, although highly effective in Zn activation, eradicates the initial oxide layer after 1 minute of the treatment. It is unfavorable as this oxide plays an essential role in the corrosion resistance properties of Zn-Al-Mg coating.

While LEIS allows us to determine the distribution of atomic fractions along the estimated depth, XPS offers a comprehensive understanding of chemical species along the virtual depth. It should be noted that LEIS was unable to detect carbon organic matter in this case, which consequently precludes the possibility of registering organic contamination, which could impact the overall composition analysis.

In the case of the reference Zn-Al-Mg sample, which has unchanged surface chemistry, Mg and Al should be in a 1:1 ratio in the oxides area [84]. The different Mg and Al ratios in the case of treated surfaces imply that in addition to the Mg/Al-oxides, $Mg(OH)_2$ and $MgCO_3$ could be present, which is observed by AR-XPS, see **Figure 3.4**.

The next point of consideration, is not supported by LEIS data the decrease in Mg-oxide concentration for sample B after 10 minutes of treatment, found by AR-

Die approbierte gedruckte Originalversion dieser Dissertation ist an der TU Wien Bibliothek verfügbar.
The approved original version of this doctoral thesis is available in print at TU Wien Bibliothek.

XPS. In this case the decrease is logical, as Mg is being dissolved in mild alkaline solutions. Furthermore, AR-XPS findings for samples C are inconclusive regarding active Al dissolution. However, Al dissolution aligns with the LEIS data, see **Figure 3.1**, and is in line with the Pourbaix diagrams and previous studies.

SIMS total count ratios within approximately 1-2 nm, as illustrated in **Figure 3.3**, closely align with AR-XPS and LEIS data, showing increased Zn signals and relatively constant Mg and Al ratios in alkaline treated samples after prolonged treatment. For the acidic sample D, SIMS reveals an increase in Zn and Al signals and a decrease in Mg, with lower signal intensities than alkaline-treated samples. All elements decrease in the signal on average. XPS also observed the increase in the signal intensities of Zn and Al, see **Figure 3.4**.

The SIMS depth profiles in **Figure 3.2** together with negative ions profiles indicate the growth of oxides following an extended treatment period for samples A and B, the removal of initial oxide for C, the dissolution of Mg, and the significant activation of Zn by an acidic solution for sample D. The increase of oxide thickness for samples A and B after prolonged treatment times is particularly observed by AR-XPS as well. The removal of initial oxides in samples C could be supported by decreased Al concentration by LEIS and Mg/Al-separation by AR-XPS. The dissolution of Mg aligns with complete absence of MgO and $Mg(OH)_2$ in depth profiles of samples D by AR-XPS and fast and constant decrease of Mg concentration by LEIS in samples D.

3.4 Conclusions

Alkaline and acidic treatments, followed by exposure to the atmosphere, form Al, Mg, and Zn-hydroxides on top of the initial Mg/Al oxide layer.

Mild alkaline treatment at a pH of around 9, created using sodium tetraborate and sodium dihydrogen phosphate, shows similar trends between the two: Mg/Al-hydroxide and a Mg-carbonate layer with small Zn-hydroxide inclusion, the latter slightly growing after increasing treatment time, followed by thick Mg/Al-oxide layer. Sodium dihydrogen phosphate, however, induces more significant Zn activation after just one minute of treatment.

Strong alkaline treatment forms a thicker and more concentrated mixture of hydroxides within one minute, leading to the dissolution of Al-oxyhydroxides and the enrichment of Zn- and Mg-hydroxides in the upper layer. This process eventually

Die approbierte gedruckte Originalversion dieser Dissertation ist an der TU Wien Bibliothek verfügbar.
The approved original version of this doctoral thesis is available in print at TU Wien Bibliothek.
TU WIEN Bibliothek Your knowledge hub

destroys the initial Mg/Al oxide layer, forming a Zn/Mg/Al-hydroxide mixture.

In acidic media, Zn-hydroxide becomes the dominant oxidation product within one minute, with Mg-oxyhydroxides dissolving completely after 10 minutes. Al undergoes significant oxidation, forming a concentrated Al-oxyhydroxide mixture that is eventually dissolved.

The integration of AR-XPS, LEIS, and SIMS techniques significantly advances our understanding of the effects of alkaline and acidic treatments on Zn-Al-Mg alloy coatings. AR-XPS excels in differentiating various chemical forms, including oxides and hydroxides, while LEIS provides precise elemental quantification as a function of the depths. SIMS complements these methods, while it is highly sensitive for Mg.

TU WIEN Bibliothek Your knowledge hub
Die approbierte gedruckte Originalversion dieser Dissertation ist an der TU Wien Bibliothek verfügbar.
The approved original version of this doctoral thesis is available in print at TU Wien Bibliothek.

Die approbierte gedruckte Originalversion dieser Dissertation ist an der TU Wien Bibliothek verfügbar.
The approved original version of this doctoral thesis is available in print at TU Wien Bibliothek.
TU WIEN Bibliothek Your knowledge hub

Chapter 4

Alkaline cleaning of Zn–Al–Mg hot-dip galvanized steels: Mechanisms and surface oxide chemistry

The following chapter is based on the article published under the same title in Journal of The Electrochemical Society [84] and reproduced under the corresponding copyright agreement. The objective of this study was to assess the effectiveness of cleaning processes on the Zn-Al-Mg coating, with a focus on surface chemistry modifications. Given the inevitable changes in surface chemistry during this process, it was of interest to determine the potential benefits or, on the opposite, unwanted results of using existing commercially available cleaners.

The experiments were performed by a group of researchers, including Jiri Duchoslav, who performed AES surface mapping and XPS measurements, Matthias Kogler, who performed LEIS depth measurements, and Gabriela Schimo-Aichorn, who measured the SKP potentials. The ICP-OES measurements were performed by the author herself, as well as the preparation of the samples for all surface measurements.

Alkaline cleaning of Zn–Al–Mg coated hot-dip galvanized steel is a central process in the industrial galvanized steel production. This process removes carbonaceous contaminants from the surface and modifies the surface chemistry profoundly. We implement a combined analytical and surface science approach to characterize the dissolution mechanism and surface chemistry of Zn-Al-Mg coatings after treatment with industrial cleaners with pH 9.3 and 12.7, respectively. Our data indicate that weak alkaline cleaning can significantly increase the surface concentration of Zn-oxide, while strong alkaline cleaning dissolves the native oxide and generates a transient Zn/Mg-hydroxide on the surface. The observed dissolution mechanisms are largely consistent with the expectations from the Pourbaix diagrams, i.e. at pH 12.7 aluminium dissolution is expected while Mg is stable and forms a transient passive film. In contrast, mild alkaline cleaning at pH 9.3 is dominated by Mg and Zn dissolution, while the native Al passive film remains stable. Hence the cleaning provides an effective direct modification of the surface chemistry for subsequent process steps during the coating. Mild alkaline cleaning offers an increase of Zn at the surface, which has important implications for subsequent conversion and adhesive applications, that have been traditionally optimized for pure Zn coatings.

4.1 Introduction

Zn–Al–Mg hot-dip galvanized steel coatings are a favoured material in the automotive industry [8]. Along with beneficial physical characteristics they exhibit high corrosion resistance, due to the formation of a passivating aluminium oxide. Their structure and chemical composition as well as the oxide layers as crucial points of these corrosion protection qualities, have been explored by advanced surface techniques such as Auger electron spectroscopy (AES), X-ray photoelectron spectroscopy (XPS) and Atomic force microscopy (AFM), Scanning electron microscopy (SEM) with Energy dispersive x-ray (EDX) analysis [90, 91]. Other practical aspects of these coatings behaviour under corrosive conditions have been intensively studied, including their corrosion products [5, 92–100], corrosion mechanisms [101], stability and protective properties [102, 103].

Alkaline cleaning is a stage in the production of hot-dip galvanized coated steel designed to remove various contaminants after industrial production and storage. Further, the state of the cleaned metallic coating can influence the subsequent surface treatments, including e.g. phosphating with importance for automotive industry. However, the effects of alkaline cleaning on the chemistry and structure of Zn–Al–Mg surfaces have not been studied in great detail.

TU Bibliothek Your knowledge hub WIEN
Die approbierte gedruckte Originalversion dieser Dissertation ist an der TU Wien Bibliothek verfügbar.
The approved original version of this doctoral thesis is available in print at TU Wien Bibliothek.

TU WIEN Bibliothek Your knowledge hub
Die approbierte gedruckte Originalversion dieser Dissertation ist an der TU Wien Bibliothek verfügbar.
The approved original version of this doctoral thesis is available in print at TU Wien Bibliothek.

Conversely, for different aluminium alloys, the cleaning process and its influence on the surface oxide layers and other properties such as adhesion with acidic and alkaline cleaners were well characterised. In addition to electrochemical methods surface analytical techniques such as AES, AFM, SEM, XPS revealed significant changes in surface chemistry [104–107]. The same surface-science oriented approach has been used by other groups of authors for stainless and hot-dip galvanized steel to study the effects of alkaline cleaning [21, 108]. In a recent work Çetinkaya et al. studied the effects of treating Zn–Al–Mg coatings with strongly alkaline and acidic solutions and concluded that the coatings can be more consistently activated by acidic cleaners due to effective increase of Zn at the surface. This, according to the authors Çetinkaya et al., should enhance the applicability of adhesives as well as conversion chemistries designed for zinc-rich substrates to yield improved bonding properties on such Zn–Al–Mg coatings activated by acidic solutions [22]. As a case in a point, Lostak et al. found, that Zn-rich cathodes are more effective as a foundation for Zr-based conversion layers on Zn-Al-Mg [32], and Fockaert et al. reported that hexafluorozirconic acid treatment improved the stability of polyester primer chemisorption by passivating zinc and magnesium oxide on metal substrates [109]. Further, for strong alkaline cleaners the dissolved elements concentrations of materials were studied by Inductively coupled plasma optical emission spectroscopy (ICP-OES) in situ, also during immersion [110–115] as well as scratch testing [116]. Monitoring of the electrochemical behavior during immersion in alkaline solutions was evaluated by electrochemical impedance spectroscopy and voltammetry [117–120]. Han et al. studied Zn–Al–Mg during alkaline cleaning in situ using ICP-OES coupled with a flow cell and open circuit potential, followed by Glow-discharge optical emission spectroscopy ex situ analysis [23]. They concluded that the effect of alkaline cleaning was a removal of oxide and selective dissolution of Al at a pH of > 12.

Here we implement a similar surface characterization approach along with dissolved elements analysis to describe an effect of mild and strong alkaline cleaning on the surface chemistry of Zn-Al-Mg coatings at pH 9.3 and 12.7, respectively. Hereby, we investigate alkaline cleaning as a process involving carbonates removal and surface chemistry changes and therefore entail a study of the kinetics of elemental dissolution as well as elemental composition and chemical states conversion on the surface and vertical layering of surface oxides.

TU WIEN Bibliothek Your knowledge hub
Die approbierte gedruckte Originalversion dieser Dissertation ist an der TU Wien Bibliothek verfügbar.
The approved original version of this doctoral thesis is available in print at TU Wien Bibliothek.

4.2 Methods and materials

4.2.1 Chemicals and Materials

Zn–Al–Mg coatings (96 wt. % Zn, 2.5 wt. % Al and 1.5 wt. % Mg) were produced by hot-dip galvanizing and subsequential skin-passing on a large-scale plant of voestalpine Stahl GmbH in Linz, Austria. The average coating weight per side was about 45 g m^{-2}, corresponding to a thickness of 6 µm. The substrate was a DX56 low carbon steel. For comparative LEIS measurements non-skin-passed Zn-Al-Mg coatings with average coating weight per side of about 60 g m^{-2} were additionally used.

Two commercial cleaners were used. Cleaner 1 (Surtec133 from Surtec) is a mild alkaline cleaner with a pH of 9.3, based on phosphates, sodium tetraborate, and anionic and non-ionic tensides. Cleaner 2 (Bonderite C-AK C 72 from Henkel) is a strong alkaline cleaner with a pH of 12.7, which is based on a mixture of alkali-based carbonates and silicates, mixed with salts of organic acids and non-ionic tensides. Cleaner solutions with a concentration of 20 g/l were prepared from the powder at 55° C.

4.2.2 IRRAS

was performed with a Vertex 70v infrared spectrometer (Bruker, USA) with a LN-MCT wide range detector in the span from 4000 to 400 cm^{-1}. The detector was cooled with liquid nitrogen prior to measurements. Spectra were recorded at an incident angle of 78° with a scan rate of 4 cm^{-1}.

4.2.3 ICP-OES

was carried out with a Spectro Arcos FHX3X system (Ametek, USA) with a vertically mounted torch at an analyte feed rate to the instrument of 30 rpm, generated by the peristaltic pump. The system was calibrated every day before the measurements using standard solutions of Zn, Al and Mg.

4.2.4 SKP

measurements were performed to indicate contact potential differences (CPD) with a Wicinski-Wicinski GbR instrument (Germany). The SKP tip consists of a Ni/Cr

(80/20) alloy and has a diameter of 174 μm. A Cu/Cu^{2+}- system was used for calibration. Measurements were conducted under atmospheric conditions at 20 % relative humidity and room temperature.

4.2.5 XPS

The surface elemental and chemical compositions of the investigated samples were determined using a Thetaprobe XPS system (Thermo Scientific, UK), equipped with a monochromated Al Kα X-Ray source and operated by the Avantage software package (Thermo Scientific, UK). Accumulated surface charge was compensated by a dual flood gun FG02. The survey spectra were recorded using a pass energy of 200 eV and an energy step of 1 eV, while 50 eV pass energy and 0.05 eV energy step were used for high resolution spectra. The recorded spectra were charge corrected with respect to the C1s peak of adventitious carbon at a binding energy of 285.0 eV. The analysis of chemical states of Zn and Mg was made using the concept of the modified Auger parameter. Furthermore, a detailed evaluation of chemical states was performed via an experimental procedure developed for the analysis of corrosion products by fitting linear combinations of spectra from reference compounds [87, 121–123]. In a short summary, the peaks in the recorded spectra were subtracted using a Shirley type background and evaluated by means of linear combination fitting taking full-shaped experimental spectra from our own spectra database. The reference spectra were collected and recorded with the same XPS instrument with identical acquisition parameters. The Wagner chemical states plot was drawn using measured data of pure chemical compounds of Zn and Mg as well as the investigated samples. The similar data for pure reference materials has been already used in our previous publication [9].

4.2.6 AES

A complimentary analysis of the surface layer with high lateral resolution was performed using a scanning AES microscope JAMP-9500 F (JEOL, JP). The system was equipped with a hemispherical electron energy analyzer, a channeltron detector and two detectors for secondary and back-scattered electrons. The elemental mappings as well as electron micrographs were recorded using an acceleration voltage of 30 kV and an electron beam current of 10 nA, which resulted in a lateral resolution of approximately 10 x 10 nm^2. The Auger elemental maps were obtained by plotting

TU WIEN Bibliothek Your knowledge hub
Die approbierte gedruckte Originalversion dieser Dissertation ist an der TU Wien Bibliothek verfügbar.
The approved original version of this doctoral thesis is available in print at TU Wien Bibliothek.

Table 4.1. Kinetic energies used to determine peak and background intensities taken for AES mappings.

Element	Kinetic energy (eV)						
	P1	P2	P3	P4	B1	B2	B3
Zn	969.3	977.8	986.3	994.8	1003.3	1011.8	1020.3
Mg	1154.3	1162.8	1171.3	1179.8	1188.3	1196.8	1205.3
Al	1363.0	1371.5	1380.0	1388.5	1397.0	1405.5	1414.0

relative intensity for the elements over the mapping area, which was split into 512 x 512 pixels (with one pixel corresponding to approx. 50 x 50 nm^2). The relative intensity (I) in each pixel was calculated as: I = (P-B)/(P+B), where P and B are the summed signal intensities measured at peak and background energy windows. The most intensive peaks from Zn LMM, Mg KLL and Al KLL transitions were selected for the mapping. Exact energies are stated in **Table 4.1**. Signal intensities at different peak and background energies were measured simultaneously for each pixel, the acquisition time was set to 20 ms and the intensity profile was recorded 3 times.

4.2.7 LEIS

measurements were performed using a high sensitivity spectrometer ION-TOF Qtac^{100} (IONTOF, Germany) with a primary beam of He^+ 3 keV at 2.5-2.7 nA, at an incident angle of 0° and scattering angle of 145°. The measurement area was 2 x 2 mm^2. The sputter beam consisted of Ar^+ 500 eV at a current of 95-105 nA and an incident angle of 59° with a sputter area of 2.5 x 2.5 mm^2. To quantify the measured data, the reference spectra of pure Zn, Al, and Mg were measured and equated to 100% concentration. Using the measured scaling factor, the concentrations of Zn, Al, and Mg in the coating samples were then calculated with respect to the densities in the metallic state.

4.2.8 Samples preparations

Reference samples for surface analyzes were successively sonicated for 10 minutes in beakers containing acetone, isopropanol, and ethanol.

Alkaline cleaned samples for the surface analyzes were prepared by immersing the samples in the heated cleaner solutions at 55° C for 1, 5 and 10 minutes. Then

Die approbierte gedruckte Originalversion dieser Dissertation ist an der TU Wien Bibliothek verfügbar.
The approved original version of this doctoral thesis is available in print at TU Wien Bibliothek.
TU WIEN Bibliothek Your knowledge hub

Die approbierte gedruckte Originalversion dieser Dissertation ist an der TU Wien Bibliothek verfügbar.
The approved original version of this doctoral thesis is available in print at TU Wien Bibliothek.
TU Bibliothek WIEN Your knowledge hub

the samples were rinsed with distilled water and dried in a stream of air.

In order to study the dissolution of coating elements during cleaning, an ex situ simulation of this process was carried out and the used cleaning solutions were subsequently analyzed by ICP-OES. A cleaning line consisting of 8 beakers filled with cleaning solution was prepared. The 8 beakers were placed in an ultrasonic bath, where a temperature of 55° C was maintained during the process. For each experiment, a total of 8 samples of 3x6 cm^2 Zn-Al-Mg were immersed in these beakers in parallel (to maintain all conditions similar) and were taken out of the cleaning solutions, with cleaning times increasing from 0.25 to 10 minutes. For ICP-OES analysis the used cleaning solutions were diluted with distilled water in a 1:10 ratio and concentrated HNO_3 was added to acidify the samples. Between each measurement the sample introduction system was rinsed with diluted HNO_3 for 30 seconds.

4.3 Results and Discussion

In this work we study how a mild alkaline (cleaner 1, pH 9.3) and a strong alkaline (cleaner 2, pH 12.7) cleaners remove carbon-based contaminants (e.g., oils) from the surface and how this cleaning process affects the oxide chemistry of a Zn-Al-Mg alloy. **Table 4.2** shows the carbon absorbance signal on the sample surface, where the signal maximum refers to the carbon content on the contaminated (uncleaned) surface.

Table 4.2. Normalized carbon absorbance measured by IRRAS at 2922 cm^{-1} with the signal maximum referring to the carbon content on the uncleaned surface.

	Absorbance, a.u.			
	0.5 min	1 min	5 min	10 min
Cleaner 1	0.124	0.042	0.015	0
Cleaner 2	0.049	0.046	0.011	0

Carbon contaminants were removed from the surface treated with Cleaner 1 virtually within the first minute, while samples treated with Cleaner 2 required only 30 seconds to achieve a similar result. After 10 minutes both surfaces were clean and free of significant carbon contaminants.

To study the influence of alkaline cleaning on the coating surface chemistry, AES measurements were conducted. The AES images shown in **Figure 4.1** indicate the elemental mapping of the surface at different stages of the cleaning process. The reference showing a degreased (solvent cleaned) surface demonstrates a predominance of Al and Mg compounds on the surface. This suggests a mixed native Al/Mg-oxide film on these surfaces, as expected for the alloy.

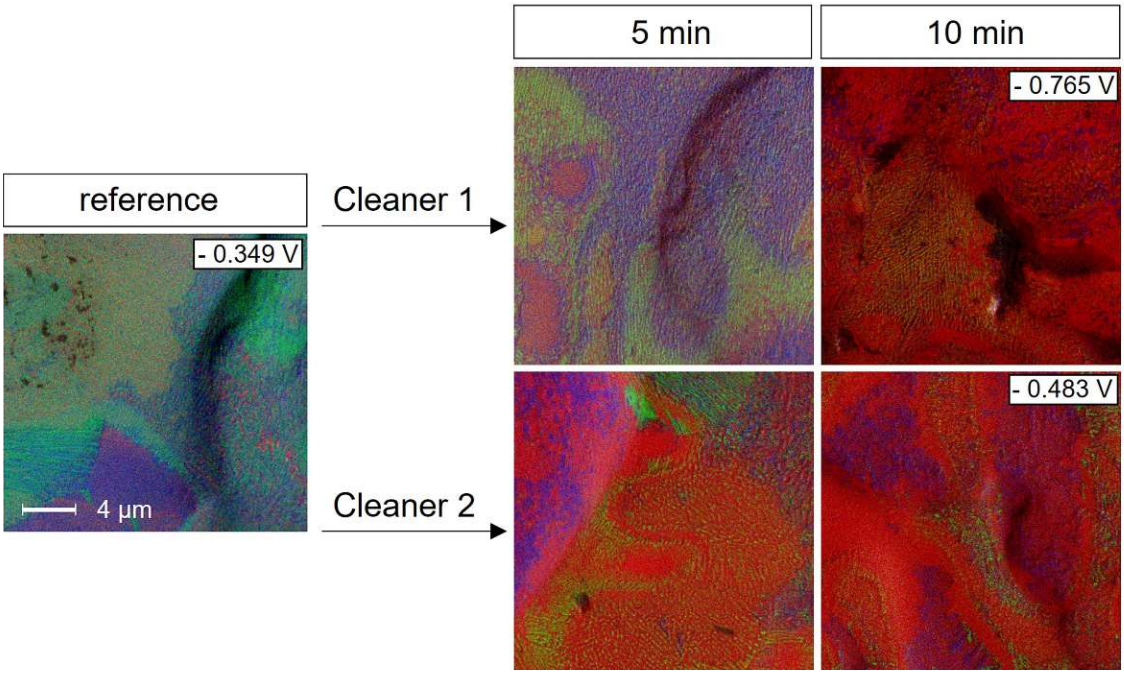

Figure 4.1. Influence of treatment with industrial cleaners on the surface chemistry of Zn–Al–Mg-coated steel, characterized by the AES surface mappings (red – Zn, blue – Al, green – Mg). The insets indicate the average CPD vs. standard hydrogen electrode (SHE), measured by SKP.

After 5 minutes of cleaning AES data imply a significant difference between the elemental surface composition for Cleaner 1 and Cleaner 2. After treatment with Cleaner 1 the surface compositions appear Al- and Mg-rich, while the surfaces treated with Cleaner 2 indicate an increasingly Zn-rich chemistry. After 10 minutes of alkaline cleaning, based on an AES analysis, the surfaces again appear nearly identical for the two different cleaners and are now both Zn-rich, indicating selective dissolution of the initial native oxide film.

Figure 4.1 also labels the resulting contact potential differences across the surface of the reference sample and the samples cleaned for 10 minutes. The potential shifts indicate that chemical changes during the cleaning process significantly affect the surface chemistry, while AES images appear rather similar after 10 minutes. This implies that the oxide and surface chemistry are different after the two different

Die approbierte gedruckte Originalversion dieser Dissertation ist an der TU Wien Bibliothek verfügbar.
The approved original version of this doctoral thesis is available in print at TU Wien Bibliothek.

cleaning processes, despite the rather similar Zn-rich AES signal.

To further assess the species dissolved during cleaning, ICP-OES of the cleaner solutions used was applied. **Figure 4.2** shows the dissolved metal content after different treatment times with the respective cleaners. These data indicate major differences in the dissolution mechanisms of the two cleaners.

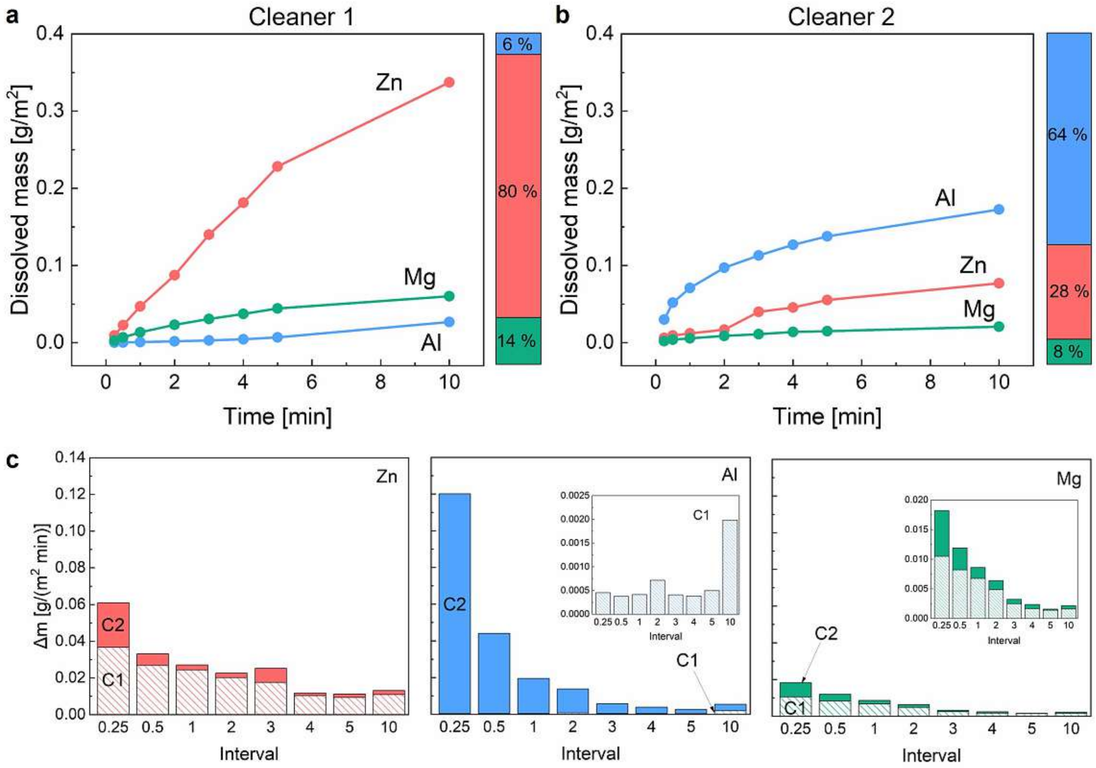

Figure 4.2. Dissolution of Zn–Al–Mg coating elements during the treatment measured by ICP-OES: a) total dissolved mass in the Cleaner 1 solution; b) total dissolved mass in the Cleaner 2 solution; c) change in dissolved mass per minute for each element by intervals: 1st interval – 0-15 s, 2nd – 15-30 s, 3rd – 30s-1 min, 4th – 1-2 min, 5th – 2-3 min, 6th – 3-4 min, 7th – 4-5 min, 8th – 5-10 min; where Cleaner 1 indicated as C1 and Cleaner 2 as C2.

First, **Figure 4.2a** designate that Cleaner 1 predominantly dissolves Zn and considerably less Al and Mg. Almost no Al dissolves in the first 5 minutes. This is not unexpected, and in line with the bulk concentration of the elements. The percentage scale next to the plot indicates that about 80 % of Zn, 6 % of Al and 14 % of Mg are dissolved from the surface during 10 minutes of cleaning. Compared to the bulk alloy composition, this still demonstrates a preferential dissolution of Mg and Al, probably from the native oxide. As can be seen in Figure 4.2b this is even

Die approbierte gedruckte Originalversion dieser Dissertation ist an der TU Wien Bibliothek verfügbar.
The approved original version of this doctoral thesis is available in print at TU Wien Bibliothek.

more pronounced for Cleaner 2, which implies a strongly preferential dissolution of Al, and to a much lesser extent a preferred dissolution of Mg, while significantly less Zn dissolves compared to the ratio expected from the bulk alloy.

Figure 4.2c further shows how the elemental dissolution rates change over time by integrating over time intervals. While Cleaner 1 can be characterized by constant decelerating dissolution for Zn and Mg, it appears that low Al dissolution accelerates slightly with time. This suggests that the native Al-oxide remains stable, while Mg and Zn are leached from the matrix. Cleaner 2 is marked by the fast initial Al dissolution, which decreases quickly. Similarly, Zn and Mg dissolution rates decrease with time. Considering the total dissolved mass over 10 minutes, this behaviour could reflect the fast initial chemical dissolution of the initial Al-oxide, as well as the formation of a transient and likely Zn/Mg-rich oxide that stabilizes during the dissolution process.

The observed elemental dissolution behavior agrees to a large extend with expectations based on the Pourbaix diagrams of the individual coating elements (see **Figure 4.3**. However, the rather significant dissolution of Zn by Cleaner 1 is surprising, since Zn is not expected to dissolve at a pH of 9.3. Nevertheless, it is the dominating product of dissolution. The discrepancy between the zinc dissolution zone and the experimental data in this case can be explained by the complex composition of the active Cleaner 1 solution, while the simple Pourbaix system does not take into account complex cleaner and material matrices, which could favour dissolution e.g. due to complexing of Zn.

Therefore, it is possible that the phosphates in Cleaner 1 solution form a complex with zinc, causing it to dissolve despite the conditions predicted by the Pourbaix diagram. Other compounds, including sodium tetraborate in Cleaner 1, alkali-carbonates and silicates in Cleaner 2 could also influence the dissolution process due to formation of the complexes with metal ions, although this effect appear less pronounced as the pH effect seems to overpower the chemical complexing effect.

Additionally, the integrated elemental dissolution shown in **Figure 4.2a/b** is quite surprising, considering that both surfaces appear similarly Zn-terminated in the AES mapping after 10 minutes of treatment. But the kinetics of elemental dissolution obtained by the ICP-OES analysis can clarify this outcome. Cleaner 1 dissolved only very small amounts of Al, mostly during extended cleaning times. Comparing with AES images for surfaces treated for 5 and 10 minutes (**Figure 4.1**) a dissolution mechanism as follows could occur. As observed, the final AES mapping

Die approbierte gedruckte Originalversion dieser Dissertation ist an der TU Wien Bibliothek verfügbar.
The approved original version of this doctoral thesis is available in print at TU Wien Bibliothek.
TU WIEN Bibliothek Your knowledge hub

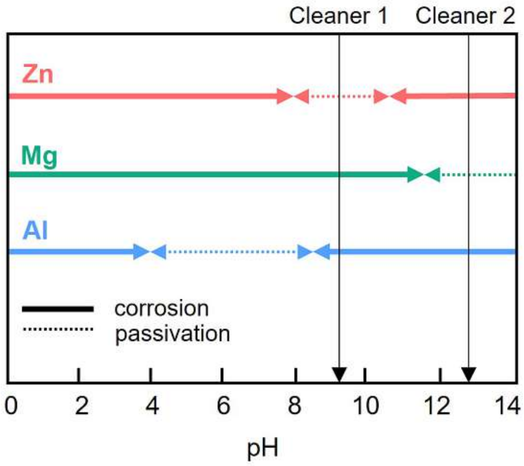

Figure 4.3. Corrosion and passivation areas in the system element-water at 25° C according to Pourbaix diagram, within potentials from -1 to 1.2 V for Zn, from -2.6 to 0.4 V for Mg and from -1.8 to 1.2 V for Al.

for Cleaner 1 indicates very low Mg and Al signals and strong Zn. Hence, given the limited Al dissolution, Mg is leached from the initial oxide layer. However, the oxide layer remains stable, and is dominated by Al, as it is shown in treated 5 minutes surface mapping. Further, Zn diffuses through the layer and covers the surface by a Zn-oxide phase, forming a Zn-enriched double layer like oxide. In contrast, the initial strong dissolution of Al for Cleaner 2, in combination with Mg dissolution, denotes a disintegration of the native oxide. The Zn-rich AES images further suggest the formation of a Zn-dominated transient oxide/hydroxide film.

To further confirm the chemistry of the formed layers XPS spectra were recorded after 10 minutes of dissolution. **Figure 4.4** shows high resolution XPS spectra of all observed species on the surface. First, for the native reference surface data indicate an Al/Mg oxide, with low Zn-content. All spectra still specify metallic signals, indicative of an oxide thickness of about 6-8 nm, given that the signal depth of XPS is about 10 nm at the selected take-off angle. Second, the XPS data reveal a clear decrease in peak intensities for both Al and Mg (see **Table 4.3**) after treatment with both cleaners, which is consistent with AES data, and displays a conversion of the initial oxide film into a Zn-rich oxyhydroxide phase at the surface. In addition, the metallic Zn peaks decrease notably after the alkaline treatment, indicating a thicker passive film.

Given the very limited amount of Al dissolution (see again **Figure 4.2**) for Cleaner 1, XPS data suggest that the native Al/Mg-oxide of the surface is cov-

Die approbierte gedruckte Originalversion dieser Dissertation ist an der TU Wien Bibliothek verfügbar.
The approved original version of this doctoral thesis is available in print at TU Wien Bibliothek.

Die approbierte gedruckte Originalversion dieser Dissertation ist an der TU Wien Bibliothek verfügbar.
The approved original version of this doctoral thesis is available in print at TU Wien Bibliothek.
TU WIEN Bibliothek Your knowledge hub

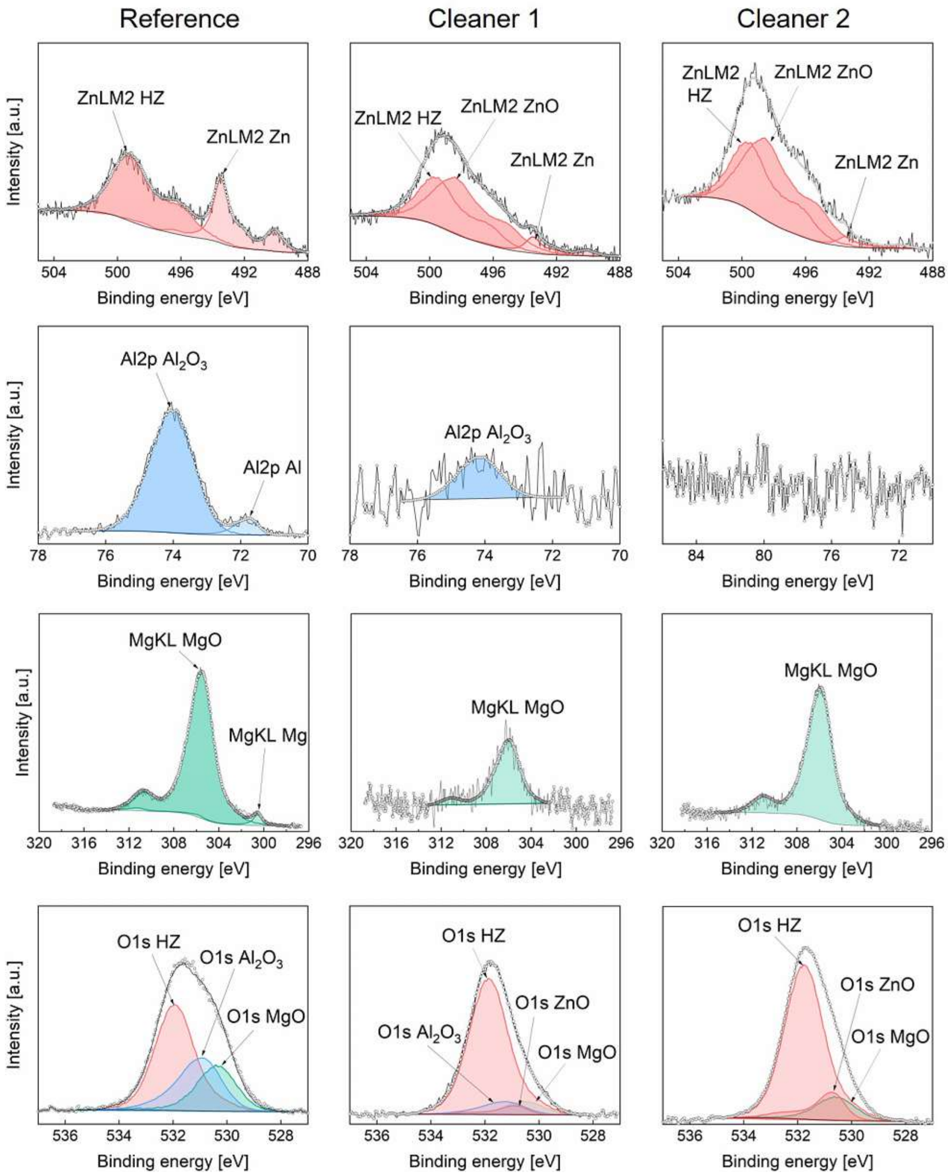

Figure 4.4. XPS scans for ZnLMM, Al2p, MgKL and O1s of the reference and samples treated 10 minutes with Cleaner 1 and Cleaner 2.

ered by a Zn-hydroxide. Further, spectra after treatment with Cleaner 2 indicate no aluminium on the surface layer at all, implying a full disintegration of the native Al/Mg-oxide. However, the intensive MgO peak suggests the formation of a Zn/Mg-rich hydroxide. The Wagner plots shown in **Figure 4.5a** further designate a shift in surface speciation for alkaline-treated surfaces from hydrozincite (HZ) to ZnO. **Figure 4.5b** specifies the Mg compounds. The predominance of MgO on the unmodified reference surface converts towards $Mg(OH)_2$ and $Mg_5(CO_3)_4(OH)_2$ after

Die approbierte gedruckte Originalversion dieser Dissertation ist an der TU Wien Bibliothek verfügbar.
The approved original version of this doctoral thesis is available in print at TU Wien Bibliothek.
TU WIEN Bibliothek Your knowledge hub

Table 4.3. Elemental composition calculated from the survey spectra.

Sample	Elemental concentration (at. %)			
	Zn2p3	Al2p	Mg2p	O1s
Reference	4.4	14.3	12.2	50.3
Cleaner 1	15.0	5.8	1.5	46.2
Cleaner 2	12.2	1.7	7.5	56.5

cleaning with both cleaners.

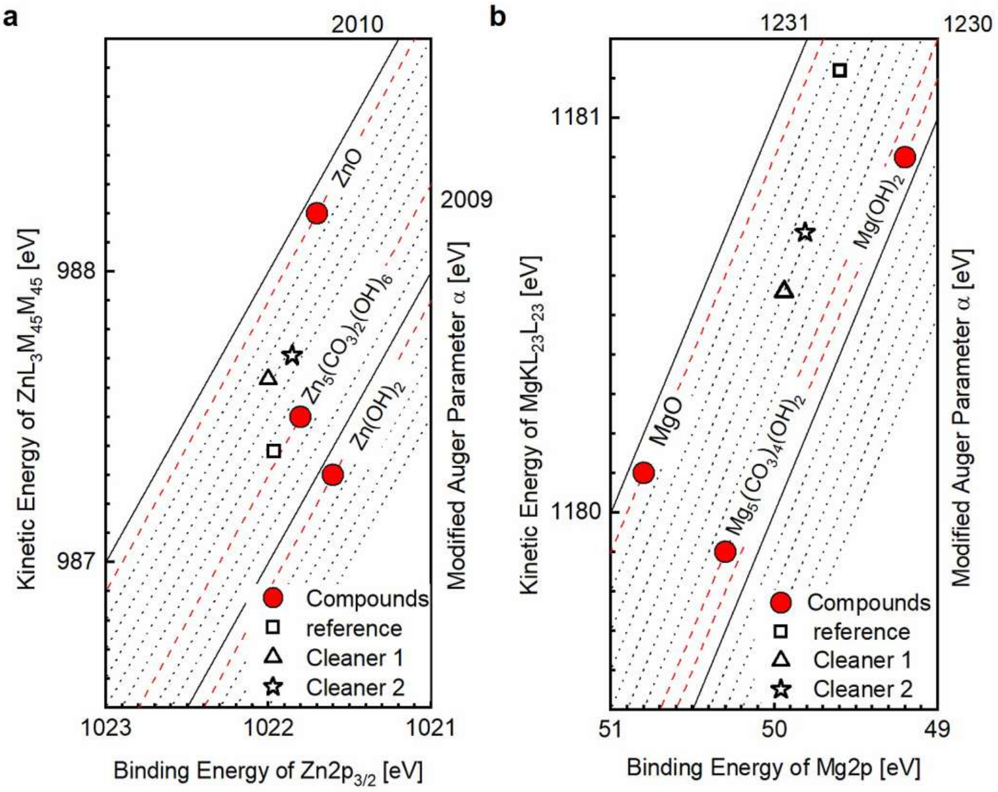

Figure 4.5. Wagner plot to determine corrosion products for Zn and Mg: a) kinetic energy of ZnLMM versus binding energy of Zn2p; b) kinetic energy of MgKLL versus binding energy of Mg2p.

Although the XPS data enable determination of the chemical states of the elements in the coating, vertical layering of oxides cannot be determined unambiguously. Hence, LEIS measurements were performed, which are quantitative and only sensitive to the topmost layer, together with sputter depth profiles [59]. **Figure 4.6** shows a quantitative comparison of coating elements in the first 5 nm in the reference sample with a native surface chemistry, and in the samples treated with alkaline cleaners 1 and 2, respectively, for 1 and 10 minutes. The reference concentrations are pure metals for each element (see methods).

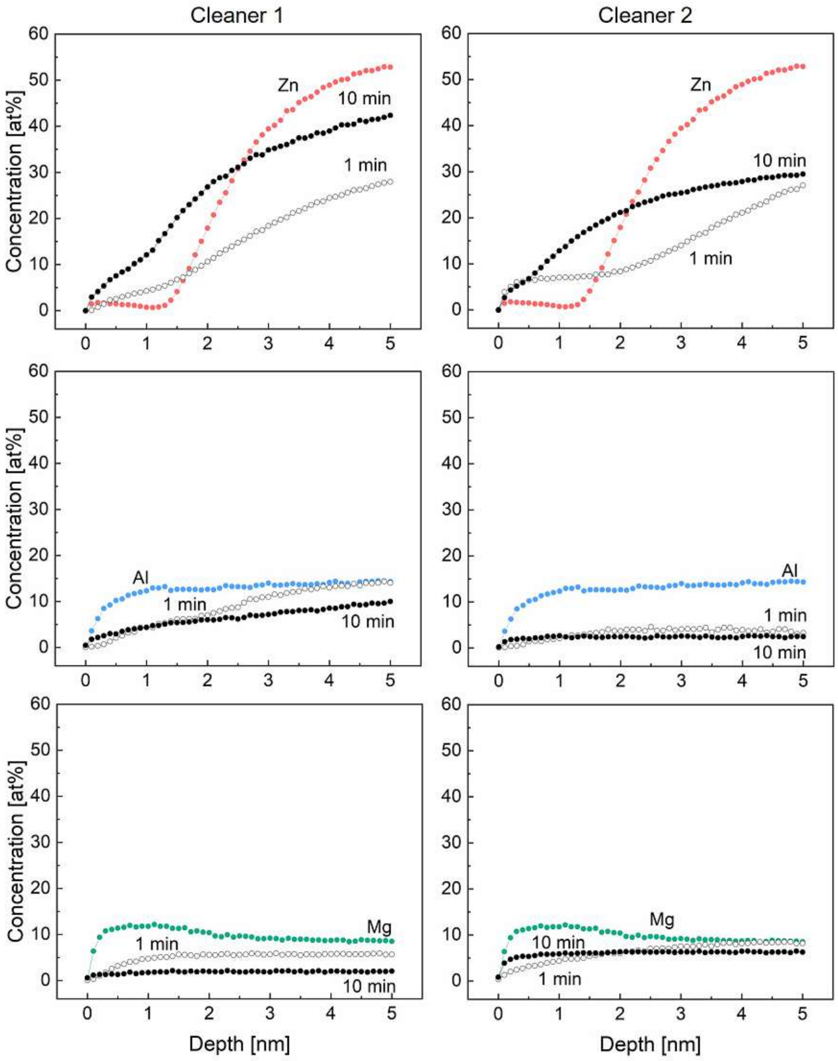

Figure 4.6. Surface oxide layers depth profile for Zn, Mg and Al after mild and strong alkaline cleaning of skin-passed Zn-Al-Mg coating during 1 and 10 minutes in comparison with depth profile for Zn, Mg and Al of reference - unchanged Zn-Al-Mg coating (colored).

First of all, the native passive film on the reference surface consists of an oxide that is enriched in Al at the top, with subsurface increase of Mg. While Zn is depleted within this Al/Mg-oxide, it is enriched further in the top layer as a possible result of Zn-diffusion through the oxide to the air/oxide interface. This may be due to the interaction with CO_2 or O_2 from the atmosphere providing a driving force for Zn-diffusion in the places of impurities or defects through the native Al/Mg.

Die approbierte gedruckte Originalversion dieser Dissertation ist an der TU Wien Bibliothek verfügbar.
The approved original version of this doctoral thesis is available in print at TU Wien Bibliothek.

In addition, the change in the surface structure as a result of industrial skin passing process may play a role. As it stated by M. Arndt et. al, skin passing destroys the Al/Mg-oxide layer in the imprinted regions, exposing underlaying Zn [2]. This may result in Zn enrichment in the top layer sensed by LEIS in the native spectra. As can be seen in the spectra, data indicate a minor enrichment with Zn, which correlates with the Zn signals in the skin-passed areas seen in the AES data (see again **Figure 4.1**). Measurements on non-skin-passed material with intact structure (not shown) indicate a less significant Zn peak. As such, skin passing indeed exposes Zn areas (within oxide defects) in the imprinted areas, while the overall oxide remains chemically identical, irrespective of skin passing.

The data further indicate that after 1 and 10 minutes of treatment with Cleaner 1 the Zn concentration increases consecutively in the first 2-2.5 nm in comparison with the reference. That trend can be a sign of the enrichment of Zn, and of a thickening of the Zn film. Notably, after 1 minute of treatment the Al concentration shows a subsurface maximum at 5 nm, while gradually increasing through the layer. Based on the low solubility of Al in the Cleaner 1 this data implies that during the first minute (**Figure 4.2**) Zn diffuses through the initial Al/Mg-oxide phase and builds up a layer on top of it. This aligns with XPS data for Al (see **Figure 4.4**), and with the increase of the Zn profile across the oxide, which indicates a diffusion towards the outer surface. The concentration of Mg exhibits a decline as the treatment time increases, hence Mg is almost depleted after 10 minutes of treatment. The Mg depletion is in accordance with the low Mg intensity in the XPS data (see **Figure 4.4**). This further underscores Zn diffusion through the Al/Mg-oxide, while the Mg-oxide part is increasingly being dissolved and the Mg concentration decreases gradually. The Al-oxide part of this Al/Mg-oxide remains as the passive film at the metal/oxide interface, which could be essential for the increased corrosion resistance.

The same trend of Zn enrichment is observable for Cleaner 2. After 10 minutes of treatment with Cleaner 2 Zn is evidently enriched in the surface layer in a mixture with Mg. In contrast Al depletes completely, which is in line with the XPS data as there is no observable spectra of Al-oxide (see **Figure 4.4**). Hence, the significant amount of Al dissolution (see again **Figure 4.2c**) appears to be due to the Al-oxide disintegration in the first minute. The surface is then covered by a Zn/Mg-rich surface film. After 10 minutes, the Mg concentration levels, and the Zn profile moves towards the top of the surface, indicative of a diffusion of Zn into the Mg-rich passive film. Again, the passive film appears to have a lower density compared to the

Die approbierte gedruckte Originalversion dieser Dissertation ist an der TU Wien Bibliothek verfügbar.
The approved original version of this doctoral thesis is available in print at TU Wien Bibliothek.

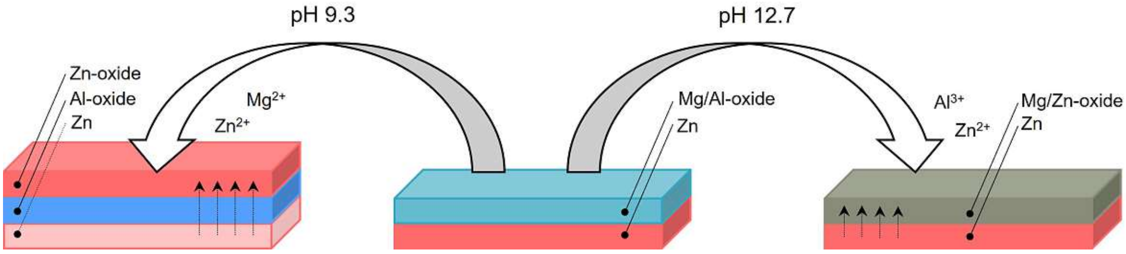

Figure 4.7. Model figure of dissolution and oxide layering process on the top surface of Zn-Al-Mg coating.

native oxide, conforming to a Mg-hydroxide formation. In general, the differences between LEIS depth profiles for the skin-passed and non-skin-passed surfaces after alkaline cleaning are insignificant (non-skin-passed data not shown). On the skin-passed samples a slightly more prominent Mg diffusion to the outer surface after the cleaning was observed. This can be explained by the initial integrity of Al/Mg-oxide layer, which is disrupted on the skin-passed surface. This minor difference does not alter the Zn overgrowth and overall Mg dissolution that is happening on both skin-passed and non-skin-passed surfaces. The overall increase/growth of a Zn-layer on both types of surfaces can also be seen in the AES images (**Figure 4.1**), which show both: areas, imprinted by skin passing, and intact plateaus, corresponding to non-skin-passed surfaces. AES (see again **Figure 4.1**) also shows that both areas overgrow similarly, with Zn/Mg-rich layers after 10 minutes of treatment.

This more thorough explanation of the topmost surface oxide layers behavior allows us to propose a simplified model of their vertical layering on the Zn-Al-Mg coatings (**Figure 4.7**) after cleaning. This figure represents an outline of the dominant elements in layers in the respective order and the main products of the dissolution. Interestingly, while skin passing may improve the real surface area for subsequent coating applications, the top-layer surface chemistry is not significantly altered after an alkaline cleaning.

4.4 Conclusion

Alkaline cleaning of Zn-Al-Mg coated hot-dip galvanized steel not only removes contaminants from the surface with different rate depending on the used cleaner, but also influences the surface chemistry profoundly. Mild and strong alkaline cleaner influence the surface chemistry and dissolve elements of the coating differently.

Die approbierte gedruckte Originalversion dieser Dissertation ist an der TU Wien Bibliothek verfügbar.
The approved original version of this doctoral thesis is available in print at TU Wien Bibliothek.

The disintegration of the native Al/Mg-oxide by Al dissolution, and subsequent formation of a transient Mg/Zn-rich passive film is the dominating mechanism at a pH of 12.7. In contrast, at a pH of 9.3 Zn dissolution and Mg leaching across a stable Al-oxide dominates the dissolution process. This results in differently layered surface structures compared to the native Al/Mg-oxide, specified by Al dominance and Zn depletion, with a Mg gradient towards the metal interface.

The observed dissolution mechanisms agree *considerably* with expectations from Pourbaix diagrams, i.e. fast Al dissolution is anticipated for a pH of 12.7, while Mg is stable and forms a transient passive film. Alternatively, mild alkaline cleaning at a pH of 9.3 is dominated by Mg and Zn dissolution, while the native Al-passive film remains stable. Hence, the choice of cleaner can offer an effective direct modification of the surface chemistry for subsequent process steps during coating of galvanized steels. Both cleaners offer an increase of Zn at the surface, which in turn can optimize the performance of consecutive conversion processes and adhesive applications, which have been traditionally optimized for neat Zn coatings.

Die approbierte gedruckte Originalversion dieser Dissertation ist an der TU Wien Bibliothek verfügbar.
The approved original version of this doctoral thesis is available in print at TU Wien Bibliothek.

Die approbierte gedruckte Originalversion dieser Dissertation ist an der TU Wien Bibliothek verfügbar.
The approved original version of this doctoral thesis is available in print at TU Wien Bibliothek.

Die approbierte gedruckte Originalversion dieser Dissertation ist an der TU Wien Bibliothek verfügbar.
The approved original version of this doctoral thesis is available in print at TU Wien Bibliothek.

Chapter 5

Effect of surface pretreatments on the formation of Zr-based conversion layers on Zn-Al-Mg alloy coated steel

The following chapter is based on the article published under the same title in Materials and Corrosion [124] and reproduced under the corresponding copyright agreement.

This study was performed essentially to evaluate the influence of mild alkaline, strong alkaline and acidic pretreatments on the characteristics of a Zr-based coating applied to a Zn-Al-Mg coating.

The experiments were performed by a group of researchers, including Jiri Duchoslav, who performed XPS measurements, Matthias Kogler, who performed LEIS depth measurements, Daniela Miano, who conducted AFM mapping, Elahe Akbari, who measured AES spectra. The author herself prepared the samples for the surface analyses, including application of pretreatment and Zr-based conversion coating, evaluated and described the data.

Zr-based conversion coatings represent an environmentally conscious alternative to traditional phosphating and chromating in the automotive industry. In this study, we employ XPS and LEIS to investigate the formation of Zr-conversion layers on Zn-Mg-Al alloy after alkaline and acidic model pretreatments. On alkaline pretreated surfaces, a Zr-oxide/oxyfluoride layer and an underlying Mg-Al-fluoride layer are formed, whereas acidic pretreatment results in only an oxidic layer. The thickness of the Zr-layer depends on pretreatment pH and immersion time. Acidic treatment achieves an approximately 23 nm-thick Zr-oxide/oxyfluoride layer after 1 minute, while prolonged treatment increases thickness of oxidic layer for strong alkaline and acidic conditions. Mild alkaline pretreatments, however, do not benefit from extended immersion. F-induced corrosion pits are observed after mild alkaline treatment. The strong alkaline pretreatment proved to be the most efficient in creating a double-layered Zr-conversion coating with increased oxidic layer thickness over time.

5.1 Introduction

For more than a decade, Zr-based conversion coatings have been used and studied as an alternative to classical toxic phosphating and chromating in the automotive industry production [125, 126].

In the late 2000s, Henkel presented a phosphate-free pretreatment composed of dilute hexafluorozirconic acid. This pretreatment, later studied on cold-rolled steel, was shown to form 20-30 nm thick zirconium oxide coatings with corrosion resistance comparable to that of samples treated in a phosphate conversion coating bath [127]. Another example is Ti/Zr-based 500 nm-thick chemical conversion coating with improved electrogalvanized steel corrosion resistance. Its uniform amorphous composition comprises nanoscale complicated oxides or hydroxides and zinc fluorides [128].

The necessity to enhance corrosion resistance and optimize process efficiency has prompted investigations into the potential of modifying zirconium coatings.

One process modification approach is adding ions or complex compounds to the conversion solutions. Thus, Han et al. discovered that in the case of Zn-Al-Mg alloy coatings, the addition of NO_3^-, serving as an oxidant and providing OH^-, contributes to more consequent ZrO_2 deposition [129]. Another group of authors found that adding Cu^{2+} or Fe^{3+} ions to the conversion solution significantly increased the film thickness on zinc alloy-coated steel sheets [130]. On the other hand, adding Mn-ions to the Zr-conversion bath didn't influence the corrosion performance and adhesion of an organic system, although the conversion layer reached improved uniformity in the bath containing 0.01 g/l Mn-ion [131]. Some additions,

Die approbierte gedruckte Originalversion dieser Dissertation ist an der TU Wien Bibliothek verfügbar.
The approved original version of this doctoral thesis is available in print at TU Wien Bibliothek.

such as polysaccharide chitosan, can improve the corrosion resistance and decrease the surface density of micro defects on a nonferrous alloy [132].

Another approach is to select optimal conditions for the existing system. Thus, the optimal conditions for a uniform and corrosion-resistant Zr-conversion layer on cold-rolled steel, established by Mohammadloo et al., are as follows: 20–30° C - temperature of the solution, 60–120 s - time of immersion, pH = 4, and acid concentration of 4% vol [133].

Pretreatment of the surface for the subsequent Zr-layer application, either cleaning, degreasing or activation, also influences the final product's properties. E.g., Cerezo et al. showed how alkaline and acidic pre-conditioning treatments influence dealloying around intermetallic parts in an Al matrix, providing a significant source of crystallization cores, affecting local Cu structures and composition of Zr-based films [134].

The mechanism of zirconium deposition is found to be driven by hydroxyl groups on the different materials. Thus, Taheri et al. studied pure zinc samples treated in alkaline, neutral, and acid solutions before and after deposition of the conversion layers and concluded that deposition of conversion layers depends on the initial surface composition and roughness, and deposition is initiated by hydroxyl removal from the zinc surfaces [135]. Fockaert et al. found that at Mg surfaces hydroxyl dissolves in an acid solution and Mg forms a zirconium oxide layer approximately 10 times thicker than zinc [136]. Likewise, for aluminum alloy, cold-rolled and hot-dip galvanized steels, the conversion layer deposition process is initiated by the oxide/hydroxide layer dissolution, which is accompanied by each metal's anodic dissolution reaction. XPS measurements have shown that most of the Zr is present in the form of ZrO_2, while Al_2O_3, ZnO, FeOOH, FeF_3, ZnF_2, and AlF_3 were found in the coatings in smaller amounts [137]. On an aluminum alloy, a higher initial hydroxyl fraction encourages the formation of a thicker Zr-based layer [138].

Lostak et al. proposed a mechanism of deposition of the Zr-conversion layer on Zn-Al-Mg alloy surfaces. After the immersion, the deposition takes place at first on the most noble Zn-rich phases, while Mg-rich and Al-rich phases undergo anodic dissolution leading to enrichment with Zn. In the case of longer immersion time, the deposition of the Zr-layer takes place over all surface [32]. In addition, Cristaudo et al. found that Zr-conversion coatings on hot-dip galvanized steel consist of a mixed Zn, Al and Zr-oxyhydroxide in combination with Zr oxy-/hydroxyfluoride on top of a complex fluoride (hydr)oxide Zn/Al layer [139].

Die approbierte gedruckte Originalversion dieser Dissertation ist an der TU Wien Bibliothek verfügbar.
The approved original version of this doctoral thesis is available in print at TU Wien Bibliothek.

Die approbierte gedruckte Originalversion dieser Dissertation ist an der TU Wien Bibliothek verfügbar.
The approved original version of this doctoral thesis is available in print at TU Wien Bibliothek.
TU WIEN Bibliothek Your knowledge hub

In our previous investigation of alkaline cleaning for Zn-Al-Mg coated steel, we identified the disintegration of the native Al/Mg-oxide and following formation of a transient Mg/Zn-rich passive film as the primary mechanism for a strong alkaline cleaner [84]. The Zn dissolution and Mg leaching across a stable Al_2O_3 were identified as the driving mechanisms for mild alkaline cleaning. According to Cetinkaya et al., although strong alkaline solution activates Zn effectively, sulphuric acid is more productive even in small concentrations [22].

The pretreatment and its impact on the surface chemistry of Zn-Al-Mg, and subsequently on the Zr layer and its characteristics, represent a crucial aspect in the conversion of Zr-based layers. Given that, we investigate similar mild and strong model alkaline solutions and an acidic one as the pretreatment activation systems for the application of Zr-conversion layers.

5.2 Methods and materials

5.2.1 Chemicals and Materials

Non-skin-passed Zn–Al–Mg coatings (96 wt% Zn, 2.5 wt% Al, and 1.5 wt% Mg) were produced by hot-dip galvanizing on a large-scale plant of voestalpine Stahl GmbH in Linz, Austria. The average coating weight per side was about 60 g m^{-2} , corresponding to a thickness of 8 µm. The substrate was a DX56 low carbon steel.

To create model solutions with different pH for the surface pretreatment before the Zr-conversion layer application, the following chemicals were used: sodium tetraborate decahydrate for a solution with a pH of 9.1-9.2, sodium dihydrogen phosphate for a solution with a pH of 9.1-9.2, sodium hydroxide for a solution with a pH of 12.7, and concentrated sulphuric acid for a model acidic treatment solution with a pH of 2.

The Zr-conversion solution was prepared using 0.76 g L^{-1} of 50 wt% hexafluorzirconic acid. Potassium nitrate was added to the Zr-conversion solution as an accelerator and potassium hydroxide was used to adjust the pH to 4.5 [129].

All chemicals were purchased from Merck.

5.2.2 Samples preparations

Samples were subsequently immersed in the pretreatment solutions, in distilled water for rinsing, and in the conversion solutions. The pretreatment and conversion

Die approbierte gedruckte Originalversion dieser Dissertation ist an der TU Wien Bibliothek verfügbar.
The approved original version of this doctoral thesis is available in print at TU Wien Bibliothek.
TU WIEN Bibliothek Your knowledge hub

solutions were heated to a temperature of 55° C, while the distilled water used for rinsing was maintained at room temperature. The pretreatment time was either 1 minute or 10 minutes, the rinsing time was 30 seconds, and the conversion time was 3 minutes. Following the completion of the conversion process, the samples were rinsed thoroughly and dried with a stream of air. Subsequently, the samples were individually packaged in aluminum foil to prevent further carbon contamination.

The model pretreatment solutions were created using four different chemical agents: sodium tetraborate decahydrate ($Na_2B_4O_7$), sodium dihydrogen phosphate (NaH_2PO_4), sodium hydroxide (NaOH), and concentrated sulphuric acid (H_2SO_4). For clarity and convenient reference, the samples have been labeled A, B, C, and D, as described in **Table 5.1**, and are hereafter referred to as such in the text and figures.

Table 5.1. Samples labeling.

sample	chemical agent	pH
A	$Na_2B_4O_7$	9.1-9.2
B	NaH_2PO_4	9.1-9.2
C	NaOH	12.7-12.8
D	H_2SO_4	2.1-2.2

5.2.3 XPS

The surface elemental and chemical compositions of the investigated samples were determined using a NEXSA G2 XPS system (Thermo Scientific, CZ), equipped with a monochromated Al Kα X-ray source and operated by the Avantage software package (Thermo Scientific, UK). The surface charge was compensated by a dual flood gun. The survey spectra were recorded using a pass energy of 200 eV and an energy step of 1 eV, while 20 eV pass energy and 0.05 eV energy step were used for high-resolution spectra. The recorded spectra were charge-corrected with respect to the C1s peak of adventitious carbon at a binding energy of 285.0 eV.

5.2.4 LEIS

Low-energy ion scattering measurements were performed using a high sensitivity spectrometer ION-TOF Qtac^{100} (IONTOF, Germany) with a primary beam of He^+ 3 keV at 1.9–2 nA, at an incident angle of 0° and scattering angle of 145°. The measurement area was 1 × 1 mm^2. The sputter beam consisted of Ar^+ 1 keV at a current of 206-226 nA and an incident angle of 59° with a sputter area of 1.5 × 1.5 mm^2. ION-TOF Surface Lab 7 was used to process the data. For quantification of Zn, Mg, Al, and Zr the measured spectra were fitted with Gaussian-type peaks considering the isotopic distribution and referenced against the respective pure metal signal.

5.2.5 AFM

The Atomic force microscopy (AFM) imaging and roughness measurements were conducted in tapping mode on an MFP-3D AFM instrument (Oxford Instruments, Asylum Research, UK) using an uncoated silicon probe (tap 300-G). The resonance frequency was 300 kHz, and the force constant was 40 N/m. The raw AFM images were corrected using the least square root method to extract an accurate height value, and the data were then approximated to a second-order flattening surface using the "Igor" software.

5.2.6 AES

The AES point spectra were collected using a multi-channel detector with a cylindrical mirror analyzer on a Phi 710 scanning Auger NanoProbe system, using a field emission electron gun at 10 kV and 10 nA. A scintillator was used for secondary electron imaging. For sputtering, an Ar-ion beam of 2.4 µA at 2 kV energy was rastered over a 1 × 1 mm^2 surface area.

5.3 Results and discussion

We evaluated the effect of mild and strong alkaline, as well as strong acid pretreatments on Zn-Al-Mg alloy coating (see experimental section for details) on formation, structure, and chemistry of Zr-based conversion coatings. First, XPS measurements were conducted to inspect the chemical species, that compose the Zr-conversion layer on these differently pretreated Zn-Al-Mg coatings.

The surface concentration of Zr in relation to Zn in the Zr-Zn pair exhibits a range of values between 80.7 % and 88.3% (see **Table 5.2**). This is consistent with the relative percentages of Zr and Zn on the surface of the Zr-converted Zn substrate, as it was determined by Cristaudo et al. using XPS [139]. Moreover,

Die approbierte gedruckte Originalversion dieser Dissertation ist an der TU Wien Bibliothek verfügbar.
The approved original version of this doctoral thesis is available in print at TU Wien Bibliothek.

slightly less Zr and more Zn were formed in strong alkaline treatment, with low statistical confidence.

Table 5.2. Elemental composition calculated from the XPS survey spectra. Samples are labeled according to the pretreatment type and the time of immersion: 1 or 10 minutes.

Sample	C	O	Zn	Zr	F	Zr/(Zn + Zr),%
A-1	31.3	39.8	2.1	14.4	12.4	87.3
A-10	25.4	41.5	2.3	15.5	15.3	86.9
B-1	19.9	45.8	2.9	16.0	15.4	84.9
B-10	23.3	43.2	2.1	16.0	15.4	88.3
C-1	19.8	43.7	3.5	16.3	16.8	82.3
C-10	16.3	46.7	4.2	17.4	15.4	80.7
D-1	30.0	37.9	2.0	14.9	15.1	88.2
D-10	22.9	40.0	2.3	17.1	17.7	87.9

Zr-conversion layers, identified by XPS peaks for Zr, F, and O, as shown in **Figure 5.1**, were formed on all samples, regardless of the type of alkaline or acidic pretreatment used. The pretreatment duration did not significantly impact the chemical speciation at the surface, as probed by XPS, which typically integrates the topmost 5-10 nm.

In order to ascertain the chemical composition of the formed layer, a detailed examination of the Zr3d peak, see **Figure 5.1** (which is representative for all samples), is required. It can be deconvoluted into two individual components: Zr 3d5/2 and Zr 3d3/2 at 182.9 and 185.3 eV, respectively. These values are in good agreement with other investigations on Zr-based conversion layers and oxidized zirconium [135, 140]. Both peaks could be assigned to ZrO_2. No ZrO_x ($x \neq 2$) seems to be formed, as according to Wang et al., it should emerge as a small peak at around 180.8 eV [140].

The peak positions are consistent with findings pertinent to fluorzirconate glass and zirconium oxyfluoride thin films for Zr3d, which could assume an oxyfluoride formation [141, 142]. Furthermore, in a later study of fluorzirconate glasses Hammer et al. attributed the peak at 530.9 eV for O1s to Zr-O-Zr bonds in Zr-oxyfluoride, which could be correlated to the O1s A peak in **Figure 5.1** [143].

While the O1s A peak could be attributed to oxides in general and the O1s B peak could be assigned to hydroxides, carbonates, oxyfluorides, and carbonyl groups, the atomic percentages of Zr, F, and O signals are in a ratio of 1:1:3, respectively. It seems that a more intricate combination of ZrO_2 with oxyfluoride is formed, we

Die approbierte gedruckte Originalversion dieser Dissertation ist an der TU Wien Bibliothek verfügbar.
The approved original version of this doctoral thesis is available in print at TU Wien Bibliothek.

Die approbierte gedruckte Originalversion dieser Dissertation ist an der TU Wien Bibliothek verfügbar.
The approved original version of this doctoral thesis is available in print at TU Wien Bibliothek.
TU WIEN Bibliothek Your knowledge hub

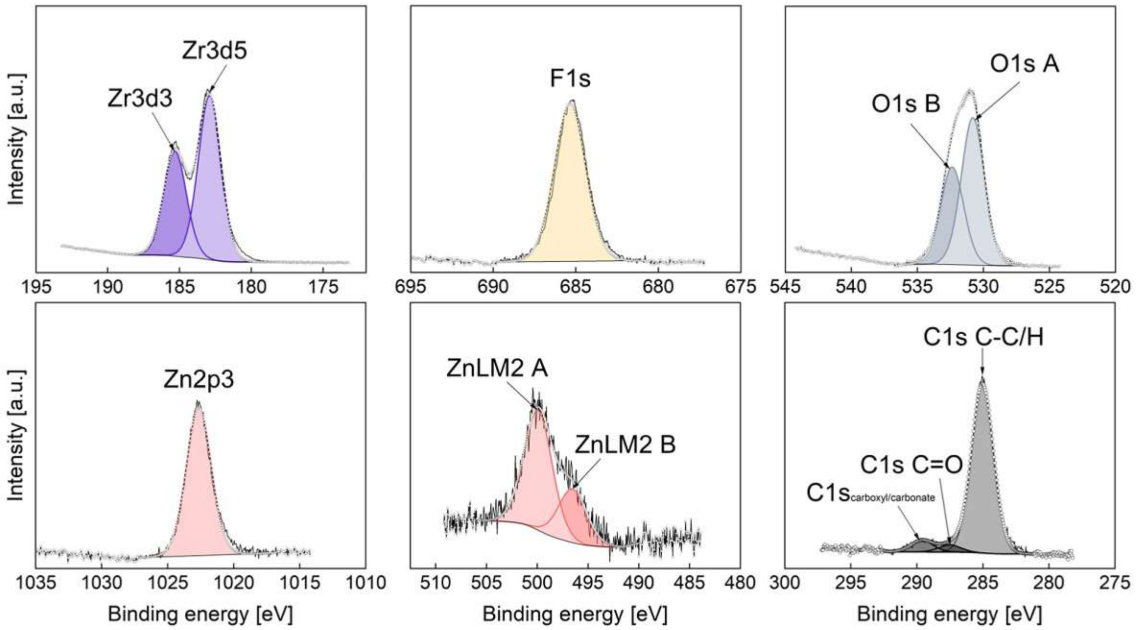

Figure 5.1. High-resolution XPS scans for Zr3d, F1s, O1s, Zn2p3, ZnLM2, and C1s of the sample A, pretreated in mild alkaline conditions after Zr-layer application.

could indicate it as ZrO_2-ZrO_xF_y.

The detected Zn peak at 1022.6 eV reveals mainly the presence of ZnO in a small concentration. The chemical analysis of the zinc peaks (Zn2p and Zn LM2) gives a modified Auger parameter (MAP) of 2009.4 eV, which indicates likely a mixture of ZnO (MAP = 2009.9 eV) and hydrozincite (2009.3 eV) or hydroxide (2008.9 eV) on the surface [9, 87, 121–123, 144].

A significant reduction in the Zn-oxyhydroxide component signal (peak ZnLM2 B in **Figure 5.1**) is observed, compared to the alkaline cleaned Zn-Al-Mg samples, that were the subject of our recent research [84]. As proposed by Cristaudo et al., this reduction can be attributed to the hydroxyl consumption by the free fluorides, prior to the deposition of the ZrO_2 film and the formation of a Zn-F complex. This complex is subsequently detached from the surface [139].

Complementary LEIS depth measurements were conducted to estimate the approximate thickness of the resulting Zr-based conversion layers on differently pretreated Zn-Al-Mg surfaces and evaluate their elemental composition along the depth.

First, as shown in **Figure 5.2** Zr the peaks overlap with the Oxygen profile (not quantitative) for all samples, indicating Zr-oxide layers with varying thicknesses. The most efficient thickness-time ratio demonstrates the acidic pretreatment D. After 1 minute of sulphuric acid treatment, the ZrO_2-ZrO_xF_y-layer thickness is approximately 23 nm. At the same time, for strongly alkaline treated samples, similar results occur only after a prolonged 10 minutes of immersion. These results practically corroborate the study, where the lower concentrations of sulphuric acid more effectively increased the surface reactivity of Zn-Al-Mg coating [22].

In contrast to XPS data, which indicate that the Zr-based conversion coating comprises zirconium oxide or oxyfluoride, LEIS profiles indicate a more complex layered structure of F and Zr. At depths beyond 10 nm, the quantitative distribution of F depth profiles in all samples traces the Mg and Al depth profiles. It can hence be assumed that F binds with Mg and Al closer to the metal/conversion layer interface, forming insoluble Al-F and highly insoluble Mg-F. Therefore, LEIS depth profiles indicate the fluoride formations. Interestingly, the fluoride formation strongly depends on the pretreatment. While alkaline pretreatments lead to a clear double-layered structure, acidic treatment leaches more Mg/Al, resulting in a less pronounced formation of fluorides.

Another conclusion derived from the LEIS analysis is that the prolonged pretreatment time affects the conversion layer thickness for strongly alkaline and acidic treated samples. For instance, the thickness of the Zr-oxide/oxyfluoride layer is increased slightly for sample C and more than twice for sample D. Therefore, the prolongation of the pretreatment time affects the surface reactivity in strong alkaline and acidic media.

Die approbierte gedruckte Originalversion dieser Dissertation ist an der TU Wien Bibliothek verfügbar.
The approved original version of this doctoral thesis is available in print at TU Wien Bibliothek.
TU WIEN Bibliothek Your knowledge hub

Die approbierte gedruckte Originalversion dieser Dissertation ist an der TU Wien Bibliothek verfügbar.
The approved original version of this doctoral thesis is available in print at TU Wien Bibliothek.

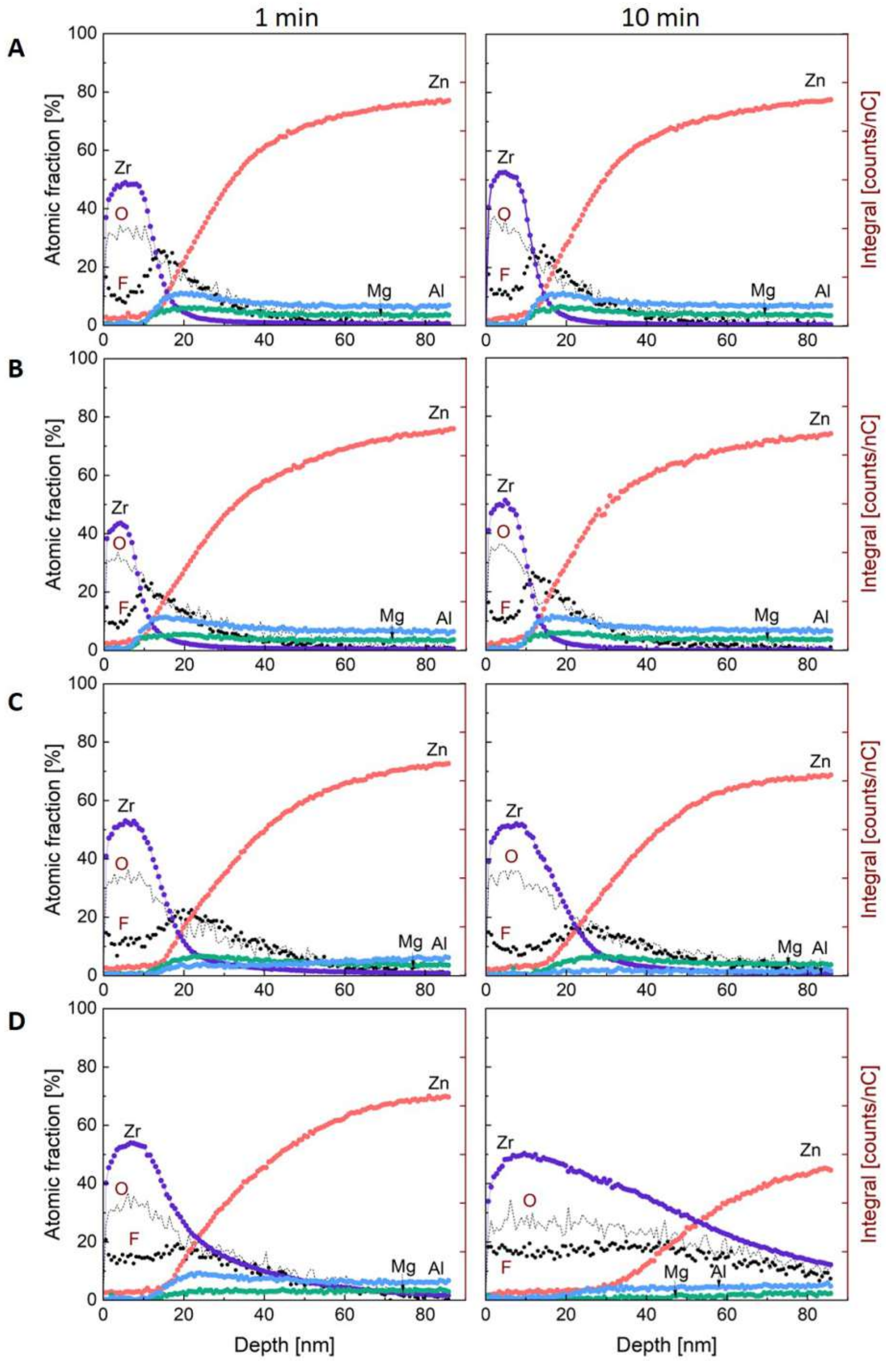

Figure 5.2. LEIS depth profiling, where A-$Na_2B_4O_7$, pH 9; B – NaH_2PO_4, pH 9; C – NaOH, pH 12.7; D – H_2SO_4, pH 2. O and F signals are not quantifiable and are presented as integral signal. The depth scale was established with the assistance of the IONTOF Surface Lab 7 software tool, which estimated the value of one sputter step to be 0.69 nm.

The difference in the behavior of Al and Mg in mild alkaline, strong alkaline, and acidic solutions can be explained by the pretreatment environment. Although in this research, commercially available cleaners were substituted by simple model solutions with the same pHs, trends of dissolution for Al and Mg are the same as those, described in our previous work[84]. In a strong alkaline solution, most of the Al was dissolved after 10 minutes of treatment. Moreover, as expected of Mg from Pourbaix diagrams, the acidic pretreatment dissolves almost all Mg after the first minute. Hence, less or no insoluble MgF_2 can form after acidic treatment.

Furthermore, the topographic imaging of Zr-converted samples A and B after 10 minutes of pretreatment with mild alkaline solutions, as shown in **Figure 5.3**, reveals the formation of holes or pits distributed over the surface. Strong alkaline and acid treatments show no pits.

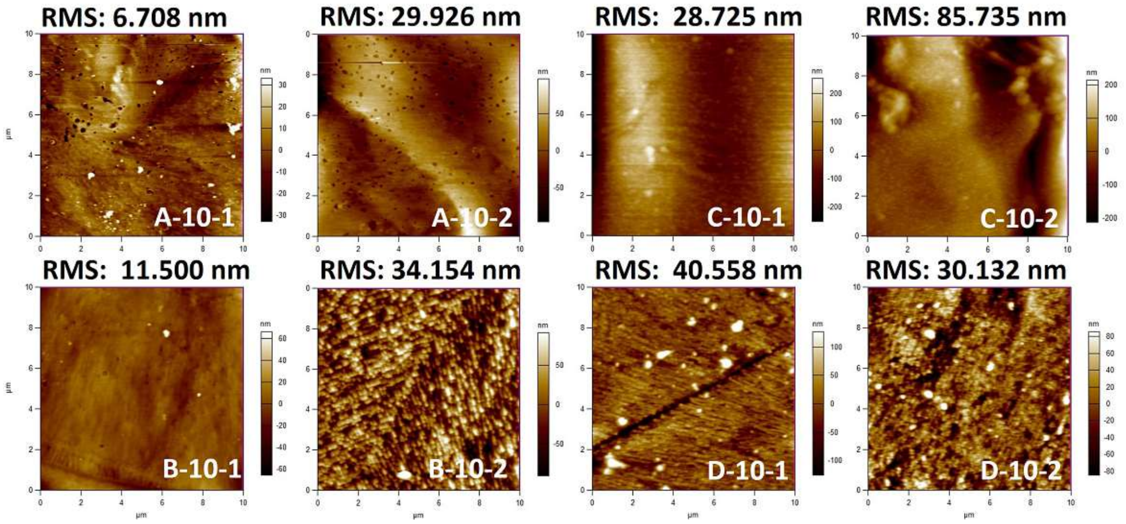

Figure 5.3. Topographic images of 10 µm^2 area on 10 minutes pretreated samples with Zr conversion layer in two spots for each. Labeling of the images refers to the type and time of pretreatment, as well as spot numbering. Root Mean Square (RMS) represents surface roughness.

To gain insight into the surface layers and examine the pit's origin closely, AES spectra with and without Argon sputtering were recorded at selected positions on the surface of sample A after 10 minutes of pretreatment.

Without sputtering, the surface is covered with adventitious carbon. The spectra at all 5 chosen locations indicate the presence of Zr-oxide/oxyfluoride on the entire surface. Further, as shown in **Figure 5.4a** (point 1), at a pit, the F concentration is significantly enlarged. In general, the Fluorine, together with Zr, O and C in the AES spectra, is similar to spectra of synthesized Zr-oxyfluoride, confirming the formation of Zr-oxyfluoride at the outermost surface [145]. This is also consistent

Die approbierte gedruckte Originalversion dieser Dissertation ist an der TU Wien Bibliothek verfügbar.
The approved original version of this doctoral thesis is available in print at TU Wien Bibliothek.
TU WIEN Bibliothek Your knowledge hub

with the slight F-signal increase in LEIS at the outermost surface (see again **Figure 5.2**).

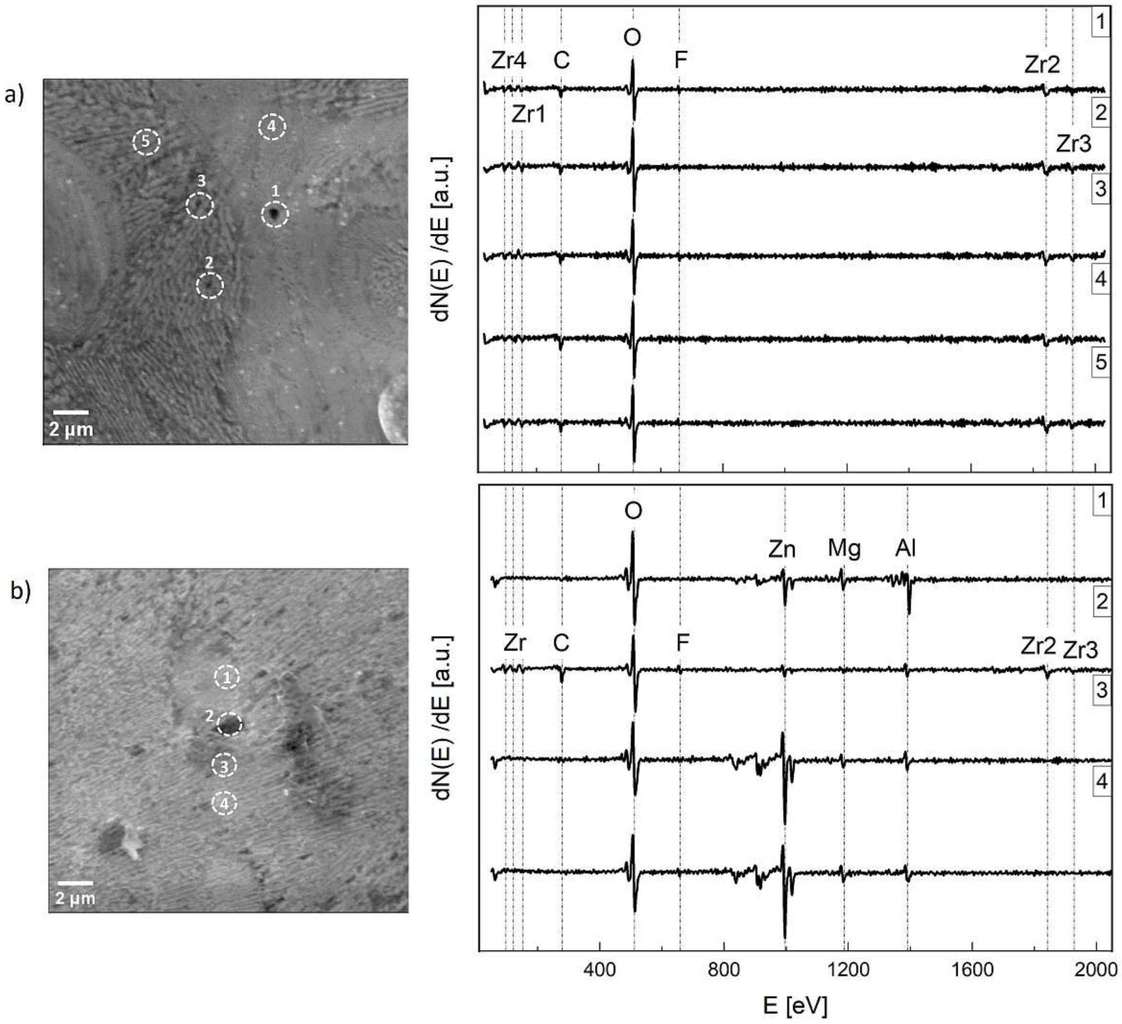

Figure 5.4. Elemental composition of selected points on the surface of sample B-10 by AES: a) as received; b) after Ar sputtering. Zr, Zr1, Zr4 correspond to Zr-MNN, Zr2, Zr3 to Zr_LMM; C to C-KLL, O to O-KLL, F to F-KLL, Zn to Zn-LMM, Mg to Mg-KLL and Al to Al-KLL.

The Ar sputtering, shown in **Figure 5.4b**, was set to remove the entire surface oxyfluoride. As can be seen, the spectra on positions 1, 3, and 4 show that only Zn, Mg, and Al bulk signals are present, while at the pit area, seen in position 2, a significant fluoride signal remained. The prevalence of Zr-oxide/oxyfluoride, accompanied by minimal Zn and Al content, suggests that the pits may result from deeper surface degradation induced by F-ions [146, 147]. It is plausible that the

Die approbierte gedruckte Originalversion dieser Dissertation ist an der TU Wien Bibliothek verfügbar.
The approved original version of this doctoral thesis is available in print at TU Wien Bibliothek.
TU WIEN Bibliothek Your knowledge hub

surface undergoes corrosion or dissolution at these sites, followed by the breaking of Zr-oxide, and forming of Zr-fluoride in the pits [148].

The vulnerability of mild alkaline-treated surfaces to F-induced corrosion could be explained by less effective surface protection by hydroxides. In particular, Mg is insoluble at higher pH (12-14), which suggests that Mg hydroxide formation may play a role in preventing pit formation.

In conclusion, the alkaline pretreatment supports the formation of an insoluble inner layer, consisting of Mg-Al-F, underneath the oxidic ZrO_2-ZrO_xF_y layer. This is due to the enrichment of Mg and Al and the preferential dissolution of Zn.

After acidic pretreatment, however, fast Mg removal during pretreatment results in a Zn-rich interface. This does not allow Mg-F bonding to happen effectively, and hence no stable inner layer is formed.

In the case of mild alkaline pretreatment, although the double layer is observable, F-induced corrosion occurs, which disrupts the integrity of the formed layer.

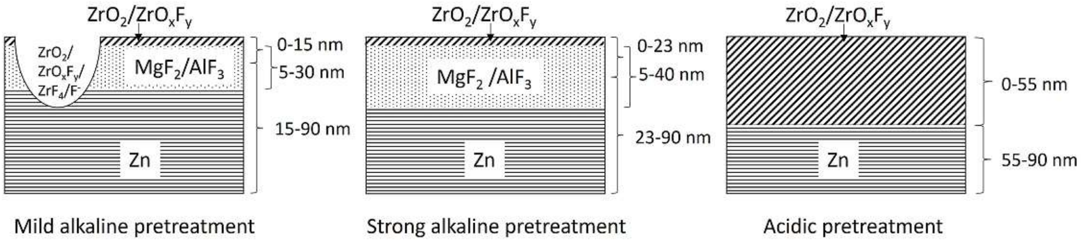

Figure 5.5. Zr-conversion coating model on differently pretreated Zn-Al-Mg surfaces, where the estimated thicknesses are provided in accordance with LEIS.

In consideration of the efficacy of the conversion process, the integrity of the coating as a foundation for the conversion layer, and surface quality, the strong alkaline pretreatment is identified as the optimal choice for the Zr-conversion layer application on Zn-Al-Mg coated steel under studied conditions. This pretreatment forms a 20-nm layer in as little as one minute, with an increase in thickness over time. Furthermore, the layer exhibits minimal susceptibility to F-induced corrosion phenomena compared to mild alkaline pretreated samples. While acidic pretreatment demonstrates the highest efficacy in terms of oxidic layer thickness, it is also known to completely remove Mg, which limits the formation of an insoluble inner fluoride layer. This is summarized and shown in **Figure 5.5**.

Die approbierte gedruckte Originalversion dieser Dissertation ist an der TU Wien Bibliothek verfügbar.
The approved original version of this doctoral thesis is available in print at TU Wien Bibliothek.

5.4 Conclusions

This work analyzes the Zr-conversion layers on Zn-Mg-Al alloy coatings activated by pretreatment with mild alkaline, strong alkaline, and acidic model solutions.

It was found that on alkaline pretreated samples, a Zr-conversion layer, consisting of zirconium oxide and zirconium oxyfluoride with undefined stoichiometry ZrO_2-ZrO_xF_y, is formed, followed by an insoluble Mg-Al-F inner layer. The acidic pretreatment removes Mg from the surface and does not allow Mg-Al-F formation; therefore, the Zr-conversion layer consists only of an oxidic part. Although mild alkaline pretreatment forms a double-layered structure, its integrity is disrupted by F-induced corrosion.

The thickness of the built Zr layer depends on the pretreatment conditions. The acidic pretreatment is the most effective in terms of thickness/time relation compared to others. After 1 minute of sulphuric acid treatment, the total thickness of the Zr-oxidic layer is estimated to be approximately 23 nm. However, long acidic treatment leads to the leaching of Mg/Al, which prevents the formation of an insoluble inner layer of fluorides.

Increasing the pretreatment time leads to a thicker Zr-oxidic layer in strong alkaline and acidic solutions. The thickness of the Zr-oxidic conversion layer is increased slightly for strongly alkaline pretreated samples and more than twice for acidic pretreated samples.

The sodium hydroxide pretreatment is advantageous in terms of producing an uniform complex Zr-conversion coating that is responsive to an increase in treatment time. The coating has a double-layered structure consisting of an oxidic and an insoluble fluoride layer. At similar conditions, it also does not overstimulate the formation of pits.

Die approbierte gedruckte Originalversion dieser Dissertation ist an der TU Wien Bibliothek verfügbar.
The approved original version of this doctoral thesis is available in print at TU Wien Bibliothek.
TU WIEN Bibliothek Your knowledge hub

Die approbierte gedruckte Originalversion dieser Dissertation ist an der TU Wien Bibliothek verfügbar.
The approved original version of this doctoral thesis is available in print at TU Wien Bibliothek.
TU WIEN Bibliothek Your knowledge hub

Chapter 6

Conclusion and Outlook

The conclusions mentioned in this section are of a general nature. The more specific findings from each study can be found at the end of the related chapters.

This thesis presented a detailed investigation of Zn-Al-Mg alloy coatings after various surface pretreatments, focusing on alkaline and acidic conditions. A scope of advanced surface-sensitive techniques, including IRRAS, XPS, LEIS, SIMS, and AES, coupled with analytical ICP-OES, was applied to study the surface oxide chemistry and mechanisms of its formation.

The application of techniques measuring depth profiles was set up to compare their ability to capture the major elemental and surface chemistry changes in the complex matrix of the industrially produced material. While LEIS estimated depth profiles could indicate the elements' distribution in the material and hint at associated surface chemistry changes, AR-XPS, capable of distinguishing between chemical species, gives a more precise understanding of surface chemistry. SIMS depth profile showed a significant sensitivity to Mg signal, still giving the understanding about the oxidational shifts.

The study of commercially available alkaline cleaners showed IRRAS to be useful for evaluating cleaning effectiveness. A simulation of the cleaning process was conducted, and ICP-OES analyzed the spent washing solutions for coating elemental content. The trends of dissolution were supported by surface-sensitive XPS, LEIS, and AES, which investigated the surface chemistry and depth profiling of the oxides. The results could be used to apply deliberate surface modifications to Zn-Al-Mg coatings, as more of present studies are focused on Zn-coated steel.

Going forward with chemical treatment analysis on Zn-Al-Mg coatings, the chemistry of pretreated differently Zr-coated surfaces was analyzed. The double-layer structure of a Zr-based coating was revealed on alkaline pretreated surfaces. At the same time, acidic pretreatment was shown to remove the bounding hydroxide layer and cover only the oxidic part of the coating. Also, fluoride-induced corrosion was shown to have an aggressive presence on surfaces subjected to mild alkaline cleaning.

Therefore, all the research questions formulated in Chapter 1.2 could be answered. The applied techniques were shown to be helpful in solving the tasks of evaluating the chemistry of Zn-Al-Mg coatings after alkaline and acidic pretreatments, commercial cleaners implication, and Zr-based conversion coatings introduction. Moreover, the pretreatment process could be optimized for specific surface qualities by choosing the right pretreatment conditions, such as the type of medium, pH, and immersion time. The optimizations to the industrial process of Zn-Al-Mg surface pretreatment can be applied in practice according to the findings presented here.

TU WIEN Bibliothek Your knowledge hub
Die approbierte gedruckte Originalversion dieser Dissertation ist an der TU Wien Bibliothek verfügbar.
The approved original version of this doctoral thesis is available in print at TU Wien Bibliothek.

Die approbierte gedruckte Originalversion dieser Dissertation ist an der TU Wien Bibliothek verfügbar.
The approved original version of this doctoral thesis is available in print at TU Wien Bibliothek.
TU WIEN Bibliothek Your knowledge hub

Bibliography

1. ISO Central Secretary. *Corrosion of Metals and Alloys—Corrosivity of Atmospheres—Classification, Determination and Estimation,2nd edition* Standard ISO 9223:2012 (International Organization for Standardization, Geneva, CH, 2021).
2. Carter, V. *Metallic coatings for corrosion control: corrosion control series* **1** (Newnes, 2013).
3. European Federation of Corrosion, EFC. *Catalogue of atmospheric corrosion field exposure sites in Europe* `https://corrosion-sites.com/`. Online; accessed 10 August 2024. 2021.
4. Thierry, D., Persson, D., Luckeneder, G. & Stellnberger, K.-H. Atmospheric corrosion of ZnAlMg coated steel during long term atmospheric weathering at different worldwide exposure sites. *Corrosion Science* **148,** 338–354 (2019).
5. Schürz, S. *et al.* Corrosion behaviour of Zn–Al–Mg coated steel sheet in sodium chloride-containing environment. *Corrosion Science* **51,** 2355–2363 (2009).
6. Yang, M., Jiang, G., Xinhua, J. & Jingli, H. TEM study on the microstructure of the Zn-Al-Mg alloy. *Materials Characterization* **129,** 336–343 (2017).
7. Dutta, M., Halder, A. K. & Singh, S. B. Morphology and properties of hot dip Zn–Mg and Zn–Mg–Al alloy coatings on steel sheet. *Surface and Coatings Technology* **205,** 2578–2584 (2010).
8. Angeli, G. *et al. The new family of European ZM coatings–a promising option for the automotive industry* in *Proc. of 4th International European Conference on Steels in Cars and Trucks (SCT), Braunschweig (Germany)* (2014).
9. Duchoslav, J. *et al.* Structure and chemistry of surface oxides on ZnMgAl corrosion protection coatings with varying alloy composition. *Surface and Coatings Technology* **368,** 51–58 (2019).

10. Duchoslav, J. *et al.* Nanoscopic view on the initial stages of corrosion of hot dip galvanized Zn–Mg–Al coatings. *Corrosion Science* **83,** 327–334 (2014).

11. Holzner, T., Luckeneder, G., Strauß, B. & Valtiner, M. Environmentally friendly layered double hydroxide conversion layers: formation kinetics on Zn–Al–Mg-coated steel. *ACS Applied Materials & Interfaces* **14,** 6109–6119 (2022).

12. Keppert, T., Luckeneder, G., Stellnberger, K.-H., Mori, G. & Antrekowitsch, H. Investigation of the corrosion behavior of Zn-Al-Mg hot-dip galvanized steel in alternating climate tests. *Corrosion* **70,** 1238–1248 (2014).

13. Keppert, T. *et al.* The effect of magnesium on the corrosion of hot-dip galvanized steel in chloride containing environments. *Materials and Corrosion* **65,** 871–880 (2014).

14. LeBozec, N. *et al.* Corrosion performance of Zn–Mg–Al coated steel in accelerated corrosion tests used in the automotive industry and field exposures. *Materials and Corrosion* **64,** 969–978 (2013).

15. Ahner, C., Maaß, P. & Peißker, P. *Handbook of hot-dip galvanization* (John Wiley & Sons, 2011).

16. Chalk, D. B. Classification and selection of cleaning processes. *ASM handbook* **5,** 13–47 (1994).

17. Wolpers, M. & Angeli, J. Activation of galvanized steel surfaces before zinc phosphating—XPS and GDOES investigations. *Applied Surface Science* **179,** 281–291 (2001).

18. Schoeman, L. & Burty, M. *Cleaning optimization of hot-dip galvanized steel surfaces in preparation for paint application* in *Materials Science Forum* **941** (2019), 1772–1777.

19. Berger, R., Bexell, U., Stavlid, N. & Grehk, T. M. The influence of alkali-degreasing on the chemical composition of hot-dip galvanized steel surfaces. *Surface and interface analysis* **38,** 1130–1138 (2006).

20. Fink, N., Wilson, B. & Grundmeier, G. Formation of ultra-thin amorphous conversion films on zinc alloy coatings: Part 1. Composition and reactivity of native oxides on ZnAl (0.05%) coatings. *Electrochimica acta* **51,** 2956–2963 (2006).

Die approbierte gedruckte Originalversion dieser Dissertation ist an der TU Wien Bibliothek verfügbar.
The approved original version of this doctoral thesis is available in print at TU Wien Bibliothek.
TU WIEN Bibliothek Your knowledge hub

21. Saarimaa, V. *et al.* Evaluation of surface activity of hot-dip galvanized steel after alkaline cleaning. *Journal of Coatings Technology and Research* **17,** 285–292 (2020).

22. Cetinkaya, B. W. *et al.* Impact of alkaline and acid treatment on the surface chemistry of a hot-dip galvanized Zn–Al–Mg coating. *Journal of Materials Research and Technology* **9,** 16445–16458 (2020).

23. Han, J., Thierry, D. & Ogle, K. Zr-based conversion coating on Zn and Zn-Al-Mg alloy coating: Understanding the accelerating effect of Cu (II) and NO3-. *Surface and Coatings Technology* **402,** 126236 (2020).

24. Van Eijnsbergen, J. F. *Duplex systems: hot-dip galvanizing plus painting* (Newnes, 2012).

25. Knudsen, O. Ø. & Forsgren, A. *Corrosion control through organic coatings* (CRC press, 2017).

26. Streitberger, H.-J. & Goldschmidt, A. *BASF handbook basics of coating technology* (European Coatings, 2018).

27. Milošev, I. & Frankel, G. Conversion coatings based on zirconium and/or titanium. *Journal of The Electrochemical Society* **165,** C127–C144 (2018).

28. Svoboda, J., Kudláček, J., Kreibich, V. & Legutko, S. *Corrosion Resistance of Alternative Chemical Pre-treatments of Hot-Dip Galvanized Zinc Surface* in *Advances in Manufacturing II: Volume 4-Mechanical Engineering* (2019), 572–581.

29. Wang, S. H., Liu, C. & Wang, L. A comparative study of zirconium-based coating on cold rolled steel. *Advanced Materials Research* **291,** 47–52 (2011).

30. Cerezo, J. *et al.* The effect of conversion bath convection on the formation of Zr-based thin-film coatings on multi-metal surfaces. *Materials and Corrosion* **67,** 361–367 (2016).

31. Taheri, P., Laha, P., Terryn, H. & Mol, J. An in situ study of zirconium-based conversion treatment on zinc surfaces. *Applied Surface Science* **356,** 837–843 (2015).

32. Lostak, T. *et al.* Zr-based conversion layer on Zn-Al-Mg alloy coated steel sheets: insights into the formation mechanism. *Electrochimica Acta* **137,** 65–74 (2014).

Die approbierte gedruckte Originalversion dieser Dissertation ist an der TU Wien Bibliothek verfügbar.
The approved original version of this doctoral thesis is available in print at TU Wien Bibliothek.
TU WIEN Bibliothek Your knowledge hub

33. Tasumi, M. *Introduction to experimental infrared spectroscopy: Fundamentals and practical methods* (John Wiley & Sons, 2014).

34. Nishikida, K., Nishio, E. & Hannah, R. W. *Selected applications of modern FT-IR techniques* (CRC Press, 2019).

35. Moore, G. L. *Introduction to inductively coupled plasma atomic emission spectrometry* (Elsevier, 2012).

36. Nölte, J. *ICP Emission Spectrometry: a practical guide* (John Wiley & Sons, 2021).

37. Hofmann, S. *Auger-and X-ray photoelectron spectroscopy in materials science: a user-oriented guide* (Springer Science & Business Media, 2012).

38. Wolstenholme, J. *Auger electron spectroscopy : practical application to materials analysis and characterization of surfaces, interfaces, and thin films* (Momentum Press, 2015).

39. Van der Heide, P. *X-ray photoelectron spectroscopy: an introduction to principles and practices* (John Wiley & Sons, 2011).

40. Zafeiratos, S. *Applications of X-ray Photoelectron Spectroscopy to Catalytic Studies: From Routine Analysis to Cutting-edge Surface Characterization* (World Scientific, 2023).

41. Van der Heide, P. *Secondary ion mass spectrometry: an introduction to principles and practices* (John Wiley & Sons, 2014).

42. Kraj, A., Desiderio, D. M. & Nibbering, N. M. *Mass spectrometry: instrumentation, interpretation, and applications* (John Wiley & Sons, 2008).

43. Wachs, I. E. & Bañares, M. A. *Springer Handbook of Advanced Catalyst Characterization* (Springer Nature, 2023).

44. Woodruff, D. P. *Modern techniques of surface science* (Cambridge university press, 2016).

45. Niemantsverdriet, J. W. *Spectroscopy in catalysis: an introduction* (John Wiley & Sons, 2007).

46. Ponomareva, M. *et al.* Comparison of LEIS, SIMS and AR-XPS as methods for surface characterization of passivated Zn-Al-Mg steel. *Materials and Corrosion* (2025).

Die approbierte gedruckte Originalversion dieser Dissertation ist an der TU Wien Bibliothek verfügbar.
The approved original version of this doctoral thesis is available in print at TU Wien Bibliothek.

47. Hantsche, H. Comparison of basic principles of the surface-specific analytical methods: AES/SAM, ESCA (XPS), SIMS, and ISS with X-ray microanalysis, and some applications in research and industry. *Scanning* **11,** 257–280 (1989).

48. Cushman, C., Grehl, T. & Linford, M. Low Energy Ion Scattering (LEIS). V. Static and Sputter Depth Profiling, and Application to Semiconductor Devices. *Vacuum Technology and Coating* (Nov. 2015).

49. Cushman, C. V. *et al.* A pictorial view of LEIS and ToF-SIMS instrumentation. *Vacuum Technology & Coating* **27** (2016).

50. Lopez, D., Schreiner, W. d., De Sánchez, S. & Simison, S. The influence of carbon steel microstructure on corrosion layers: an XPS and SEM characterization. *Applied surface science* **207,** 69–85 (2003).

51. Galicia, P., Batina, N. & Gonzalez, I. The relationship between the surface composition and electrical properties of corrosion films formed on carbon steel in alkaline sour medium: An XPS and EIS study. *The Journal of Physical Chemistry B* **110,** 14398–14405 (2006).

52. Barroux, A. *et al.* Combined XPS/TEM study of the chemical composition and structure of the passive film formed on additive manufactured 17-4PH stainless steel. *Surfaces and Interfaces* **22,** 100874 (2021).

53. Steiner Petrovič, D., Nagode, A. & Mandrino, D. XRD and AES/XPS investigations of the oxidation behavior of high-manganese electrical steel in air. *JOM* **72,** 962–969 (2020).

54. Zhidkov, I. S. *et al.* XPS characterization of surface layers of stainless steel nitrided in electron beam plasma at low temperature. *Surface and Coatings Technology* **386,** 125492 (2020).

55. Detriche, S. *et al.* XPS fast depth profile of the native oxide layers on AISI 304, 316 and 430 commercial stainless steels and their evolution with time. *Journal of Electron Spectroscopy and Related Phenomena* **243,** 146970 (2020).

56. Donik, Č., Mandrino, D. & Jenko, M. Depth profiling and angular dependent XPS analysis of ultra thin oxide film on duplex stainless steel. *Vacuum* **84,** 1266–1269 (2010).

Die approbierte gedruckte Originalversion dieser Dissertation ist an der TU Wien Bibliothek verfügbar.
The approved original version of this doctoral thesis is available in print at TU Wien Bibliothek.
TU WIEN Bibliothek Your knowledge hub

57. Kalina, L., Bilek Jr, V., Bušo, M., Koplík, J. & Masilko, J. Thickness determination of corrosion layers on iron using XPS depth profiling. *Materiali in tehnologije* **52,** 537–540 (2018).

58. Cushman, C. V. *et al.* Low energy ion scattering (LEIS). A practical introduction to its theory, instrumentation, and applications. *Analytical Methods* **8,** 3419–3439 (2016).

59. Brongersma, H. H., Draxler, M., De Ridder, M. & Bauer, P. Surface composition analysis by low-energy ion scattering. *Surface Science Reports* **62,** 63–109 (2007).

60. Druce, J., Ishihara, T. & Kilner, J. Surface composition of perovskite-type materials studied by Low Energy Ion Scattering (LEIS). *Solid State Ionics* **262,** 893–896 (2014).

61. Caporali, S., Bardi, U. & Lavacchi, A. X-ray photoelectron spectroscopy and low energy ion scattering studies on 1-buthyl-3-methyl-imidazolium bis (trifluoromethane) sulfonimide. *Journal of Electron Spectroscopy and Related Phenomena* **151,** 4–8 (2006).

62. Stowe, K., Chryssoulis, S. & Kim, J. Mapping of composition of mineral surfaces by TOF-SIMS. *Minerals engineering* **8,** 421–430 (1995).

63. Kovochich, M. *et al.* Chemical mapping of tire and road wear particles for single particle analysis. *Science of the Total Environment* **757,** 144085 (2021).

64. Straub, F. *et al.* Imaging the microstructure of duplex stainless steel samples with TOF-SIMS. *Surface and interface analysis* **42,** 739–742 (2010).

65. Saito, K., Kato, T., Tsuji, Y. & Fukushima, K. Identifying the characteristic secondary ions of lignin polymer using ToF- SIMS. *Biomacromolecules* **6,** 678–683 (2005).

66. Tardio, S., Abel, M.-L., Carr, R. H., Castle, J. E. & Watts, J. F. Comparative study of the native oxide on 316L stainless steel by XPS and ToF-SIMS. *Journal of Vacuum Science & Technology A* **33** (2015).

67. Parker, G. D., Plymale, A., Hager, J., Hanley, L. & Yu, X.-Y. Studying microbially induced corrosion on glass using ToF-SIMS. *Biointerphases* **19** (2024).

Die approbierte gedruckte Originalversion dieser Dissertation ist an der TU Wien Bibliothek verfügbar.
The approved original version of this doctoral thesis is available in print at TU Wien Bibliothek.
TU WIEN Bibliothek Your knowledge hub

68. Taylor, M. J. *et al.* Atomistic simulations for investigation of substrate effects on lipid in-source fragmentation in secondary ion mass spectrometry. *Biointerphases* **18** (2023).

69. Wang, L., Seyeux, A. & Marcus, P. Thermal stability of the passive film formed on 316L stainless steel surface studied by ToF-SIMS. *Corrosion Science* **165,** 108395 (2020).

70. Nabizadeh, M. *et al.* Unraveling the mechanism of the conversion treatment on Advanced High Strength Stainless Steels (AHSSS). *Applied Surface Science* **572,** 151418 (2022).

71. Saarimaa, V., Markkula, A., Juhanoja, J. & Skrifvars, B.-J. Determination of surface topography and composition of cr-free pretreatment layers on hot dip galvanized steel. *Journal of Coating Science and Technology* **1,** 88–95 (2014).

72. Gaderbauer, W. *et al.* Effects of alloying elements on surface oxides of hot–dip galvanized press hardened steel. *Surface and Coatings Technology* **404,** 126466 (2020).

73. Lakshmi, R., Bera, P., Aruna, S. & Barshilia, H. C. in *Polymer-Based Nanoscale Materials for Surface Coatings* 167–194 (Elsevier, 2023).

74. Koltsov, A., Cornu, M.-J. & Loison, D. Characterization by different analytical techniques of SiO2 and silane thin films deposited on rough hot-dip galvanized steel surfaces. *Surface and Coatings Technology* **206,** 2759–2768 (2012).

75. Lei, Y. *et al.* Enhanced mechanical properties and corrosion resistance of 316L stainless steel by pre-forming a gradient nanostructured surface layer and annealing. *Acta Materialia* **208,** 116773 (2021).

76. Saarimaa, V. *et al.* Microscale distribution of Ti-based conversion layer on hot dip galvanized steel. *Surface and Coatings Technology* **206,** 4173–4179 (2012).

77. Obada, D., Mamede, A.-S., Nuns, N., Grégoire, A.-C. & Gasnot, L. Combined ToF-SIMS and XPS characterization of 304L surface after interaction with caesium iodide under PWR severe accident conditions. *Applied Surface Science* **459,** 23–31 (2018).

Die approbierte gedruckte Originalversion dieser Dissertation ist an der TU Wien Bibliothek verfügbar.
The approved original version of this doctoral thesis is available in print at TU Wien Bibliothek.

Die approbierte gedruckte Originalversion dieser Dissertation ist an der TU Wien Bibliothek verfügbar.
The approved original version of this doctoral thesis is available in print at TU Wien Bibliothek.

78. Bhattacharya, D. *et al.* Liquid metal embrittlement susceptibility of two Zn-Coated advanced high strength steels of similar strengths. *Materials Science and Engineering: A* **823,** 141569 (2021).

79. Mamede, A.-S. *et al.* Multitechnique characterisation of 304L surface states oxidised at high temperature in steam and air atmospheres. *Applied Surface Science* **369,** 510–519 (2016).

80. Šutara, F., Matolınová, I., Skála, T., Mašek, K. & Matolın, V. Residual surface oxide on ZrV getter—XPS, LEIS and SIMS study. *Vacuum* **74,** 305–309 (2004).

81. Knust, S., Kuhlmann, A., de Los Arcos, T. & Grundmeier, G. Surface modification of ZnMgAl-coated steel by dielectric-barrier discharge plasma. *RSC advances* **9,** 35077–35088 (2019).

82. Ghatei-Kalashami, A., Khan, M. S., Lee, M.-Y. & Zhou, Y. N. High-temperature phase evolution of the ZnAlMg coating and its effect on mitigating liquid-metal-embrittlement cracking. *Acta Materialia* **229,** 117836 (2022).

83. Saarimaa, V., Markkula, A., Arstila, K., Manni, J. & Juhanoja, J. Effect of hot dip galvanized steel surface chemistry and morphology on titanium hexafluoride pretreatment. *Advances in Materials Physics and Chemistry* **7,** 28–41 (2017).

84. Ponomareva, M. *et al.* Alkaline Cleaning of Zn–Al–Mg Hot-Dip Galvanized Steels: Mechanisms and Surface Oxide Chemistry. *Journal of The Electrochemical Society* **170,** 061506 (2023).

85. Havelund, R., Seah, M. & Gilmore, I. Sampling depths, depth shifts, and depth resolutions for Bi n+ ion analysis in argon gas cluster depth profiles. *The Journal of Physical Chemistry B* **120,** 2604–2611 (2016).

86. Guilhaus, M. Mass spectrometry— time-of-flight (2005).

87. Duchoslav, J., Arndt, M., Keppert, T., Luckeneder, G. & Stifter, D. XPS investigation on the surface chemistry of corrosion products on ZnMgAl-coated steel. *Analytical and bioanalytical chemistry* **405,** 7133–7144 (2013).

88. Duchoslav, J. *et al.* Principal investigation on the surface chemistry of phosphated zinc coatings treated by hot active plasma. *Applied Surface Science* **665,** 160308 (2024).

89. Kogler, M. Understanding corrosion passivation layers on high entropy alloys using High Sensitivity–Low Energy Ion Scattering Spectroscopy (LEIS) (2023).

90. Arndt, M. *et al.* Nanoscale analysis of surface oxides on ZnMgAl hot-dip-coated steel sheets. *Analytical and bioanalytical chemistry* **403,** 651–661 (2012).

91. Commenda, C. & Pühringer, J. Microstructural characterization and quantification of Zn–Al–Mg surface coatings. *Materials characterization* **61,** 943–951 (2010).

92. Prosek, T., Larché, N., Vlot, M., Goodwin, F. & Thierry, D. Corrosion performance of Zn–Al–Mg coatings in open and confined zones in conditions simulating automotive applications. *Materials and Corrosion* **61,** 412–420 (2010).

93. Schürz, S. *et al.* Chemistry of corrosion products on Zn–Al–Mg alloy coated steel. *Corrosion Science* **52,** 3271–3279 (2010).

94. Rai, P. K., Rout, D., Satish Kumar, D., Sharma, S. & Balachandran, G. Effect of magnesium on corrosion behavior of hot-dip Zn-Al-Mg coating. *Journal of Materials Engineering and Performance* **30,** 4138–4147 (2021).

95. Rai, P. K., Rout, D., Kumar, D. S., Sharma, S. & Balachandran, G. Corrosion behaviour of hot-dip Zn-Al-Mg coatings with different Al content. *Anti-Corrosion Methods and Materials* **69,** 29–37 (2022).

96. Yao, C. *et al.* Effect of Mg content on microstructure and corrosion behavior of hot dipped Zn–Al–Mg coatings. *Journal of Alloys and Compounds* **670,** 239–248 (2016).

97. De Bruycker, E., Zermout, Z. & De Cooman, B. C. *Zn-Al-Mg coatings: thermodynamic analysis and microstructure related properties* in *Materials Science Forum* **539** (2007), 1276–1281.

98. Stoulil, J. *et al.* Electrochemical properties of corrosion products formed on Zn-Mg, Zn-Al and Zn-Al-Mg coatings in model atmospheric conditions. *Materials and Corrosion* **66,** 777–782 (2015).

99. Walkner, S. & Hassel, A. W. Combined chemical and EIS study of the reaction of zinc coatings under alkaline conditions. *Electrochimica Acta* **131,** 130–136 (2014).

Die approbierte gedruckte Originalversion dieser Dissertation ist an der TU Wien Bibliothek verfügbar.
The approved original version of this doctoral thesis is available in print at TU Wien Bibliothek.
TU WIEN Bibliothek Your knowledge hub

100. Azevedo, M. S., Allély, C., Ogle, K. & Volovitch, P. Corrosion mechanisms of Zn (Mg, Al) coated steel: 2. The effect of Mg and Al alloying on the formation and properties of corrosion products in different electrolytes. *Corrosion Science* **90,** 482–490 (2015).

101. Azevedo, M. S., Allély, C., Ogle, K. & Volovitch, P. Corrosion mechanisms of Zn (Mg, Al) coated steel: the effect of HCO3- and NH4+ ions on the intrinsic reactivity of the coating. *Electrochimica Acta* **153,** 159–169 (2015).

102. Prosek, T. *et al.* Effect of the microstructure of Zn-Al and Zn-Al-Mg model alloys on corrosion stability. *Corrosion Science* **110,** 71–81 (2016).

103. Vimalanandan, A., Bashir, A. & Rohwerder, M. Zn Mg and Zn Mg Al alloys for improved corrosion protection of steel: Some new aspects. *Materials and Corrosion* **65,** 392–400 (2014).

104. Joshi, S., Fahrenholtz, W. G. & O'Keefe, M. J. Effect of alkaline cleaning and activation on aluminum alloy 7075-T6. *Applied Surface Science* **257,** 1859–1863 (2011).

105. Golru, S. S., Attar, M. & Ramezanzadeh, B. Effects of different surface cleaning procedures on the superficial morphology and the adhesive strength of epoxy coating on aluminium alloy 1050. *Progress in Organic Coatings* **87,** 52–60 (2015).

106. Chen, S.-Y., Huang, C.-Y. & Lin, C.-S. Microstructure inhomogeneity of the constituent particles of 7075-T6 aluminum alloy after alkaline cleaning and desmutting. *Corrosion Science* **184,** 109354 (2021).

107. Moffitt, C., Wieliczka, D. & Yasuda, H. An XPS study of the elemental enrichment on aluminum alloy surfaces from chemical cleaning. *Surface and Coatings Technology* **137,** 188–196 (2001).

108. Xavier, C. C., Braga, J. O., Pessoa, M. O., Matencio, T. & Lins, V. F. Corrosion resistance of stainless-steel surgical tools in enzymatic and alkaline detergent. *Materials Today Communications* **33,** 104453 (2022).

109. Fockaert, L. *et al.* Chemisorption of polyester coatings on zirconium-based conversion coated multi-metal substrates and their stability in aqueous environment. *Applied Surface Science* **508,** 144771 (2020).

TU Bibliothek WIEN Your knowledge hub
Die approbierte gedruckte Originalversion dieser Dissertation ist an der TU Wien Bibliothek verfügbar.
The approved original version of this doctoral thesis is available in print at TU Wien Bibliothek.

110. Vu, T. N., Volovitch, P. & Ogle, K. The effect of pH on the selective dissolution of Zn and Al from Zn–Al coatings on steel. *Corrosion Science* **67,** 42–49 (2013).

111. Gharbi, O., Birbilis, N. & Ogle, K. In-situ monitoring of alloy dissolution and residual film formation during the pretreatment of Al-alloy AA2024-T3. *Journal of The Electrochemical Society* **163,** C240 (2016).

112. Mokaddem, M., Volovitch, P. & Ogle, K. The anodic dissolution of zinc and zinc alloys in alkaline solution. I. Oxide formation on electrogalvanized steel. *Electrochimica Acta* **55,** 7867–7875 (2010).

113. Han, J. & Ogle, K. The anodic and cathodic dissolution of α-phase Zn-68Al in alkaline media. *Corrosion Science* **148,** 1–11 (2019).

114. Vu, T., Mokaddem, M., Volovitch, P. & Ogle, K. The anodic dissolution of zinc and zinc alloys in alkaline solution. II. Al and Zn partial dissolution from 5% Al–Zn coatings. *Electrochimica Acta* **74,** 130–138 (2012).

115. Ejaz, A. *et al.* The effects of hydrogen on anodic dissolution and passivation of iron in alkaline solutions. *Corrosion Science* **101,** 165–181 (2015).

116. Yan, Y. *et al.* Investigating ion release using inline ICP during in situ scratch testing of an Mg-Li (-Al-Y-Zr) alloy. *Electrochemistry Communications* **99,** 46–50 (2019).

117. Castaneda, H., Sosa, E. & Espinosa-Medina, M. A. Film properties and stability influence on impedance distribution during the dissolution process of low-carbon steel exposed to modified alkaline sour environment. *Corrosion science* **51,** 799–806 (2009).

118. Sánchez-Moreno, M., Takenouti, H., García-Jareño, J., Vicente, F. & Alonso, C. A theoretical approach of impedance spectroscopy during the passivation of steel in alkaline media. *Electrochimica Acta* **54,** 7222–7226 (2009).

119. Pereira, M., Barbosa, L., Souza, C., De Moraes, A. & Carlos, I. A. The influence of sorbitol on zinc film deposition, zinc dissolution process and morphology of deposits obtained from alkaline bath. *Journal of applied electrochemistry* **36,** 727–732 (2006).

Die approbierte gedruckte Originalversion dieser Dissertation ist an der TU Wien Bibliothek verfügbar.
The approved original version of this doctoral thesis is available in print at TU Wien Bibliothek.

120. Freire, L., Carmezim, M., Ferreira, M. & Montemor, M. The electrochemical behaviour of stainless steel AISI 304 in alkaline solutions with different pH in the presence of chlorides. *Electrochimica Acta* **56,** 5280–5289 (2011).

121. Wagner, C. Auger lines in x-ray photoelectron spectrometry. *Analytical Chemistry* **44,** 967–973 (1972).

122. Powell, C. J. Recommended Auger parameters for 42 elemental solids. *Journal of Electron Spectroscopy and Related Phenomena* **185,** 1–3 (2012).

123. Wagner, C. Auger parameter in electron spectroscopy for the identification of chemical species. *Analytical Chemistry* **47,** 1201–1203 (1975).

124. Ponomareva, M. *et al.* Effect of Surface Pretreatments on the Formation of Zr-Based Conversion Layers on Zn–Al–Mg Alloy-Coated Steel. *Materials and Corrosion* (2024).

125. Shahini, M. H., Eivaz Mohammadloo, H. & Ramezanzadeh, B. Recent advances in steel surface treatment via novel/green conversion coatings for anti-corrosion applications: a review study. *Journal of Coatings Technology and Research* **19,** 159–199. ISSN: 1547-0091 1935-3804 (2021).

126. Giles, T. R., Goodreau, B. H., Fristad, W. E., Kroemer, J. & Frank, M. An update of new conversion coating for the automotive industry. *SAE International Journal of Materials and Manufacturing* **1,** 575–581 (2009).

127. Adhikari, S. *et al.* Hexafluorozirconic acid based surface pretreatments: Characterization and performance assessment. *Electrochimica Acta* **56,** 1912–1924. ISSN: 00134686 (2011).

128. Guan, Y., Liu, J.-g. & Yan, C.-w. Novel Ti/Zr Based Non-Chromium Chemical Conversion Coating for the Corrosion Protection of Electrogalvanized Steel. *International Journal of Electrochemical Science* **6,** 4853–4867. ISSN: 14523981 (2011).

129. Han, J., Thierry, D. & Ogle, K. Zr-based conversion coating on Zn and Zn-Al-Mg alloy coating: Understanding the accelerating effect of Cu(II) and NO3. *Surface and Coatings Technology* **402.** ISSN: 02578972 (2020).

130. Lostak, T. *et al.* Formation and characterization of Fe3+-/Cu2+-modified zirconium oxide conversion layers on zinc alloy coated steel sheets. *Electrochimica Acta* **112,** 14–23. ISSN: 00134686 (2013).

Die approbierte gedruckte Originalversion dieser Dissertation ist an der TU Wien Bibliothek verfügbar.
The approved original version of this doctoral thesis is available in print at TU Wien Bibliothek.

131. Mohammad Hosseini, R., Sarabi, A. A., Eivaz Mohammadloo, H. & Sarayloo, M. The performance improvement of Zr conversion coating through Mn incorporation: With and without organic coating. *Surface and Coatings Technology* **258,** 437–446. ISSN: 02578972 (2014).

132. Pan, J., Ding, Y.-j., Zhao, R.-c., Zhang, J. & Li, Y. Zirconium-based conversion coating modified by different amount of chitosan on hot-dip Zn-Al alloy coated steel sheet. *Corrosion Communications* **12,** 1–10. ISSN: 26672669 (2023).

133. Eivaz Mohammadloo, H. *et al.* A comprehensive study of the green hexafluorozirconic acid-based conversion coating. *Progress in Organic Coatings* **77,** 322–330. ISSN: 03009440 (2014).

134. Cerezo, J. *et al.* The effect of surface pre-conditioning treatments on the local composition of Zr-based conversion coatings formed on aluminium alloys. *Applied Surface Science* **366,** 339–347. ISSN: 01694332 (2016).

135. Taheri, P., Lill, K., de Wit, J. H. W., Mol, J. M. C. & Terryn, H. Effects of Zinc Surface Acid-Based Properties on Formation Mechanisms and Interfacial Bonding Properties of Zirconium-Based Conversion Layers. *The Journal of Physical Chemistry C* **116,** 8426–8436. ISSN: 1932-7447 1932-7455 (2012).

136. Fockaert, L. I. *et al.* Zirconium-based conversion film formation on zinc, aluminium and magnesium oxides and their interactions with functionalized molecules. *Applied Surface Science* **423,** 817–828. ISSN: 01694332 (2017).

137. Cerezo, J. *et al.* Initiation and growth of modified Zr-based conversion coatings on multi-metal surfaces. *Surface and Coatings Technology* **236,** 284–289. ISSN: 02578972 (2013).

138. Cerezo, J. *et al.* Influence of surface hydroxyls on the formation of Zr-based conversion coatings on AA6014 aluminum alloy. *Surface and Coatings Technology* **254,** 277–283. ISSN: 02578972 (2014).

139. Cristaudo, V. *et al.* A combined XPS/ToF-SIMS approach for the 3D compositional characterization of Zr-based conversion of galvanized steel. *Applied Surface Science* **562.** ISSN: 01694332 (2021).

140. Wang, Y., Li, Y., Wong, P. & Mitchell, K. XPS studies of the stability and reactivity of thin films of oxidized zirconium. *Applied surface science* **72,** 237–244 (1993).

TU WIEN Bibliothek Your knowledge hub
Die approbierte gedruckte Originalversion dieser Dissertation ist an der TU Wien Bibliothek verfügbar.
The approved original version of this doctoral thesis is available in print at TU Wien Bibliothek.

141. Pantano, C. G. & Brow, R. K. Hydrolysis reactions at the surface of fluorozirconate glass. *Journal of the American Ceramic Society* **71,** 577–581 (1988).

142. Gibson, U. & Cornett, K. Reactive ion beam assisted deposition of zirconium oxyfluoride thin films. *Journal of Vacuum Science & Technology A: Vacuum, Surfaces, and Films* **14,** 2056–2061 (1996).

143. Hammer, P., Rizzato, A., Pulcinelli, S. H. & Santilli, C. V. XPS study on water corrosion of fluorzirconate glasses and their protection by a layer of surface modified tin dioxide nanoparticles. *Journal of electron spectroscopy and related phenomena* **156,** 128–134 (2007).

144. Duchoslav, J. *et al.* The effect of plasma treatment on the surface chemistry and structure of ZnMgAl coatings. *Applied Surface Science* **504,** 144457 (2020).

145. Taylor, D. & Meyer III, H. Wet-chemical synthesis of zirconium oxyfluoride. *Journal of materials science* **40,** 2655–2658 (2005).

146. Cox, B., Wong, Y.-M. & Dume, P. Effect of fluoride contamination on the growth of ZrO2 films. *Journal of nuclear materials* **250,** 200–215 (1997).

147. Yau, T.-L. & Schweitzer, P. Corrosion of zirconium. *CORROSION TECHNOLOGY-NEW YORK AND BASEL-* **11,** 195–252 (1996).

148. Gwinner, B. *et al.* A step towards a better understanding of corrosion of zirconium in nitric acid with additions of fluorine: Focus on the role of the presence of an initial oxide film. *Corrosion Science* **201,** 110284 (2022).

Die approbierte gedruckte Originalversion dieser Dissertation ist an der TU Wien Bibliothek verfügbar.
The approved original version of this doctoral thesis is available in print at TU Wien Bibliothek.
TU WIEN Bibliothek Your knowledge hub

Die approbierte gedruckte Originalversion dieser Dissertation ist an der TU Wien Bibliothek verfügbar.
The approved original version of this doctoral thesis is available in print at TU Wien Bibliothek.
TU WIEN Bibliothek Your knowledge hub

List of Figures

Die approbierte gedruckte Originalversion dieser Dissertation ist an der TU Wien Bibliothek verfügbar.
The approved original version of this doctoral thesis is available in print at TU Wien Bibliothek.

Die approbierte gedruckte Originalversion dieser Dissertation ist an der TU Wien Bibliothek verfügbar.
The approved original version of this doctoral thesis is available in print at TU Wien Bibliothek.
TU Bibliothek WIEN Your knowledge hub

List of Tables

Die approbierte gedruckte Originalversion dieser Dissertation ist an der TU Wien Bibliothek verfügbar.
The approved original version of this doctoral thesis is available in print at TU Wien Bibliothek.
TU WIEN Bibliothek Your knowledge hub

Die approbierte gedruckte Originalversion dieser Dissertation ist an der TU Wien Bibliothek verfügbar.
The approved original version of this doctoral thesis is available in print at TU Wien Bibliothek.
TU WIEN Bibliothek Your knowledge hub

List of publications

Accepted

- M. Ponomareva, J. Duchoslav, D. Stifter, M. Kogler, F. Fahrnberger, H. Hutter, G. Luckeneder, L. Hader-Kregl, M. Valtiner. Comparison of LEIS, SIMS and AR-XPS as methods for surface characterization of passivated Zn-Al-Mg steel, Materials and Corrosion (2025). DOI:10.1002/maco.202414776

Published

- M. Ponomareva, J. Duchoslav, D. Stifter, M. Kogler, D. Miano, E. Akbari, A. Bleij, G. Luckeneder, T. Singewald, M. Valtiner. Effect of surface pretreatments on the formation of Zr-based conversion layers on Zn-Al-Mg alloy coated steel, Materials and Corrosion (2024). DOI:10.1002/maco.202414664
- M. Ponomareva, M. Nadlinger, G. Schimo-Aichhorn, J. Duchoslav, D. Stifter, G. Luckeneder, M. Valtiner. Alkaline Cleaning of Zn–Al–Mg Hot-Dip Galvanized Steels: Mechanisms and Surface Oxide Chemistry, Journal of The Electrochemical Society (2023). DOI:10.1149/1945-7111/acdc58
- A. Bleij, M. Ponomareva, M. Nadlinger, G. Schimo-Aichhorn, D. Bingemann, C. Rathmell, G. Luckeneder, G. Haslehner, P. Gattinger, M. Brandstetter, P. Bilotto, M. Valtiner. In situ Raman Spectroscopy Monitors the Corrosion of Mild Steel in a Salt Fog Chamber, SPECTROSCOPY (2022). DOI:10.56530/spectroscopy.vl2866a9

Die approbierte gedruckte Originalversion dieser Dissertation ist an der TU Wien Bibliothek verfügbar.
The approved original version of this doctoral thesis is available in print at TU Wien Bibliothek.

Die approbierte gedruckte Originalversion dieser Dissertation ist an der TU Wien Bibliothek verfügbar.
The approved original version of this doctoral thesis is available in print at TU Wien Bibliothek.
TU WIEN Bibliothek Your knowledge hub

Copyright clearances

Marketplace by Copyright Clearance Center 09.10.24, 22:40

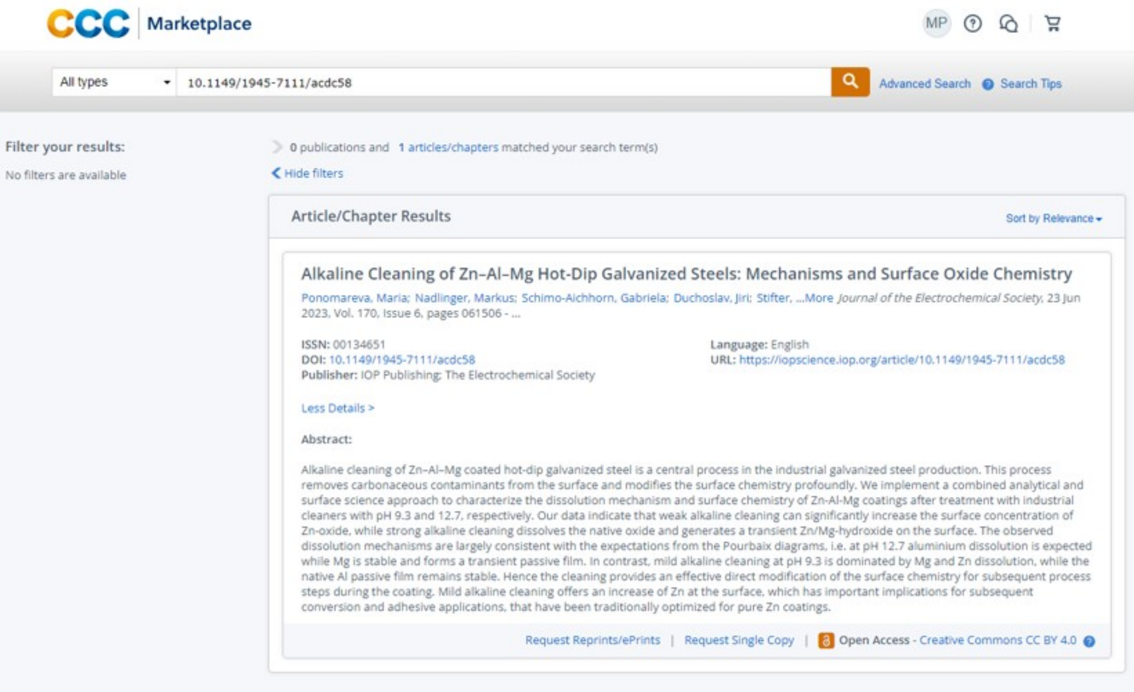

10.1149/1945-7111/acdc58

0 publications and 1 articles/chapters matched your search term(s)

Alkaline Cleaning of Zn–Al–Mg Hot-Dip Galvanized Steels: Mechanisms and Surface Oxide Chemistry

Ponomareva, Maria; Nadlinger, Markus; Schimo-Aichhorn, Gabriela; Duchoslav, Jiri; Stifter, ...More *Journal of the Electrochemical Society*, 23 Jun 2023, Vol. 170, Issue 6, pages 061506 - ...

ISSN: 00134651
DOI: 10.1149/1945-7111/acdc58
Publisher: IOP Publishing; The Electrochemical Society
Language: English
URL: https://iopscience.iop.org/article/10.1149/1945-7111/acdc58

Abstract:

Alkaline cleaning of Zn–Al–Mg coated hot-dip galvanized steel is a central process in the industrial galvanized steel production. This process removes carbonaceous contaminants from the surface and modifies the surface chemistry profoundly. We implement a combined analytical and surface science approach to characterize the dissolution mechanism and surface chemistry of Zn-Al-Mg coatings after treatment with industrial cleaners with pH 9.3 and 12.7, respectively. Our data indicate that weak alkaline cleaning can significantly increase the surface concentration of Zn-oxide, while strong alkaline cleaning dissolves the native oxide and generates a transient Zn/Mg-hydroxide on the surface. The observed dissolution mechanisms are largely consistent with the expectations from the Pourbaix diagrams, i.e. at pH 12.7 aluminium dissolution is expected while Mg is stable and forms a transient passive film. In contrast, mild alkaline cleaning at pH 9.3 is dominated by Mg and Zn dissolution, while the native Al passive film remains stable. Hence the cleaning provides an effective direct modification of the surface chemistry for subsequent process steps during the coating. Mild alkaline cleaning offers an increase of Zn at the surface, which has important implications for subsequent conversion and adhesive applications, that have been traditionally optimized for pure Zn coatings.

Open Access - Creative Commons CC BY 4.0

https://marketplace.copyright.com/rs-ui-web/mp/search/all/10.1149%2F1945-7111%2Facdc58

Page 1 of 1

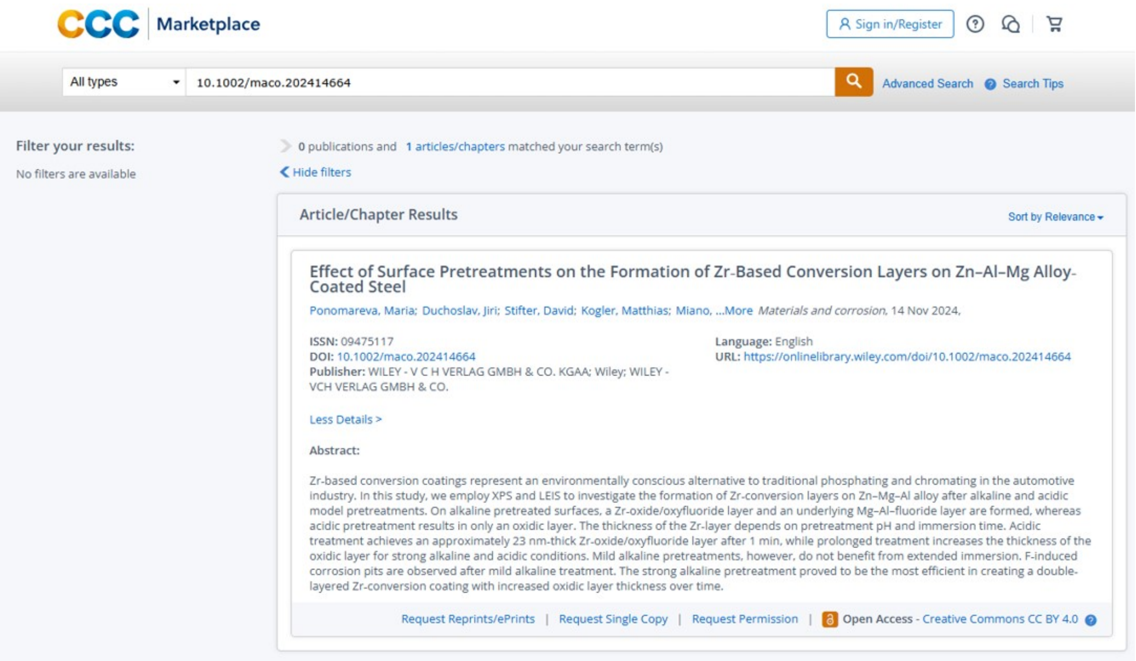

Filter your results:

No filters are available

0 publications and **1** articles/chapters matched your search term(s)

Hide filters

Article/Chapter Results

Effect of Surface Pretreatments on the Formation of Zr-Based Conversion Layers on Zn–Al–Mg Alloy-Coated Steel

Ponomareva, Maria; Duchoslav, Jiri; Stifter, David; Kogler, Matthias; Miano, ...More *Materials and corrosion*, 14 Nov 2024,

ISSN: 09475117
DOI: 10.1002/maco.202414664
Publisher: WILEY - V C H VERLAG GMBH & CO. KGAA; Wiley; WILEY - VCH VERLAG GMBH & CO.
Language: English
URL: https://onlinelibrary.wiley.com/doi/10.1002/maco.202414664

Less Details >

Abstract:

Zr-based conversion coatings represent an environmentally conscious alternative to traditional phosphating and chromating in the automotive industry. In this study, we employ XPS and LEIS to investigate the formation of Zr-conversion layers on Zn–Mg–Al alloy after alkaline and acidic model pretreatments. On alkaline pretreated surfaces, a Zr-oxide/oxyfluoride layer and an underlying Mg–Al–fluoride layer are formed, whereas acidic pretreatment results in only an oxidic layer. The thickness of the Zr-layer depends on pretreatment pH and immersion time. Acidic treatment achieves an approximately 23 nm-thick Zr-oxide/oxyfluoride layer after 1 min, while prolonged treatment increases the thickness of the oxidic layer for strong alkaline and acidic conditions. Mild alkaline pretreatments, however, do not benefit from extended immersion. F-induced corrosion pits are observed after mild alkaline treatment. The strong alkaline pretreatment proved to be the most efficient in creating a double-layered Zr-conversion coating with increased oxidic layer thickness over time.

Open Access - Creative Commons CC BY 4.0

Die approbierte gedruckte Originalversion dieser Dissertation ist an der TU Wien Bibliothek verfügbar.
The approved original version of this doctoral thesis is available in print at TU Wien Bibliothek.
TU Bibliothek WIEN Your knowledge hub

Curriculum Vitae

Personal Data

Name:	Ponomareva, Maria
E-Mail:	maria.n.ponomareva@gmail.com

Education

since 03/2021	**Vienna University of Technology, Vienna** Doctoral programme in Engineering Sciences Diploma programme: Technical Physics Doctoral thesis: Surface chemistry and treatment effects on Zn-Al-Mg coatings: insights into oxidic and zirconium conversion layer formation (working title)
09/2017 – 07/2019	**Tomsk Polytechnic University, Tomsk** Master program in Chemical Technology Thesis Title: L-arginine determination in dietary supplements by voltammetry Degree: Master of Science
10/2013 – 07/2017	**Tomsk Polytechnic University, Tomsk** Bachelor program in Chemical Technology Thesis Title: Determination of ethyl nitrite in model environment by voltammetry Degree: Bachelor of Science

Work Experience

02/2020 – 12/2023	**CEST Centre for Electrochemistry and Surface Technology GmbH, Linz** Junior researcher
09/2019 – 12/2019	**Language school „Friends“, Tomsk** German language tutor
07/2017	**Internship, „Art-Life” Quality control department, Tomsk** Trainee

Die approbierte gedruckte Originalversion dieser Dissertation ist an der TU Wien Bibliothek verfügbar.
The approved original version of this doctoral thesis is available in print at TU Wien Bibliothek.
TU WIEN Bibliothek Your knowledge hub

Skills

Languages:	• Russian, native speaker • English, advanced • German, advanced
Computer:	• MS Office (Word, Power-Point, Excel), advanced skills • Origin Pro, EndNote, Citavi, Overleaf LaTex

Conference contributions

- EuroCorr2021 (Talk): "Study on the impact of strong alkaline cleaning for hot dip galvanized Zn–Al–Mg coatings".

- COAST2022 (Poster): "Impact of alkaline cleaning on hot-dip galvanized steel Zn-Al-Mg coating".

- EuroCorr2022 (Talk): "Extended insights into corrosion during neutral salt spray testing by coupling to advanced analytics".

- COAST2023 (Poster): "Modifications to the surface chemistry of ZM coatings in the complex alkaline cleaners".

- EuroCorr2023 (Talk): "Complex study of mild and strong alkaline cleaning of Zn-Al-Mg hot-dip galvanized steel".

Die approbierte gedruckte Originalversion dieser Dissertation ist an der TU Wien Bibliothek verfügbar.
The approved original version of this doctoral thesis is available in print at TU Wien Bibliothek.
TU WIEN Bibliothek Your knowledge hub

Appendices

A.1 SIMS to LEIS depth profile signal ratio for Zn, Al and Mg relative to Zn

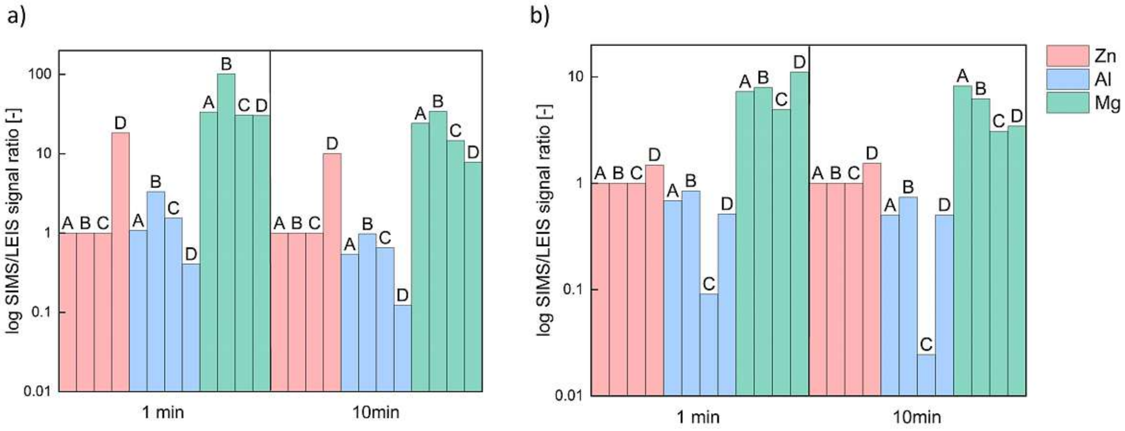

Figure A.1. SIMS to LEIS depth profile signal ratio for Zn, Al and Mg relative to Zn at: a) approximately 8 nm in depth, b) a depth profile signal plateau, corresponding to app. 8 nm for LEIS, and 1000 s for SIMS.

Die approbierte gedruckte Originalversion dieser Dissertation ist an der TU Wien Bibliothek verfügbar.
The approved original version of this doctoral thesis is available in print at TU Wien Bibliothek.
TU WIEN Bibliothek Your knowledge hub

A.2 Not quantified SIMS depth profile of AlO$^-$, MgO$^-$, ZnO$^-$, O2$^-$ and O$^-$ in alkaline and acidic treated samples after 1- and 10- minutes treatment

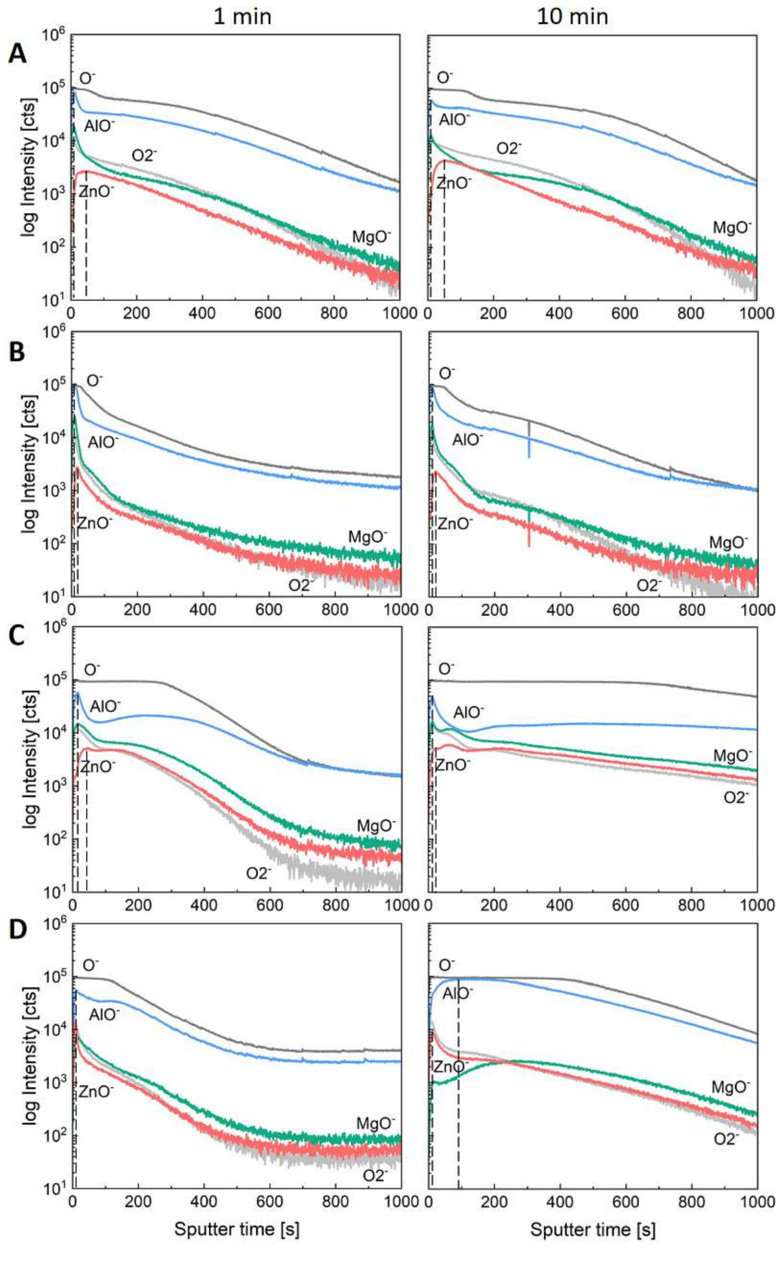

Figure A.2. Not quantified SIMS depth profile of AlO$^-$, MgO$^-$, ZnO$^-$, O2$^-$ and O$^-$ in alkaline and acidic treated samples after 1- and 10- minutes treatment by SIMS.

Die approbierte gedruckte Originalversion dieser Dissertation ist an der TU Wien Bibliothek verfügbar.
The approved original version of this doctoral thesis is available in print at TU Wien Bibliothek.
TU WIEN Bibliothek Your knowledge hub

A.3 High-resolution XPS spectra of Zn (ZnLMM), Al (Al2p) and Mg (MgKLL)

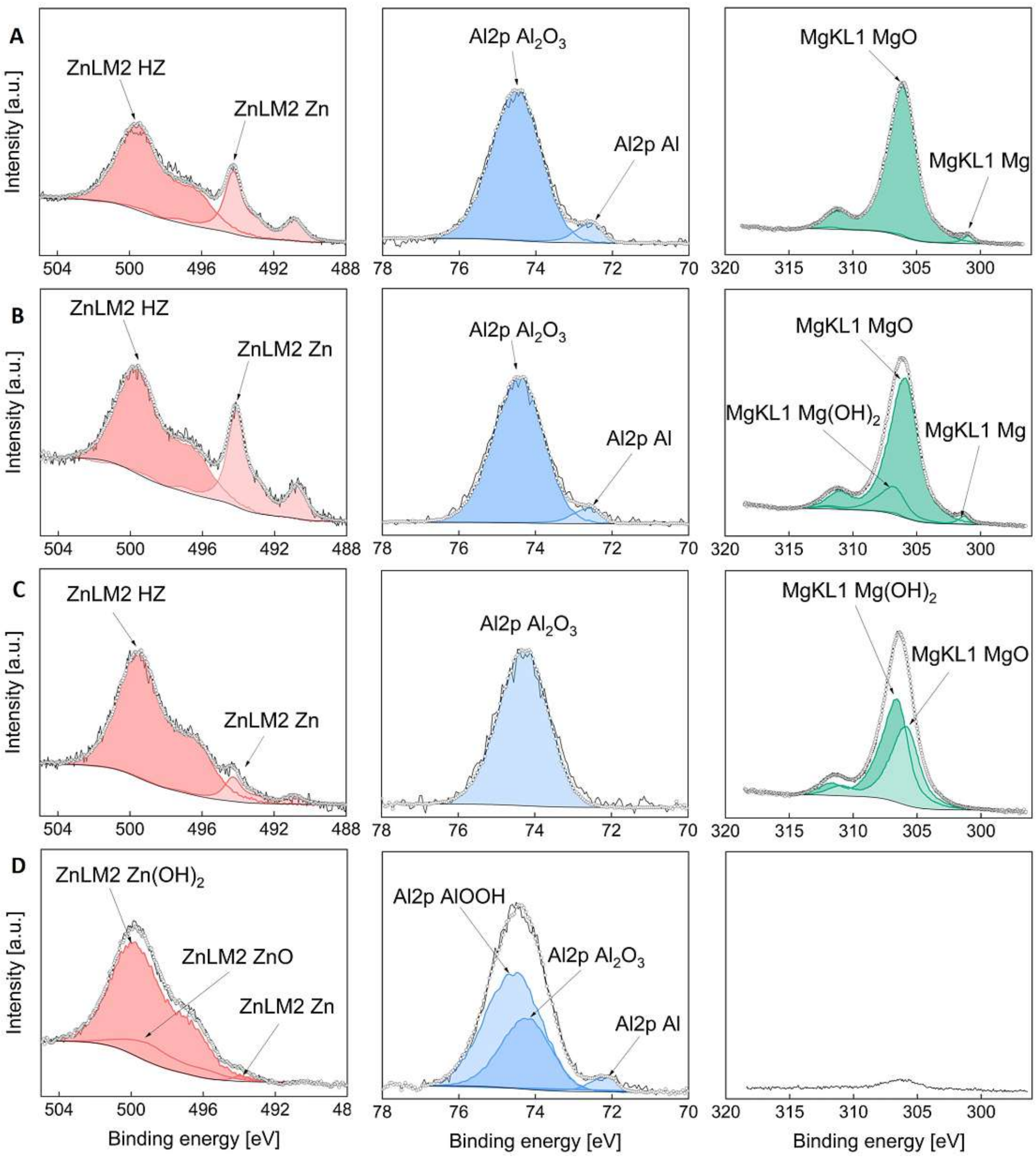

Figure A.3. High-resolution XPS spectra of Zn (ZnLMM), Al (Al2p) and Mg (MgKLL) in samples A, B, C and D after 1 minute of pretreatment.

Die approbierte gedruckte Originalversion dieser Dissertation ist an der TU Wien Bibliothek verfügbar.
The approved original version of this doctoral thesis is available in print at TU Wien Bibliothek.
TU WIEN Bibliothek Your knowledge hub

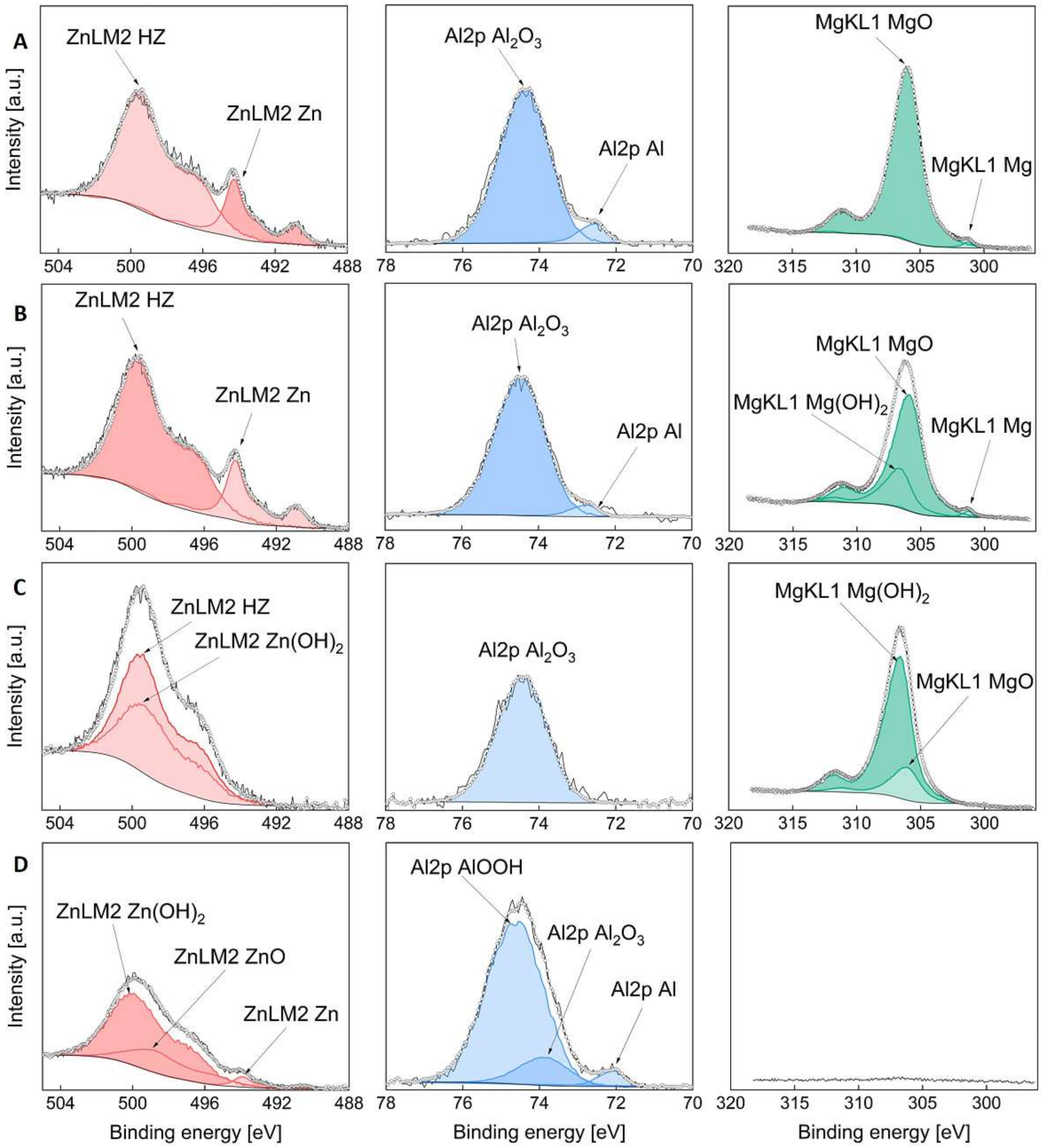

Figure A.4. High-resolution spectra of Zn (ZnLMM), Al (Al2p) and Mg (MgKLL) in samples A, B, C and D after 10 minutes of pretreatment.

Die approbierte gedruckte Originalversion dieser Dissertation ist an der TU Wien Bibliothek verfügbar.
The approved original version of this doctoral thesis is available in print at TU Wien Bibliothek.